ENHANCING THERMOELECTRIC CONVERSION EFFICIENCY: FROM N-TYPE $CaMnO_3$ MODULES IN MULTI-LAYER CONCRETE BRICK TO ULTRA-HIGH RGO CONTENT OF $C_{12}A_7$-RGO COMPOSITES

KEERATI MANEESAI

A THESIS SUBMITTED IN PARTIAL FULFILLMENT OF THE REQUIREMENT FOR THE DEGREE OF DOCTOR OF PHILOSOPHY IN APPLIED PHYSICS

DEPARTMENT OF PHYSICS SCHOOL OF SCIENCE
KING MONGKUT'S INSTITUTE OF TECHNOLOGY LADKRABANG

2025

KMITL-2025-SC-D-030-015

Thesis Title	Enhancing Thermoelectric Conversion Efficiency: From N-Type $CaMnO_3$ Modules in Multi-layer Concrete Brick to Ultra High rGO Content of $C_{12}A_7$-rGO Composites
Student Name	Keerati Maneesai
Student ID	61605017
Degree	Doctor of Philosophy (Applied physics)
Department	Physics
Year	2025
Thesis Advisor	Associate Professor Dr. Chesta Ruttanapun

Abstract

Thermoelectric materials play a critical role in converting waste heat into electricity, offering promising solutions for sustainable energy. This research is driven by three key objectives. The first objective is to optimize the thermoelectric performance of n-type $CaMnO_3$ by integrating these modules into multi-layer concrete bricks, thereby enhancing energy-harvesting capabilities in structural materials. The second objective is to investigate the impact of ultra-high rGO content in $C_{12}A_7$ composites, aiming to significantly improve electrical conductivity and achieve high figures of merit (ZT). Finally, the third objective is to develop and apply Finite Element Method (FEM) simulations to model and optimize the heat and charge transport processes in these systems, providing a robust computational foundation for their real-world applications.

This thesis focuses on enhancing the thermoelectric conversion efficiency of two key systems: n-type $CaMnO_3$ modules embedded in multi-layer concrete bricks and ultra-high rGO content composites of $C_{12}A_7$-rGO. The first part of the research investigates the performance of $CaMnO_3$, a stable perovskite oxide, as an n-type thermoelectric material for high-temperature applications. The integration of n-type

$CaMnO_3$ modules into structural components, such as concrete bricks, enables energy harvesting within building materials. FEM simulations were employed to optimize the design and performance of the $CaMnO_3$ modules, particularly focusing on the effects of embedding these modules into multi-layered concrete structures to improve both heat and charge transport. The results indicate that this novel integration significantly enhances energy efficiency in modern building applications by improving the Seebeck coefficient and power output, demonstrating the potential of these materials for practical implementation in sustainable architecture.

The second part of the research explores the synthesis and characterization of $C_{12}A_7$-rGO composites with ultra-high content of reduced graphene oxide (rGO). $C_{12}A_7$, a calcium aluminate material, is known for its wide bandgap and excellent thermal stability but has limited thermoelectric performance due to its low electrical conductivity. To overcome this, rGO was incorporated into the $C_{12}A_7$ matrix to enhance electrical conductivity while maintaining low thermal conductivity, which are key parameters for improving the ZT. Through extensive characterization techniques, including XRD, Raman spectroscopy, and SEM, the impact of rGO content on the electrical and thermal properties was analyzed. The results reveal that increasing rGO content up to 70 wt% leads to a threefold improvement in electrical conductivity and a significant boost in the Seebeck coefficient, enhancing the overall thermoelectric performance with ZT values reaching 0.7 at high temperatures. However, challenges were observed in achieving homogeneity in rGO dispersion, and thermal conductivity increased slightly with higher rGO content, requiring further optimization to maintain low thermal conductivity.

In conclusion, the integration of n-type $CaMnO_3$ modules into multi-layer concrete bricks, supported by FEM simulations, demonstrated that this system can efficiently convert waste heat into usable electricity while maintaining the structural integrity of building materials. On the other hand, the ultra-high rGO content in $C_{12}A_7$ composites provided a promising pathway for boosting thermoelectric performance, with a critical trade-off between electrical and thermal properties. The overall ZT improvement observed in these materials highlights the importance of nanostructuring and compositional optimization. By addressing the thermoelectric properties of both

$CaMnO_3$-based modules and $C_{12}A_7$-rGO composites, this thesis contributes to the development of more efficient thermoelectric materials. The integration of thermoelectric modules into structural components and the use of rGO to enhance electrical conductivity in ceramic-based composites offer innovative pathways for energy harvesting and waste heat recovery in both industrial and residential settings. This research not only pushes the boundaries of thermoelectric material applications but also contributes to the broader goal of achieving sustainable energy solutions.

Keywords: N-type $CaMnO_3$ modules, $C_{12}A_7$-rGO composites, Multi-layer concrete bricks, Finite Element Method

Acknowledgements

This thesis happened because I got kindness, help, and support from many funding sources, organizations, and people. This gave me chances and inspiration that led to the success of this thesis. I would like to thank Associate Professor Dr. Samak Pimarnpaeng, from the Department of Physics, Faculty of Science, Srinakharinwirot University, who was the chairman of the proposal and thesis examination committee and examined the thesis. Thank you to Assistant Professor Dr. Prathan Buranasiri, Assistant Professor Dr. Chawal Srivong, and Assistant Professor Dr. Metaya Kitiwan, who were also on the committee for the proposal and thesis examination.

This thesis got research funding from the King Mongkut's Institute of Technology Ladkrabang Ph.D. Scholarship Project, contract number KDS2018/007. I want to thank King Mongkut's Institute of Technology Ladkrabang very much. I want to thank the administrators of the Faculty of Science and Engineering, Kasetsart University, Chalermphrakiat Sakon Nakhon Province Campus, for approving my study leave. Thank you to all the staff in the physics department for their work during my study leave.

The main success of this thesis is because I got the chance and kindness from my thesis advisor, Associate Professor Dr. Chettha Ratanapan. He gave me the chance, was kind to give advice, and was a good example in every part of my research topic. He also gave suggestions, and checked my writing of articles. This helped my work get published in an international academic journal that is well-known and made this thesis finish well. Thank you to the post-doctoral researchers and all Ph.D., Master's, and Bachelor's degree students at the Center of Excellence in Research and Innovation for Smart Materials. They gave useful advice and helped with experiments. Thank you to the Center of Excellence in Research and Innovation for Smart Materials, Department of Physics, Faculty of Science, King Mongkut's Institute of Technology Ladkrabang (KMITL), for providing equipment, experimental tools, and a place for research.

Finally, I want to thank my wife, my son and my daughter, who have always been a good support and encouragement behind the scenes. For any good things that come from this thesis, I want to give them to my father, my mother and all my respected teachers who gave me knowledge and shared good experiences, as well as everyone not mentioned here.

Mr. Keerati Maneesai

Table of contents

Table of contents (cont.)

Table of contents (cont.)

Table of contents (cont.)

Table of contents (cont.)

List of tables

List of figures

List of figures (cont.)

List of Abbreviations

T	Absolute temperature
ρ	Density
ZT	Dimensionless figure of merit
σ	Electrical conductivity
I	Electric current
FEM	Finite element method
GO	Graphene oxide
$\dot{Q}$	Heat transferred per unit time
I_D	Intensity of D-band
I_G	Intensity of G-band
I_D/I_G	Intensity ratio of D-band to G-band
V_{oc}	Open-circuit voltage
π_A and π_B	Peltier coefficients of the two materials
PF	Power factor
rGO	Reduced graphene oxide
SEM	Scanning electron microscopy
S	Seebeck coefficient
Cp	Specific heat capacity
ΔT	Temperature difference
κ	Thermal conductivity
α	Thermal diffusivity
TEGs	Thermoelectric generators
wt%	Weight percent
XRD	X-ray diffraction

Chapter 1
Introduction

1.1 Overview of thermoelectric materials

Thermoelectric materials are essential for converting temperature differences into electrical energy. This conversion relies on the Seebeck, Peltier, and Thomson effects. Thermoelectric materials are typically semiconductors because their band structure allows for better performance compared to metals. In semiconductors, the Fermi energy is below the conduction band, enabling asymmetrical state density that facilitates charge transport. On the other hand, metals have a symmetric state density around the Fermi energy, which reduces their efficiency in thermoelectric applications.

The efficiency of thermoelectric materials is measured by the dimensionless figure of merit (ZT), defined as $ZT = \left(\frac{S^2\sigma}{\kappa}\right)T$, where S is the Seebeck coefficient, σ is the electrical conductivity, T is the absolute temperature, and κ is the thermal conductivity. A higher ZT value indicates better thermoelectric performance (Frontiers in Electronic, 2021). Key properties of efficient thermoelectric materials include high electrical conductivity, low thermal conductivity, and a high Seebeck coefficient. These properties ensure efficient charge transport, maintain the necessary temperature gradient, and maximize voltage generation from temperature differences.

Thermoelectric materials are increasingly important in energy harvesting and waste heat recovery, providing sustainable solutions to improve energy efficiency. Their ability to convert thermal gradients into electricity makes them essential components in future energy systems, particularly in reducing environmental impact. Thermoelectric systems, utilizing the Seebeck effect, can generate power for low-energy devices like sensors and wearable technologies, eliminating the need for batteries [1, 2], continuous power generation, harvesting ambient thermal energy, is especially valuable in Internet of Things (IoT) applications, where autonomous sensor operation over long periods are required [3, 4].

The most widely used thermoelectric materials include bismuth telluride (Bi_2Te_3) and lead telluride (PbTe). Bi_2Te_3 is known for its favorable ZT values at room temperature, making it suitable for various applications [5]. However, its performance

drops at higher temperatures, and concerns about the scarcity and toxicity of tellurium limit PbTe large-scale use [6]. PbTe, on the other hand, is effective at higher temperatures, up to around 900 K, making it ideal for industrial waste heat recovery. However, its toxicity and high production costs also pose challenges for widespread adoption.

1.2 Role of $CaMnO_3$ and $C_{12}A_7$-rGO composites

Calcium manganese oxide ($CaMnO_3$) has emerged as a promising n-type thermoelectric material, especially for high-temperature applications. Its perovskite crystal structure provides flexibility for doping and compositional adjustments, which can improve thermoelectric performance. By controlling the oxygen content and adding elements like niobium (Nb), the electrical conductivity and Seebeck coefficient of non-stoichiometric $CaMnO_3$ ($CaMnO_{3-\delta}$) can be optimized. Nb-doped $CaMnO_3$ has achieved a ZT of 0.32 at 800°C, showing potential for high-temperature use [7, 8]. Unlike traditional thermoelectric materials that often contain toxic elements, $CaMnO_3$ is environmentally friendly, making it suitable for sustainable technologies. Thin films of $CaMnO_3$ can be created using sputtering techniques, which facilitates integration into modern microelectronics [8]. However, despite recent progress, $CaMnO_3$'s ZT values remain lower than those of leading thermoelectric materials.

$C_{12}A_7$, or calcium aluminate, combined with reduced graphene oxide (rGO) is gaining attention for its potential to enhance thermoelectric performance. $C_{12}A_7$ has a perovskite-like structure and excellent thermal stability, making it suitable for high-temperature applications. Doping $C_{12}A_7$ with various elements can improve both its electrical conductivity and Seebeck coefficient. However, pure $C_{12}A_7$ tends to have lower ZT values compared to other thermoelectric materials, requiring further optimization. A major challenge with $C_{12}A_7$-based materials is balancing electrical conductivity and thermal conductivity, as improving one often compromises the other.

Reduced graphene oxide (rGO) is derived from graphene oxide and has superior electrical conductivity while retaining some oxygen functionalities. Its high surface area and mechanical strength make it a promising candidate for composite materials. When combined with other materials, rGO can significantly enhance the power factor of thermoelectric composites. However, rGO's relatively high thermal conductivity poses

a challenge for thermoelectric applications, where low thermal conductivity is essential. Achieving uniform dispersion of rGO within a composite matrix is difficult but crucial for optimizing performance. Combining $C_{12}A_7$ with rGO can create a synergistic effect, where the electrical properties of rGO complement the structural benefits of $C_{12}A_7$. Nanostructuring these composites can help scatter phonons, reducing thermal conductivity without affecting electrical transport properties significantly.

The introduction of rGO significantly enhances the electrical conductivity of $C_{12}A_7$ composites. The Seebeck coefficient increases with higher rGO content, indicating improved thermoelectric performance. This enhancement is attributed to the increased density of free charge carriers facilitated by rGO [9]. While thermal conductivity also increases with higher rGO content, careful optimization is necessary to maintain a favorable balance between electrical and thermal conductivities for optimal thermoelectric performance. The power factor (PF) and the figure of merit (ZT) are both temperature-dependent and increase with the amount of rGO incorporated into the composite. These metrics indicate that higher rGO content can lead to better thermoelectric efficiency (Chen and et al., 2022).

The demand for more efficient thermoelectric materials is increasing due to the need for sustainable energy solutions and waste heat recovery. Traditional thermoelectric materials like Bi_2Te_3 and PbTe have limitations, such as narrow operating temperature ranges and environmental concerns. While these materials achieve ZT values of 0.8 to 1.0 at room temperature [9], their performance decreases at higher temperatures. Recent research has shown that layered materials like half-Heusler (hH) alloys can reach ZT values of 1.47 at 973 K by optimizing both composition and design [10]. Nanostructuring techniques, which create superlattice structures, offer a promising approach to improving both electrical and thermal properties, leading to better overall efficiency in thermoelectric systems.

1.3 Integration of thermoelectric materials with structural materials

Integrating thermoelectric materials into structural components such as bricks and concrete offers a new approach to energy harvesting and waste heat recovery. This integration enhances the traditional role of building materials by adding energy efficiency functions. Thermoelectric materials like $CaMnO_3$, when combined with

structural materials, provide a promising solution for converting heat into electrical energy in construction applications. Although challenges remain in balancing electrical conductivity and thermal insulation, recent advancements in material science are improving the performance of such systems. These innovations can potentially increase both the energy efficiency and functionality of modern buildings.

The finite element method (FEM) is an important computational tool for designing and optimizing thermoelectric materials and devices. FEM allows detailed simulations of the thermal and electrical properties of thermoelectric systems. It can model temperature distribution, electric potentials, and heat flow within thermoelectric generators (TEGs). Through these simulations, researchers can predict how temperature gradients affect the voltage output and overall efficiency of thermoelectric materials [11]. FEM simulations provide insights into the behavior of different thermoelectric materials under various conditions. By inputting key parameters like electrical conductivity, Seebeck coefficient, and thermal conductivity, researchers can identify optimal material combinations and configurations that maximize the ZT [12], which is a measure of thermoelectric performance. Additionally, FEM allows researchers to explore different geometric designs of thermoelectric modules, such as leg configurations or module layouts, and evaluate their effects on power output and efficiency [11]. One of the strengths of FEM is its ability to simulate and optimize thermoelectric system architecture for real-world applications. For example, variations in the structure of $CaMnO_3$ thermoelectric modules embedded in concrete bricks can be simulated to analyze their thermal distributions and electrical outputs. These simulations can then be compared with experimental data to verify the accuracy of the model. Studies have shown that FEM simulations often align well with experimental results, demonstrating its value as a reliable predictive tool in the development of thermoelectric materials integrated into structural systems [13].

1.4 Motivation for the study

The demand for sustainable energy solutions has led to growing interest in thermoelectric materials due to their ability to convert waste heat into electricity. However, current thermoelectric materials face limitations in efficiency, particularly at higher temperatures. Traditional materials like Bi_2Te_3 and PbTe suffer from narrow

operating temperature ranges and environmental concerns, prompting the need for alternative materials. This study aims to explore two key thermoelectric materials, $CaMnO_3$ and $C_{12}A_7$-rGO composites, for enhancing thermoelectric efficiency. $CaMnO_3$ is a promising n-type material for high-temperature applications, with its environmentally friendly properties and doping potential. In addition to material exploration, this research integrates thermoelectric modules into multi-layer concrete bricks, offering a novel approach to waste heat recovery in structural materials. The study also employs FEM simulations to model thermal and electrical behaviors, aiding in the design and optimization of thermoelectric systems.

$C_{12}A_7$, composited with rGO, offers the potential to improve thermoelectric performance through optimized electrical conductivity and reduced thermal conductivity. However, achieving a balance between these properties remains a challenge.

1.5 Research problem and knowledge gap

Despite advancements in thermoelectric materials, significant gaps remain in several areas. First, there is a lack of comprehensive studies focusing on ultra-high rGO content in $C_{12}A_7$-rGO composites. Research has explored the potential of these composites, but detailed investigations on the effects of extremely high rGO content, especially in relation to thermoelectric performance, are still limited. Another notable gap is the limited research on integrating thermoelectric materials like $CaMnO_3$ into practical, large-scale applications, particularly within multi-layered structural materials such as concrete bricks. The combination of thermoelectric modules with structural components has the potential to enhance energy efficiency in buildings but has not been extensively studied or optimized. This thesis aims to address these gaps by investigating the impact of ultra-high rGO content in $C_{12}A_7$-rGO composites and by exploring the integration of $CaMnO_3$ thermoelectric modules into multi-layer concrete bricks.

1.6 Objectives of the study

The primary objective of this research is to enhance thermoelectric performance through material innovation and system integration. The specific goals are outlined as follows:

Synthesis and characterization of ultra-high rGO content $C_{12}A_7$-rGO composites

1) To synthesize $C_{12}A_7$-rGO composites with ultra-high rGO content using solid-state reaction techniques, including 3D ball-milling.

2) To characterize the composites using various techniques such as X-ray diffraction (XRD), scanning electron microscopy (SEM), Raman spectroscopy, and UV-Visible (UV-VIS) spectroscopy.

3) To evaluate the electrical conductivity, dielectric properties, and thermoelectric properties of the composites, with a focus on understanding the impact of ultra-high rGO content.

Design and construction of n-type $CaMnO_3$ modules in multi-layer concrete brick

1) To design and optimize n-type $CaMnO_3$ thermoelectric modules using FEM simulations, with a focus on improving heat and charge transport.

2) To integrate these thermoelectric modules into multi-layer concrete bricks and measure their electrical properties under both open and closed-circuit conditions, assessing their performance in practical applications.

1.7 Research hypotheses

This research is based on two main hypotheses:

Hypothesis for $C_{12}A_7$-rGO composites

The hypothesis is that ultra-high rGO content in $C_{12}A_7$-rGO composites will significantly enhance both electrical conductivity and thermoelectric properties. This enhancement is expected to result from increased charge carrier mobility and reduced phonon scattering, leading to improved thermoelectric performance.

Hypothesis for n-type $CaMnO_3$ modules in multi-layer concrete bricks

It is hypothesized that integrating $CaMnO_3$-based thermoelectric modules into multi-layer concrete bricks will improve energy conversion efficiency without compromising the structural integrity and functionality of the bricks. This will allow the bricks to serve dual purposes: structural support and energy generation.

1.8 Scope of the thesis

This thesis covers several key areas of thermoelectric material research and application:

Material synthesis

The study focuses on synthesizing $C_{12}A_7$, $C_{12}A_7$-rGO composites and n-type $CaMnO_3$ using solid-state reaction methods, with particular emphasis on varying rGO content to explore its effects on thermoelectric performance.

Characterization

The structural, spectroscopic, and electrical properties of the composites will be thoroughly characterized using techniques such as XRD, SEM, Raman, and UV-VIS spectroscopy. These characterizations will help establish correlations between material composition and thermoelectric performance.

Thermoelectric property evaluation

The thesis will evaluate key thermoelectric properties of the $C_{12}A_7$, $C_{12}A_7$-rGO composites and n-type $CaMnO_3$, including the Seebeck coefficient, electrical conductivity, thermal conductivity, and the calculation of the ZT.

FEM simulation and module design

The study will utilize FEM simulations to design and optimize n-type $CaMnO_3$ thermoelectric modules. These simulations will focus on enhancing the heat and charge transport properties of the modules, contributing to their overall thermoelectric efficiency.

Integration of n-type $CaMnO_3$ modules into structural materials

The research will examine the integration of n-type $CaMnO_3$ thermoelectric modules into multi-layer concrete bricks. Experimental evaluations will be conducted to assess their performance in practical settings, particularly in terms of energy generation and structural integrity.

1.9 Research significance and applications

This study has the potential to make significant contributions to both thermoelectric material science and sustainable energy technologies. The research will advance knowledge on the synthesis and application of $C_{12}A_7$-rGO composites, particularly regarding the effects of ultra-high rGO content on thermoelectric

properties. It will also contribute to the development of $CaMnO_3$ thermoelectric modules for integration into structural materials, opening new possibilities for energy-efficient building designs. This dual approach aims to provide innovative solutions for waste heat recovery and sustainable energy generation.

1.10 Thesis structure overview

This thesis is organized into five main chapters. Chapter 1 introduces the background and motivation of the research, outlines the research problem, defines the objectives, and highlights the scope and significance of the study. Chapter 2 provides a comprehensive review of the literature on thermoelectric materials, focusing on graphene-based composites, oxides, and thermoelectric module design. It also discusses the application of the FEM in thermoelectric research. Chapter 3 details the materials and methodologies used in the research, including synthesis techniques, characterization methods, and FEM simulations. Chapter 4 presents and discusses the results of the structural, electrical, dielectric, and thermoelectric property measurements, as well as FEM simulation and experimental validation. Finally, Chapter 5 concludes the study, summarizing key findings, contributions, limitations, and suggestions for future research. The thesis also includes references and appendices for additional data and detailed information

Chapter 2
Theory and literature reviews

2.1 Introduction to thermoelectric materials

2.1.1 Thermoelectric effect and its applications

The Seebeck and Peltier effects are fundamental thermoelectric phenomena that enable the direct conversion of thermal energy to electrical energy and vice versa. These effects are essential for energy conversion, refrigeration, and temperature measurement.

Seebeck effect

The Seebeck effect occurs when a temperature difference between two conductive materials generates an electromotive force (EMF). When two dissimilar metals are connected at two junctions and one junction is heated while the other is kept cool, an electric current flow through the circuit. Discovered by Thomas Johann Seebeck in 1821, this effect is commonly used in thermocouples to measure temperature. The voltage generated is approximately linear with respect to the temperature difference and is expressed as $V = S\Delta T$, where V is the voltage, S is the Seebeck coefficient, and ΔT is the temperature difference.

Peltier effect

The Peltier effect, discovered by Jean Charles Athanase Peltier in 1834, is the reverse of the Seebeck effect. When an electric current flow through a circuit of two different conductors, heat is absorbed at one junction and released at another. This effect is used in heating or cooling applications depending on the direction of the current. The heat transfer rate due to the Peltier effect is given by $\dot{Q} = (\pi_A - \pi_B)I$, where $\dot{Q}$ is the heat transferred per unit time, π_A and π_B are the Peltier coefficients of the two materials, and I is the electric current.

Significance in energy conversion

Both effects play a critical role in thermoelectric devices, which convert heat into electrical energy or provide temperature control. Thermoelectric generators (TEGs) convert waste heat from industrial processes or automotive exhaust into electricity, enhancing energy efficiency. Thermoelectric coolers (TECs) utilize the Peltier effect for cooling in devices like portable refrigerators and electronic components. Thermocouples use the Seebeck effect for precise temperature measurements, particularly in industrial and scientific settings. Thermoelectric modules are lightweight, compact, and provide precise temperature control, making them suitable for applications in medical devices and laboratory equipment.

2.1.2 Thermoelectric figure of merit (ZT)

Definition and importance of ZT

The dimensionless figure of merit (ZT) is a key parameter used to evaluate the performance of thermoelectric materials. It quantifies how efficiently a material can convert heat into electricity or provide cooling. ZT is expressed as $ZT = \left(\frac{S^2\sigma}{\kappa}\right)T$, where S is the Seebeck coefficient, measuring voltage per unit temperature difference, σ is the electrical conductivity, indicating how well the material conducts electricity, T is the absolute temperature in Kelvin and κ is the thermal conductivity, which reflects the material's ability to conduct heat.

Higher ZT values indicate more efficient thermoelectric materials, making it a crucial metric for thermoelectric applications. As ZT increases, the maximum conversion efficiency approaches the Carnot limit. Achieving high ZT requires balancing Seebeck coefficient, electrical conductivity, and thermal conductivity, which are interdependent. Materials with high Seebeck coefficients tend to have low electrical conductivity, and those with high electrical conductivity often have high thermal conductivity, reducing ZT. Generally, materials with ZT values greater than 1 are considered suitable for practical applications such as energy harvesting and cooling systems. A ZT value of around 1.5 is often cited as a threshold for effective thermoelectric generators (TEGs). Research continues to explore new materials and methods to push ZT values beyond conventional limits. Techniques such as nano-

structuring, doping, and novel compounds are being developed to improve thermoelectric performance.

State-of-the-art materials with high ZT values

Several thermoelectric materials with high ZT values have been developed, improving energy conversion efficiency. These materials are crucial for applications such as thermoelectric generators (TEGs) and cooling systems. **Table 2.1** summarizes key materials and their ZT values.

Table 2.1 Prominent thermoelectric materials with high ZT values

Material	ZT Value	Applications
Bi_2Te_3	~1.0 (room temperature)	refrigeration, power generation
PbTe	>1.5 (high temperatures)	waste heat recovery
Skutterudites	1.0-1.5	mid to high temperature applications
Half-Heusler alloys	~1.0 or higher	automotive, aerospace
Zintl phases	>1.0	medium-temperature applications
Thermoelectric oxides	~1.0	various environments

Bismuth telluride (Bi_2Te_3) and its alloys have achieved ZT values up to 2.4 due to nano-structuring techniques that improve electrical conductivity while maintaining low thermal conductivity. Bi_2Te_3's ZT is approximately 1.0 at room temperature, making it suitable for refrigeration and power generation applications near room temperature. Lead telluride (PbTe) is known for its high Seebeck coefficient and has been enhanced

through doping and alloying. PbTe's ZT exceeds 1.5 at high temperatures, making it suitable for high-temperature applications like waste heat recovery. Skutterudites materials have complex crystal structures that facilitate phonon scattering, which reduces thermal conductivity while maintaining good electrical properties. Skutterudites exhibit ZT values around 1.0 to 1.5 and are effective for mid- to high-temperature applications. Half-Heusler alloys compounds exhibit good mechanical stability and can be alloyed to optimize thermoelectric properties. ZT values can reach up to 1.0 or higher, particularly at elevated temperatures, making them suitable for automotive and aerospace applications. Zintl phases materials possess low lattice thermal conductivity and high electrical conductivity due to their complex crystal structures. Some compounds, like $Yb_{14}MnSb_{11}$, have ZT values exceeding 1.0, making them suitable for medium-temperature applications. Thermoelectric oxides like $Ca_3Co_4O_9$ show promise due to their high Seebeck coefficients and moderate thermal conductivity. With ZT values of up to 1.0, these oxides are stable in various environments, making them suitable for broader applications.

Strategies to improve ZT for efficient thermoelectric conversion

Enhancing ZT involves optimizing Seebeck coefficient, electrical conductivity, and thermal conductivity. Key approaches include nano-structuring, doping, grain size control, composite materials, and advanced fabrication techniques aimed to develop thermoelectric materials that efficiently convert waste heat into energy or provide effective cooling solutions.

Nanostructures can decouple thermal and electrical transport properties, reducing thermal conductivity while maintaining or enhancing electrical conductivity. Nanoscale features scatter phonons, effectively lowering thermal conductivity. This has been successful in materials like graphene and transition metal dichalcogenides. Techniques such as nanoscale lithography can fine-tune material properties. Introducing dopants can enhance the Seebeck coefficient and electrical conductivity by optimizing carrier concentration. For example, doping Bi_2Te_3 improves its thermoelectric properties. Similarly, alloys can combine materials that have high electrical conductivity with those that reduce thermal conductivity, enhancing ZT. Reducing grain size increases grain boundaries, which scatter phonons and reduce

thermal conductivity. This approach has been effective in materials such as ZnO and PbTe, where smaller grains improve ZT through enhanced phonon scattering. Incorporating conductive nanoparticles into a thermoelectric matrix improves charge carrier mobility while reducing thermal conductivity. For example, metal nanoparticles in a thermoelectric matrix can improve performance by enhancing electrical properties and scattering phonons at interfaces. Advanced fabrication Techniques such as 3D printing and layer-by-layer deposition enable precise control of microstructures, allowing for complex geometries that optimize thermoelectric performance. These methods help to enhance electrical conductivity, Seebeck coefficient, and reduce thermal conductivity. Improving ZT is a multi-faceted challenge. By employing nano-structuring, doping, grain size control, composite materials, and advanced fabrication techniques, researchers aim to develop thermoelectric materials that efficiently convert waste heat into energy or provide effective cooling solutions.

2.2 Advances in thermoelectric materials

2.2.1 N-type thermoelectric materials

Role of n-type thermoelectric materials

N-type thermoelectric materials play a crucial role in thermoelectric modules, converting thermal energy into electrical energy. These materials conduct electricity via negatively charged electrons and are essential for improving thermoelectric device efficiency. They generally exhibit high electrical conductivity, which is necessary for efficient charge transport under a temperature gradient. In n-type materials, the Seebeck coefficient is negative, meaning electrons flow from the hot side to the cold side, generating a voltage. Low thermal conductivity is also important to maintain a temperature difference for efficient energy conversion. **Table 2.2** summarizes key n-type thermoelectric materials, their ZT values, their applications and key features.

Table 2.2 Prominent n-type thermoelectric materials

Material	ZT value	Applications	Key features
Bi_2Te_3	~1.0 (room temperature)	commercial thermoelectric devices	enhancements in nanostructured forms
In2O3	up to 0.15	high-temperature applications	high power factor due to excellent electrical conductivity
SnSe	up to 2.8	thermoelectric generators	favorable thermoelectric properties
Half-Heusler alloys	~1.0 or higher (elevated temperatures)	automotive applications	good mechanical properties
Skutterudites	1.0-1.5	mid to high temperature applications	ability to reduce thermal conductivity while maintaining electrical properties

Performance metrics of n-type thermoelectric materials

N-type thermoelectric material performance varies with temperature. For example, Bi_2Te_3 shows ZT values around 1.4 at room temperature, while SnSe reaches up to 2.8 at elevated temperatures. Recent improvements in Bi_2Te_3-based materials demonstrate efficiencies up to 6.6% at a temperature gradient of 235 K. Doping strategies have significantly improved electrical conductivity and Seebeck coefficients while reducing thermal conductivity.

2.2.2 $CaMnO_3$ as an n-type thermoelectric material

Structure and synthesis of $CaMnO_3$

Calcium manganese oxide ($CaMnO_3$) is a perovskite-type oxide, known for its stability and suitability in high-temperature thermoelectric applications. It has a distorted perovskite structure with tilted MnO_6 octahedra, which influences its

electronic properties and thermoelectric performance. This distortion is important for optimizing the material's Seebeck coefficient and electrical conductivity.

Various synthesis methods have been used to improve $CaMnO_3$'s properties, including:

1) Solid-state reaction: A common method using CaO and MnO_2 at high temperatures. While simple, it may result in large grain sizes and inhomogeneous distributions.

2) Sol-Gel method: Provides better control over particle size and morphology, yielding high-purity and homogeneous materials.

3) Co-precipitation: Produces fine powders with controlled stoichiometry.

4) RF magnetron sputtering: Offers high deposition rates and better control over film composition.

5) Glycine-Nitrate synthesis: Utilizes glycine as a fuel to control morphology.

6) Chemical vapor deposition (CVD): Creates thin films with precise control over thickness and composition.

Thermoelectric properties of $CaMnO_3$

$CaMnO_3$'s thermoelectric properties—electrical conductivity, Seebeck coefficient, and thermal conductivity—are key to its performance. Although it suffers from low electrical conductivity, doping improves this significantly. For example, Nb-doped $CaMnO_3$ shows enhanced conductivity and a resistivity of 0.077 Ω·cm at elevated temperatures. The Seebeck coefficient of $CaMnO_3$ ranges between -200 and -550 μV/K, and its relatively high thermal conductivity (around 4 W/m·K) poses challenges for achieving high ZT values. The best reported ZT value for Nb-doped $CaMnO_3$ is approximately 0.32. Doping can also increase the power factor, with Nb-doped $CaMnO_3$ reaching up to 21.6 μV/m·K² at room temperature.

Challenges and opportunities in $CaMnO_3$ thermoelectric applications

$CaMnO_3$ holds promise as an n-type thermoelectric material, but several challenges remain, including low electrical conductivity, high thermal conductivity, and modest ZT values. Its high resistivity, ranging from 0.12 to 20 Ω·cm, limits its competitiveness. Additionally, the polaron hopping mechanism within the Mn-O framework contributes to inefficiency. High thermal conductivity diminishes the temperature gradient needed for efficient energy conversion. Despite these issues, opportunities for improvement exist. Doping strategies (e.g., with Nb, La, or Dy) can enhance both electrical conductivity and the Seebeck coefficient. Advanced synthesis techniques like sol-gel processes and nano-structuring could further optimize $CaMnO_3$'s thermoelectric properties, making it more viable for practical applications.

Research on enhancing the thermoelectric performance of $CaMnO_3$

Enhancing the thermoelectric performance of $CaMnO_3$ is a multifaceted challenge that involves various strategies, including doping, structural modifications, and composite formation. The inherent properties of $CaMnO_3$, such as its high Seebeck coefficient and n-type conductivity, make it a promising candidate for thermoelectric applications; however, its high electrical resistivity limits its efficiency [14, 15, 16].

One effective approach to improve the thermoelectric performance of $CaMnO_3$ is through doping with various elements. For instance, vanadium doping has been shown to enhance the electronic properties by increasing the hybridization between Mn d and O p orbitals, which facilitates electron conduction via the Mn-O-Mn pathways [17]. Similarly, the dual doping of Pr and Yb has resulted in a significant increase in the ZT, reaching values approximately three times higher than that of undoped $CaMnO_3$ [16]. Other studies have indicated that Sr doping can effectively enhance thermoelectric performance by optimizing the electronic transport properties [15]. Furthermore, the introduction of cerium ions has been reported to improve the Seebeck coefficient and overall thermoelectric efficiency [18].

Structural modifications also play a crucial role in enhancing the thermoelectric properties of $CaMnO_3$. For example, the substitution of metal ions into the $CaMnO_3$ lattice can lead to improved carrier mobility and reduced thermal conductivity, which

are essential for high thermoelectric performance [19, 20]. The introduction of A-site vacancies has been shown to create a glass-like thermal conductivity, which can further enhance the thermoelectric efficiency by reducing heat loss [21]. Additionally, the synthesis of porous $CaMnO_3$ nanostructures has demonstrated improved electrocatalytic activity, which can be beneficial for thermoelectric applications [22]. Composite materials that incorporate $CaMnO_3$ with other thermoelectric materials or insulating matrices have also been explored. Such composites can optimize the thermal and electrical transport properties, leading to enhanced thermoelectric performance [23, 24]. For instance, the use of hybrid p-n junctions with $CaMnO_3$ has shown promising results in terms of power output and efficiency in thermoelectric modules [25].

2.3 Thermoelectric composites with rGO

2.3.1 Reduced graphene oxide in thermoelectric

Structure, properties, and applications of graphene and rGO

Graphene, graphene oxide (GO), and reduced graphene oxide (rGO) are carbon-based materials with distinct structural characteristics that influence their properties and applications. Graphene consists of a single layer of carbon atoms arranged in a hexagonal lattice, giving it exceptional mechanical, electrical, and thermal properties. Its high surface area and strength make it suitable for applications such as transistors, sensors, batteries, and reinforcement of polymers for improved mechanical properties. GO is produced by oxidizing graphene, which introduces functional groups like hydroxyl and carboxyl, improving its dispersibility in water. GO's layered structure varies from single to multi-layer forms. Key applications of GO include drug delivery, tissue engineering, water purification, and corrosion protection. Reduced graphene oxide (rGO) is obtained by chemically or thermally reducing GO, which removes some oxygen groups and restores the electrical and mechanical properties of graphene while retaining some hydrophilicity. rGO is used in applications such as chemical sensors, biosensors, fuel cells, and polymer reinforcement. A critical distinction between GO and rGO lies in their electrical conductivity. GO's insulating nature results from

disrupted π-conjugation, while rGO regains conductivity as oxygen functionalities are removed, enabling its use in electronic applications. **Table 2.3** summarizes properties of Graphene, GO, and rGO.

Table 2.3 Properties of Graphene, GO, and rGO

Property	Graphene	Graphene Oxide	Reduced Graphene Oxide
Electrical Conductivity	Excellent conductor	Insulator due to oxygen groups	Good conductor but less than graphene
Mechanical Strength	Exceptional	Reduced compared to graphene	Improved compared to GO
Hydrophilicity	Hydrophobic	Highly hydrophilic	Moderately hydrophilic
Surface Area	High	High	High
Chemical Stability	Very stable	Stable but reactive	Stable with some reactivity

Role of rGO in enhancing electrical conductivity and carrier mobility in composite materials

Reduced graphene oxide (rGO) plays a crucial role in enhancing electrical conductivity and carrier mobility in composite materials. Its sp^2 hybridized carbon structure, restored during the reduction process, significantly improves conductivity. For instance, Choi et al. demonstrated that reducing GO to rGO restores sp^2 clusters, leading to better charge transport and higher conductivity compared to oxidized graphene [26].

The incorporation of rGO into thermoelectric composites also boosts carrier mobility. For example, the addition of rGO to nonstoichiometric $SrTiO_3$-δ composites resulted in a power factor three times higher than that of pristine $SrTiO_3$ due to the increased electrical conductivity and Seebeck coefficient [27]. Similarly, rGO in $NiMoO_4$ composites improved carrier mobility by reducing energy barriers between grains, leading to enhanced electrical conductivity and Seebeck coefficient [28].

Hybridization of rGO with two-dimensional materials like tungsten disulfide (WS_2) has shown promising control over electrical and thermal transport properties. Kim et al. reported that adding rGO to WS_2 composites improved electrical conductivity, although it reduced the Seebeck coefficient as rGO content increased, indicating the need for optimized rGO ratios for desired thermoelectric properties [29].

In addition to enhancing conductivity, rGO also improves the thermal management of composites. For example, rGO in TiO_2-rGO nanocomposites reduced thermal conductivity while maintaining high electrical conductivity, which is crucial for improving the ZT [30]. This dual enhancement makes rGO an essential component in thermoelectric applications.

Current state of research on rGO-based thermoelectric composites

Reduced graphene oxide (rGO) has emerged as a significant material in the development of thermoelectric composites due to its unique electrical and thermal properties. The incorporation of rGO into various matrices has been shown to enhance the thermoelectric performance of these composites, primarily by improving electrical conductivity while maintaining low thermal conductivity, which is crucial for effective thermoelectric applications.

One of the key advantages of rGO is its ability to enhance the electrical conductivity of composite materials. For instance, studies have demonstrated that the hybridization of rGO with other two-dimensional materials, such as tungsten disulfide (WS2), significantly improves the electrical transport properties of the resulting composites. This improvement is attributed to the effective charge carrier transport facilitated by rGO, which acts as a conductive pathway within the composite structure [29]. Similarly, rGO has been utilized in the creation of nanocomposites with polyaniline (PANI), where the interactions between rGO and PANI lead to increased carrier mobility and enhanced thermoelectric power [31]. The combination of rGO with other conductive polymers has been shown to yield composites with superior thermoelectric performance compared to their individual components.

Moreover, the structural modifications introduced by rGO can lead to a reduction in thermal conductivity, which is beneficial for thermoelectric applications.

For example, the introduction of rGO into $Bi_6Cu_2Se_4O_6$ matrices has been shown to optimize microstructure and enhance thermoelectric performance by reducing thermal conductivity through phonon scattering mechanisms [32]. This is consistent with findings that highlight the role of rGO in lowering thermal conductivity while improving the Seebeck coefficient, thus enhancing the overall ZT of the composites [33].

In addition to its role in enhancing electrical properties, rGO's compatibility with various materials allows for the development of flexible and lightweight thermoelectric devices. The integration of rGO into cotton threads has been explored, resulting in increased electrical conductivity and potential applications in wearable technology [34]. This flexibility is crucial for the advancement of thermoelectric materials in practical applications, particularly in the context of smart textiles and wearable electronics [35].

Furthermore, the versatility of rGO enables its use in various composite formulations, including those with metal oxides like ZnO, where rGO serves to enhance the thermoelectric performance through improved charge transport and reduced thermal conductivity [36]. The ability to tailor the properties of rGO through chemical reduction and functionalization further expands its applicability in thermoelectric materials, allowing for the optimization of performance based on specific application requirements [37].

2.3.2 $C_{12}A_7$ for thermoelectric composites

Structure and properties of $C_{12}A_7$ in dielectric and electrical applications

$C_{12}A_7$ (Dodecacalcium heptaaluminate, $Ca_{12}Al_{14}O_{33}$) is a ceramic material recognized for its unique cubic structure, which contains 12 nano-cages. Two of these cages house mobile oxygen ions, contributing to its ionic conductivity. $C_{12}A_7$, with a wide bandgap of around 7 eV, is an insulator in its pure form, but doping can modify its electrical properties, making it useful in various dielectric and electrical applications.

The dielectric constant of $C_{12}A_7$ has been observed to increase with the incorporation of graphene oxide (GO). For example, $C_{12}A_7$-GO composites exhibit a dielectric constant ranging from 6.61 for pristine $C_{12}A_7$ to 21.11 for composites with higher GO concentrations at 1 kHz. This improvement is attributed to the interfacial

polarization effects and the high density of free electron charges introduced by GO. The loss tangent ($\tan\delta$) also rises with increased GO content, indicating enhanced capacitive behavior. The maximum specific capacitance of 21.514 was recorded at a current density of 0.2 A/g for the $C_{12}A_7$-GO composite.

$C_{12}A_7$'s electrical conductivity can be enhanced through doping or thermal treatments. For instance, polycrystalline $C_{12}A_7$'s conductivity reached 7.65 S/cm at 573 K after Mg heat treatment, demonstrating its potential for conductive applications. The incorporation of rGO or other dopants further improves conductivity by introducing charge carriers and enhancing charge transport mechanisms. In addition to electrical properties, $C_{12}A_7$ composites exhibit improved mechanical characteristics with increasing GO content. Vickers hardness measurements showed the highest value of 117.8 HV for a $C_{12}A_7$-GO composite, indicating enhanced structural integrity.

Due to its high dielectric constant and low loss tangent, $C_{12}A_7$ is suitable for capacitors and other electronic components where low leakage currents are critical. The incorporation of rGO enhances its dielectric properties, improving performance in electrical double-layer capacitors (EDLCs) for energy storage. The improved electrical conductivity also makes $C_{12}A_7$ applicable in electronic devices like sensors and conductive coatings. Moreover, doping or composite formation with rGO opens opportunities for $C_{12}A_7$ in optoelectronics and fuel cells. Studies suggest that $C_{12}A_7$ composites doped with rGO could exhibit thermoelectric properties, driven by enhanced charge transport and stable structure.

Synthesis methods for $C_{12}A_7$-based composites

Various synthesis methods have been developed for $C_{12}A_7$-based composites, focusing on solid-state reactions. These methods are energy-intensive but effective in producing high-quality materials.

Solid-state reaction techniques

$C_{12}A_7$ is synthesized by mixing calcium carbonate ($CaCO_3$) and aluminum oxide (Al_2O_3) in a 12:7 ratio and heating the mixture at high temperatures (around 1300 °C). This method can take several hours to days, with $C_{12}A_7$ forming at elevated

temperatures following the crystallization of phases like C5A3 and C3A. The formation of $C_{12}A_7$ highlights the importance of precise temperature control during synthesis.

Direct mixing with graphene oxide (GO)

C12A7/GO composites are prepared by mixing $C_{12}A_7$ powder with GO suspension at room temperature, which allows GO incorporation without high-temperature treatment. X-ray diffraction (XRD) and Raman spectroscopy confirm that GO integrates into the $C_{12}A_7$ matrix, enhancing electrical and dielectric properties.

Ultra-high rGO content composites

For composites with ultra-high rGO content (up to 70 wt%), a solid-state reaction method is used, followed by hydraulic pressing and heat treatment in an inert atmosphere (such as argon) at around 773 K. This process improves electrical transport properties, resulting in higher Seebeck coefficient and ZT values.

Alternative synthesis methods

A novel method using a double-fuel mixture combined with oxalic acid allows the production of mesoporous $C_{12}A_7$ without long annealing times. This method enhances the material's textural properties while reducing energy consumption. Additionally, the conversion of oxy- $C_{12}A_7$ to electride $C_{12}A_7$ through solid-state techniques has been shown to enhance electrical conductivity via anionic vacancy formation.

Studies on thermoelectric performance of $C_{12}A_7$ related oxides

$C_{12}A_7$ related oxide materials have been explored for their thermoelectric properties. For example, layered oxides such as tin oxides (SnO) and cobalt oxides (e.g., $LaCoO_3$) have been studied for their potential as n-type thermoelectric materials. These materials exhibit interesting electronic properties due to the presence of lone pair electrons and polaronic conduction mechanisms, which can enhance their thermoelectric performance [38, 39]. The exploration of high-entropy oxides has also shown promise, as they can provide a balance between thermal stability and electrical performance, making them suitable for high-temperature applications [40].

Moreover, the stability of oxide thermoelectric materials under various environmental conditions is a significant advantage over traditional thermoelectric materials like Bi_2Te_3 and PbTe. Oxides tend to maintain their structural integrity and performance at elevated temperatures, which is critical for practical applications in thermoelectric generators [41, 42]. However, challenges remain in achieving competitive ZT values compared to established materials, primarily due to limitations in electrical conductivity and the need for further optimization of their microstructural properties [43].

2.3.3 Ultra high rGO content in $C_{12}A_7$ composites

Challenges in achieving high rGO content while maintaining material stability and homogeneity

Incorporating high levels of rGO into $C_{12}A_7$ composites poses several challenges related to stability and homogeneity. As the rGO content increases, the tendency of rGO sheets to agglomerate becomes a significant issue. Agglomeration leads to non-uniform distribution within the composite, which can hinder the formation of effective conductive pathways, crucial for improving electrical properties. This uneven dispersion also weakens mechanical integrity, reducing the overall performance of the material in thermoelectric applications. Higher rGO content also makes the composite more sensitive to oxidative conditions during processing and operation. Excessive rGO may become overactivated, compromising the stability of the composite under harsh conditions. In addition, high rGO content can negatively impact the thermal stability of the composite, as rGO decomposition at elevated temperatures may result in structural degradation and altered material properties. Although rGO improves electrical conductivity, excessive amounts can lead to inconsistent performance due to poor dispersion and increased resistance at interfaces between agglomerated regions. This variability in conductivity can limit the expected improvements in thermoelectric performance. Similarly, the Seebeck coefficient may not increase as anticipated if rGO is not well-dispersed, limiting gains in thermoelectric efficiency. Achieving a uniform distribution of high rGO content requires complex processing methods, such as sonication or chemical functionalization, which complicate synthesis and increase production costs. Moreover, heat treatment must be carefully controlled to prevent

degradation of both $C_{12}A_7$ and rGO. Inconsistent heating can cause phase separation or incomplete reactions, adversely affecting the composite's properties. Excessive rGO content can also alter grain boundary characteristics in $C_{12}A_7$ composites. While some studies suggest that rGO enhances grain boundary interfaces, too much rGO can lead to rough boundaries that impede electron transport, degrading overall performance. High rGO levels can introduce defects into the crystal structure of $C_{12}A_7$, potentially causing undesirable changes in mechanical and electrical properties.

Review on rGO-doped composites in terms of improved ZT

Reduced graphene oxide (rGO)-doped composites have emerged as a significant area of research in the field of thermoelectric materials due to their potential to enhance the ZT. The incorporation of rGO into various thermoelectric matrices has been shown to improve electrical conductivity, reduce thermal conductivity, and optimize the Seebeck coefficient, all of which contribute to higher ZT values. One of the primary mechanisms by which rGO enhances thermoelectric performance is through its high electrical conductivity. For instance, Ding et al. demonstrated that the addition of rGO to bismuth telluride (Bi_2Te_3) nanoplates significantly improved the power factor, a critical parameter for thermoelectric efficiency, due to enhanced charge carrier mobility [44]. The rGO acts as a conductive network within the composite, facilitating better charge transport and reducing the overall resistivity of the material. This is particularly important in thermoelectric applications, where maximizing electrical conductivity while minimizing thermal conductivity is essential for achieving high ZT values. Moreover, the structural properties of rGO can lead to effective phonon scattering, which helps in reducing thermal conductivity. This phenomenon is crucial because lower thermal conductivity allows for a greater temperature gradient, which is beneficial for thermoelectric applications. For example, Biswas et al. reported that the introduction of rGO into metal oxide composites can enhance ZT by effectively scattering phonons while maintaining good electrical conductivity [45]. This balance between electrical and thermal properties is vital for optimizing the thermoelectric performance of the composite.

In addition to improving conductivity and reducing thermal conductivity, rGO can also influence the Seebeck coefficient. Ding et al. reported that the incorporation

of rGO into bismuth telluride (Bi_2Te_3) nanoplates led to a significant enhancement in the Seebeck coefficient, which is a measure of the voltage generated in response to a temperature difference [44]. The synergistic effect of rGO in these composites allows for improved thermoelectric performance, as the Seebeck coefficient is a critical factor in determining ZT.

Furthermore, the use of rGO in combination with other thermoelectric materials has shown promising results. For instance, Huang et al. suggested that combining rGO with SnSe could lead to considerable improvements in ZT values through optimized doping strategies and texture control [46]. This indicates that the potential for enhancing thermoelectric performance through rGO is not limited to its standalone effects but can be significantly amplified when used in conjunction with other materials.

The versatility of rGO also extends to its ability to form composites with various matrices, including polymers and metal oxides. For example, the incorporation of rGO into polymeric thermoelectric composites has been shown to enhance the overall thermoelectric properties, as the rGO provides a conductive pathway that improves charge transport while maintaining the flexibility of the composite [47]. Similarly, rGO-doped metal oxides have demonstrated improved thermoelectric performance due to the effective charge carrier dynamics facilitated by the rGO network [45].

2.4 Structural thermoelectric modules

2.4.1 Integration of thermoelectric materials in structural applications

Thermoelectric modules embedded in structural components for energy harvesting

Recent developments in materials science have enabled the integration of thermoelectric modules into structural components like concrete and bricks for energy harvesting. These innovations aim to capture waste heat and ambient energy, enhancing energy efficiency and sustainability in construction.

Energy-harvesting concrete

Energy-harvesting concrete uses mechanisms such as the Seebeck effect, pyroelectric effect, and piezoelectric effect to convert thermal, mechanical, and light energy into electricity. This allows concrete structures to generate energy autonomously, reducing reliance on external power sources. Functional fillers, such as carbon fibers and conductive polymers, are often added to improve the concrete's electrical conductivity and energy conversion efficiency.

Energy-storing bricks

Energy-storing bricks are designed to store renewable energy, such as solar power, and release it when needed. These bricks utilize a chemical process that converts pigments into conductive plastics, functioning as supercapacitors for quick energy storage and release. Some designs incorporate phase change materials (PCMs) to absorb and release heat, helping reduce building heating and cooling loads.

Thermoelectric modules in pavement

Thermoelectric modules have also been integrated into pavement for energy harvesting. These cement-based composites not only convert thermal gradients into electricity but also help lower surface temperatures, contributing to urban heat management. Adding conductive materials like carbon fibers improves the thermoelectric properties of the pavement, allowing cities to capture waste heat from vehicles and the environment.

Challenges and future directions

Maintaining the durability of embedded thermoelectric systems in structural components is crucial. Research is ongoing to develop materials that can withstand environmental stresses while maintaining performance. Effective integration techniques are needed to avoid compromising the structural integrity of concrete or bricks. Innovations such as 3D printing may help improve integration and reduce production costs. Scaling up production for large-scale applications while keeping costs manageable remains a challenge.

Advantages and challenges of embedding thermoelectric materials into structural elements

Embedding thermoelectric materials in structural components offers innovative solutions for energy harvesting but comes with several advantages and challenges.

Advantages

Thermoelectric materials can convert waste heat into electricity, enhancing energy efficiency and sustainability. Structures embedded with these materials can become self-sufficient, powering sensors, lighting, and electronic devices. Embedding thermoelectric materials allows traditional building elements to serve both structural and energy-generating functions. These systems can also enable smart building technologies, allowing for real-time monitoring of energy usage and structural health, improving operational efficiency. Additionally, thermoelectric materials can help manage urban heat by dissipating excess heat from structures, contributing to better local climate conditions. Their durability, when embedded in concrete or bricks, may lead to long-lasting energy-harvesting systems.

Challenges

The differing thermal expansion coefficients between thermoelectric materials and concrete or bricks may cause stress and cracking, compromising structural integrity. Ensuring thermoelectric materials remain stable in the alkaline environment of concrete is vital for long-term performance. Embedding these materials can be complex and costly, requiring advanced manufacturing techniques. Achieving uniform distribution within the composite matrix is challenging, and optimizing the thermoelectric performance while maintaining the mechanical properties of concrete or bricks is difficult. Effective energy harvesting requires maintaining temperature gradients, which necessitates adequate thermal insulation around the embedded modules. The high initial investment for integrating thermoelectric materials raises concerns about economic feasibility compared to traditional energy solutions. Evaluating the long-term benefits versus initial costs is essential for justifying their use in construction projects.

Studies on thermoelectric materials integrated into building materials for energy-efficient buildings

The integration of thermoelectric materials into building materials represents a significant advancement in the pursuit of energy-efficient buildings. This approach not only enhances energy recovery from waste heat but also contributes to the overall sustainability of building designs. Recent studies have highlighted various thermoelectric materials and their composites, demonstrating their potential to improve the ZT when incorporated into construction materials.

One of the key studies in this area is by Iyer, which emphasizes the importance of integrating thermoelectric systems within building structures rather than treating them as standalone entities. The research indicates that buildings account for a substantial portion of energy loss, primarily due to heat loss through their fabric and ventilation systems. By embedding thermoelectric materials into building components, it is possible to harness waste heat and convert it into usable electrical energy, thereby improving overall energy efficiency [48]. This integration can lead to significant reductions in energy consumption and operational costs.

Research on thermoelectric properties of geopolymer mortars, such as those doped with graphite powder, has also shown promising results. Hotěk's study indicates that the thermoelectric function of these materials can be enhanced through the addition of conductive admixtures, which improve the electrical conductivity and, consequently, the thermoelectric performance [49]. This finding supports the notion that building materials can be engineered to not only provide structural integrity but also to actively participate in energy generation. Moreover, the exploration of new thermoelectric materials, such as those discussed by Tan et al., highlights the ongoing advancements in material science aimed at improving thermoelectric efficiency. The study underscores the potential of novel materials to be implemented in thermoelectric modules specifically designed for power generation, which could be integrated into building systems [50]. This aligns with the broader goal of developing robust thermoelectric modules that can effectively convert thermal energy into electrical energy.

The concept of using thermoelectric materials in combination with traditional building materials is further supported by the work of Wang et al., who discuss the coordination of carriers and phonons in solids to achieve efficient thermoelectric conversion. Their findings suggest that optimizing the thermoelectric properties of these materials can significantly contribute to energy recovery in building applications [51]. This is particularly relevant as the construction industry seeks to adopt more sustainable practices. In addition to these advancements, the development of functionally graded materials, as explored by Ma et al., indicates that spatial variation in thermoelectric properties can enhance heat distribution and energy recovery in thermoelectric systems [52]. This approach can be particularly beneficial in building applications where temperature gradients are prevalent. Furthermore, the integration of thermoelectric devices into existing heating systems, as discussed by Xiao et al., demonstrates the potential for enhancing energy utilization efficiency in residential applications. By embedding thermoelectric generators into boilers or heating systems, it is possible to recover waste heat and convert it into electrical energy, thereby improving the overall energy efficiency of the building [53].

2.4.2 $CaMnO_3$ in multi-layer concrete brick modules

Potential benefits of such integration for energy efficiency in modern buildings

The integration of thermoelectric modules into structural elements, such as concrete and bricks, offers significant potential for improving energy efficiency in modern buildings. Thermoelectric modules can convert waste heat from sources like sunlight, HVAC systems, and human activity into electricity. This reduces dependence on external power sources and increases building energy self-sufficiency. By harnessing ambient thermal gradients, buildings can generate on-site clean energy to power lighting, sensors, and other devices. Thermoelectric materials also help regulate indoor temperatures by converting excess heat into electricity, reducing the load on heating and cooling systems and lowering energy consumption. Additionally, integrating thermoelectric modules can optimize HVAC operations by providing real-time data on temperature differentials for more efficient climate control. The use of thermoelectric modules supports the development of net-zero buildings, which produce as much energy as they consume. These embedded systems can complement other renewable

energy sources, like solar panels, to enhance overall energy efficiency and reduce reliance on fossil fuels. This multifunctionality allows concrete and bricks to provide structural support while also generating electricity, contributing to innovative and efficient building designs.

Integrating thermoelectric systems helps create smart buildings that dynamically monitor and adjust their energy use, improving occupant comfort and reducing waste. By generating renewable energy on-site and optimizing energy usage, such buildings contribute to lower greenhouse gas emissions. This approach aligns with sustainable construction practices by improving the lifecycle performance of building materials and reducing environmental impacts. Buildings equipped with integrated thermoelectric modules can also lower energy costs due to reduced reliance on grid electricity and optimized HVAC performance. These energy-efficient features can increase property value, attracting environmentally conscious buyers and tenants.

Experimental results or simulations involving concrete as a host for thermoelectric modules

The experimental results and simulations involving thermoelectric modules embedded in concrete highlight the significant potential for enhancing energy efficiency in building materials. Studies have demonstrated the feasibility of energy conversion from concrete, the performance characteristics of thermoelectric modules in concrete applications, and the potential for monitoring heat flow. These findings pave the way for further research and development of integrated thermoelectric systems in sustainable building designs. The integration of thermoelectric materials into concrete as a host for thermoelectric modules has been the focus of several experimental studies and simulations aimed at enhancing energy efficiency in building applications. This approach leverages the ability of thermoelectric materials to convert waste heat generated within concrete structures into usable electrical energy, thereby contributing to sustainable building practices.

One significant study by Félix-Herrán et al. explored the implementation of thermoelectric modules mounted on concrete structures. The research involved the electrical characterization of a commercially available thermoelectric module (TEC1-12710) embedded in a concrete slab. The results demonstrated the feasibility of energy

conversion from concrete using thermoelectric modules, highlighting the potential for integrating such systems into building materials to harness waste heat effectively [54]. This study provides a foundational understanding of how thermoelectric modules can operate within concrete, paving the way for further advancements in energy-efficient building designs. Murata et al. also contributed to this field by fabricating a prototype thermoelectric module that operates using the Nernst effect. Although their primary focus was on the Nernst effect, the findings provide insights into the performance characteristics of thermoelectric modules that could be adapted for integration into concrete structures [55]. The study emphasizes the importance of understanding the operational principles of thermoelectric modules, which can inform their application in building materials. Leephakpreeda's research further supports the integration of thermoelectric modules into concrete by experimentally determining the parameters of thermoelectric modules and modeling their performance for heating and cooling control. The study involved three thermoelectric modules with varying capacities, providing valuable data on their operational characteristics when embedded in concrete [56]. This information is crucial for optimizing the design and implementation of thermoelectric systems in building applications.

Additionally, the work of Sippawit and Leephakpreeda demonstrated the viability of using thermoelectric modules to detect heat flow through thermal walls. Their experimental studies showed that thermoelectric modules could effectively measure heat flow by observing the generated electric voltage, further supporting the potential for integrating these systems into concrete structures for energy monitoring and management [57].

2.5 FEM analysis in thermoelectric design

2.5.1 Overview of FEM in material science

The FEM is a widely used numerical technique for solving complex engineering and mathematical problems, often represented by partial differential equations. It is applied in various fields such as structural analysis, heat transfer, fluid dynamics, and electromagnetism. FEM divides a large system into smaller, manageable parts called

finite elements, a process known as discretization. These elements can be one-dimensional, two-dimensional, or three-dimensional, and are interconnected to form a mesh representing the entire domain. Each element behaves according to a set of equations that describe its response to various conditions like stress or heat. Material properties are defined at the nodes, where the elements are connected. The equations governing individual elements are assembled into a global system, which is then solved using numerical methods to approximate unknown variables, such as displacements or temperatures. Applying appropriate boundary conditions ensures that the simulation accurately reflects real-world constraints.

FEM offers high accuracy, even with relatively simple approximation functions, and allows for detailed visualization of complex behaviors. It is extensively used in structural analysis to predict stress distributions and deformation patterns, heat transfer to model temperature distributions, and electromagnetic simulations to study field propagation in materials. The method is also useful in understanding the mechanical behavior of materials and in solving multi-physics problems where different physical phenomena occur simultaneously.

Role of FEM in thermoelectric material design

FEM plays a key role in designing and analyzing thermoelectric materials by simulating their thermal and electrical behaviors. It allows for the optimization of material properties and provides insights into the interactions within thermoelectric systems.

Modeling heat transfer

FEM enables the simulation of temperature distributions in thermoelectric materials. For example, in thermoelectric concrete bricks embedded with $CaMnO_3$ modules, FEM predicts heat flow through various layers, helping to maximize the temperature gradient necessary for efficient energy conversion. These simulations can guide the selection of insulating materials and optimize structural designs for better thermal performance. Results are often validated against experimental data to ensure accuracy.

Modeling electrical conductivity

FEM is used to simulate electric field distributions within thermoelectric materials, allowing for the assessment of material composition and its effect on electrical conductivity. It also helps model electrical interface resistances between different materials, providing critical insights into current flow and voltage generation.

Thermoelectric properties simulation

FEM is instrumental in calculating the Seebeck coefficient by simulating how temperature gradients cause charge carrier movement. By integrating thermal and electrical conductivity models, FEM helps evaluate the power factor (PF) and identify materials with a high ZT for energy conversion. Advanced FEM simulations can couple thermal, electrical, and mechanical behaviors, offering a comprehensive view of material performance.

2.5.2 FEM studies on thermoelectric modules

Optimization strategies for improving thermoelectric module performance

Optimizing thermoelectric modules in real-world conditions requires careful consideration of material selection, structural design, and operational strategies. Recent studies have proposed several approaches to enhance thermoelectric device performance. One approach involves using high-entropy materials, like GeTe-based compounds, which exhibit optimized band structures and efficient electronic transport at elevated temperatures. Doping and alloying have been shown to improve thermoelectric performance, especially in the low-temperature range where intrinsic carrier concentration often limits efficiency.

Another strategy focuses on manipulating the electron mean free path (MFP) in Dirac materials to enhance thermoelectric performance through MFP filtering. This approach improves transport behaviors, increasing the overall efficiency of thermoelectric materials.

Doping strategies have also been effective in improving thermoelectric performance. Regulating free carrier concentration in organic semiconductors through doping has led to substantial improvements in thermoelectric response.

Structural innovations have further enhanced thermoelectric performance. For example, research on compliant and stretchable thermoelectric coils for energy harvesting in flexible devices has shown that improving packing efficiency and stacking designs can increase energy conversion efficiency.

Additionally, optimizing the mechanical properties of thermoelectric materials is crucial for practical applications. Introducing carbon materials to improve toughness while maintaining thermoelectric efficiency has shown promise for enhancing the durability of thermoelectric modules.

FEM has also been applied to optimize thermoelectric generator (TEG) designs, particularly for high-temperature environments like aviation. Effective heat transfer coefficients and optimized thermocouple configurations can maximize energy recovery from waste heat.

Moreover, studies on n-type PbS thermoelectric materials have demonstrated the potential of lattice expansion and interstitial doping to suppress thermal conductivity and enhance electrical performance, improving ZT values.

Finally, geometry optimization of thermoelectric modules is another critical factor for enhancing performance. Careful design considerations, such as optimized geometric structures, can significantly improve power output and conversion efficiency in thermoelectric systems.

Review of using FEM to optimize thermoelectric materials and module designs

The application of the FEM in optimizing thermoelectric materials and module designs has gained traction in recent years, particularly as researchers seek to enhance the efficiency and performance of thermoelectric devices. FEM provides a powerful numerical tool for simulating the thermal and electrical behaviors of thermoelectric materials and systems, allowing for the optimization of their geometrical and material properties.

One significant study by Sahu et al. emphasizes the importance of a bottom-up design approach for developing thermoelectric hybrid materials using chalcogenides. The authors utilized FEM to model the thermal and electrical properties

of these materials, demonstrating how structural modifications can lead to improved thermoelectric performance quantified by the ZT [58]. This study highlights the potential of FEM in guiding the design of new thermoelectric materials by predicting their performance based on various structural configurations. Lu et al. conducted a cooling and mechanical performance analysis of a trapezoidal thermoelectric cooler (TEC) using FEM. Their research focused on optimizing the geometry of the TEC to enhance its cooling performance while maintaining structural integrity. The results indicated that specific geometric configurations could significantly improve the conversion efficiency of the thermoelectric module, showcasing the utility of FEM in optimizing module designs for practical applications [59].

In another study, Hotěk explored the thermoelectric properties of geopolymer mortar doped with graphite powder. The research employed FEM to simulate the effects of doping on the thermoelectric performance of the composite material. The findings suggested that optimizing the doping concentration could lead to enhanced power factors, which are critical for improving the overall efficiency of thermoelectric systems [49]. This work illustrates how FEM can be used to optimize material compositions for better thermoelectric performance. Zhu et al. further demonstrated the application of FEM in the geometrical design and optimization of thermoelectric generators. Their study utilized artificial neural networks in conjunction with FEM to accurately predict the performance of thermoelectric generators based on various design parameters. This hybrid approach allowed for the identification of optimal geometrical configurations that maximize thermoelectric efficiency [60]. The integration of machine learning with FEM represents a promising direction for future research in thermoelectric optimization.

Kishore et al. employed FEM to conduct a Taguchi optimization of bismuth-telluride-based thermoelectric coolers. Their study analyzed a comprehensive set of parameters affecting the performance of thermoelectric modules, including material properties and operational conditions. The results indicated that FEM could effectively predict the performance of thermoelectric devices under varying conditions, providing valuable insights for optimizing module designs [61]. Additionally, Shittu et al. investigated the electrical and mechanical performance of a segmented solar

thermoelectric generator using FEM. Their numerical study focused on the impact of non-uniform heat flux on the thermoelectric performance and mechanical reliability of the generator. The results demonstrated that FEM could be used to optimize the design of thermoelectric generators for enhanced performance and longevity [62].

2.5.3 Application of FEM for $CaMnO_3$ and multi-layer concrete brick modules

Using FEM to simulate thermoelectric performance of n-type $CaMnO_3$ in multi-layer concrete bricks

FEM is a powerful tool for simulating and optimizing the thermoelectric performance of materials like n-type $CaMnO_3$ embedded within multi-layer concrete bricks. FEM enables detailed analysis of heat transfer, electrical conductivity, and overall thermoelectric efficiency under various conditions.

Modeling thermal distribution

FEM can simulate thermal distribution within multi-layer concrete bricks containing $CaMnO_3$ modules. By modeling different configurations (such as I-layer and III-layer bricks), it is possible to evaluate how thermal insulation affects temperature gradients across the thermoelectric module. These simulations incorporate boundary conditions that reflect real-world scenarios, such as ambient temperature changes and heat sources. For example, simulations have shown that III-layer bricks maintain a larger temperature difference (up to 172°C) compared to simpler configurations.

Electrical conductivity simulation

FEM allows for the simulation of electrical current flow through the n-type $CaMnO_3$ module when exposed to thermal gradients. This includes modeling how changes in load resistance affect output voltage and power generation. It also accounts for electrical interface resistances between the $CaMnO_3$ module and the surrounding concrete, providing critical insights into overall electrical performance.

Thermoelectric properties assessment

FEM is useful for modeling the Seebeck coefficient and power factor of n-type $CaMnO_3$ under different temperature conditions. By simulating various temperature

ranges (e.g., 300 K to 600 K), researchers can predict how these properties evolve and adjust material composition for improved thermoelectric performance. For instance, FEM can predict output voltage for different operational conditions, and studies show that III-layer brick configurations produce higher output voltages than I-layer bricks due to better thermal management.

Experimental validation

FEM simulations are typically validated against experimental results to ensure accuracy. Studies have shown a good agreement between simulated and measured temperature differences and output voltages in different configurations of thermoelectric concrete bricks. This iterative process helps refine material properties and configurations based on predicted performance.

Multi-physics simulations

Advanced FEM simulations can couple thermal and electrical behaviors, providing a holistic view of thermoelectric systems. This approach helps in understanding the interactions between heat transfer and electrical conduction, enabling researchers to optimize material properties and geometric configurations for maximum efficiency.

Challenges in FEM simulations: material heterogeneity and boundary conditions

While FEM is highly effective, it faces challenges, especially when simulating heterogeneous materials and establishing boundary conditions. Heterogeneous materials, such as composites or polycrystalline substances, have varying properties at the microstructural level, making it difficult to predict their macroscopic behavior. Factors like grain size and morphology influence the overall material response, requiring detailed microstructural modeling. High-resolution models are often needed, which increases computational costs and simulation time. Creating accurate meshes for FEM simulations of heterogeneous materials is time-consuming and prone to convergence issues due to discontinuities in material properties. Techniques like using tomographic images can help but add complexity to the mesh generation process.

Establishing proper boundary conditions is essential for accurate simulation results. Inaccurate or overly simplistic boundary conditions can introduce significant errors. For example, periodic boundary conditions may not always be suitable for non-periodic microstructures. Recent advancements, such as soft periodic boundary conditions, aim to improve realism, but they are complex and require careful calibration. In multi-scale simulations, linking boundary conditions between macro and micro scales is challenging, as the macroscopic model must accurately reflect the microscopic behavior.

Studies for FEM analysis of thermoelectric materials in structural applications

The optimization of thermoelectric materials and modules through FEM analysis is a critical area of research that enhances the performance of thermoelectric devices in structural applications. FEM provides a robust framework for simulating the thermal, electrical, and mechanical behaviors of thermoelectric materials, allowing for the identification of optimal designs and configurations.

One significant application of FEM in thermoelectric materials is illustrated in the work by Ziółkowski et al., who studied the design of thermoelectric generators (TEGs) for waste heat recovery in aviation applications. Their research utilized FEM to model the thermal and electrical performance of TEGs integrated into jet engine nozzles. By applying computational fluid dynamics (CFD) results as boundary conditions, they were able to simulate various thermocouple configurations and optimize the heat transfer coefficients, thereby enhancing the efficiency of the thermoelectric modules [63]. This study exemplifies how FEM can be employed to refine the design of thermoelectric systems in real-world applications.

In another study, Zhang and Wang conducted FEM analysis on the temperature and electric potential fields of interface cracks in layered thermoelectric materials. Their research focused on the nonlinear fully coupled thermoelectric behavior, incorporating factors such as Joule heating, Fourier's heat conduction, and the Peltier effect. The findings highlighted the importance of understanding the interactions between thermal and electrical fields in optimizing thermoelectric materials for structural applications [15]. This approach underscores the versatility of FEM in addressing complex thermoelectric phenomena. Wolf et al. explored the geometric

optimization of thermoelectric modules using FEM simulations. Their study compared different module designs to assess the impact of geometric configurations on power output and conversion efficiency. By analyzing the thermoelectric parameters of various materials, they demonstrated that careful design considerations could lead to significant improvements in thermoelectric performance [64]. This research illustrates the potential of FEM to guide the engineering of thermoelectric modules for enhanced functionality.

Additionally, the work by Zhu introduced a nonlocal numerical simulation approach to analyze thermoelectric coupling fields. This method provides a mathematical framework for understanding the intrinsic relationships between material parameters and output properties, facilitating the performance analysis of thermoelectric structures [65]. Such advanced modeling techniques can offer deeper insights into the optimization of thermoelectric materials. The optimization of thermoelectric materials through structural modifications is further supported by the findings of Qian et al., who investigated the effects of material anisotropy on the transverse thermoelectricity of layered composites. Their study utilized FEM to analyze how anisotropic properties could enhance thermoelectric performance, particularly in applications where decoupling electric current and heat flux is advantageous [66]. This highlights the role of FEM in exploring new material configurations for improved thermoelectric efficiency. Moreover, the research conducted by Jiang et al. examined the effects of hole and crack geometries on the multi-field behaviors of thermoelectric materials under oblique loads. Their FEM simulations provided valuable insights into how structural defects influence thermoelectric performance, emphasizing the importance of considering mechanical stresses in the design of modules [67].

2.6 Synthesis and characterization techniques for thermoelectric materials

2.6.1 Solid-state reaction techniques

Overview of solid-state reaction methods

Solid-state reaction methods are commonly used for synthesizing thermoelectric materials due to their ability to produce high-purity compounds with controlled stoichiometry. One such technique, 3D ball milling, has gained attention for preparing fine powders, which can enhance thermoelectric performance. Solid-state reactions involve reacting solid precursors at elevated temperatures to form the desired compound. Precursors like metal oxides or carbonates are mixed in stoichiometric ratios and heated to promote chemical reactions and phase formation. Precise temperature control is essential to prevent unwanted phase changes.

3D ball milling

3D ball milling involves rotating a chamber filled with grinding media and materials to reduce particle size and improve homogeneity. This process helps distribute precursor materials uniformly, which is critical for consistent thermoelectric properties. Adjusting milling time and conditions optimizes the microstructure and composition for better performance.

Applications in thermoelectric materials

For example, magnesium silicide (Mg_2Si) powders have been synthesized through ball milling and thermal annealing under inert conditions, enhancing thermoelectric performance. Similarly, Bi_2Te_3-based thermoelectric materials, prepared via solid-state methods combined with selective laser melting, exhibit improved mechanical properties while retaining favorable thermoelectric characteristics.

Challenges and considerations

Maintaining the correct temperature profile during calcination is crucial, as excessive heat may cause undesired phase changes or degradation. Particle size variability can affect thermoelectric performance, and while techniques like ball milling help mitigate these issues, they require careful optimization. Scaling up these processes for industrial use presents additional challenges related to consistency and cost.

Factors affecting material synthesis

Temperature plays a key role in solid-state reactions by influencing reaction rates and phase formation. Higher temperatures can increase reaction efficiency, but must be controlled to prevent unwanted transformations. For instance, specific annealing temperatures are required for phase formation in materials like magnesium silicide (Mg_2Si). Applying pressure during synthesis can enhance material densification and improve thermoelectric properties. However, the increased energy requirements and safety concerns associated with high-pressure environments must be considered. Longer milling times typically result in smaller particles and better mixing. However, excessive milling can introduce defects or amorphization. Studies indicate that optimal milling durations depend on the material; for example, magnesium and silicon powders showed reduced grain sizes after milling, with thermal annealing required for phase formation. Precise control over reactant ratios is essential for achieving desired thermoelectric properties. Incorrect ratios can result in phase segregation or incomplete reactions, leading to heterogeneous microstructures that negatively affect material performance.

2.6.2 Characterization techniques

X-ray diffraction (XRD) is widely used to identify crystal structures and assess phase purity in thermoelectric materials. By analyzing diffraction patterns, researchers can determine crystallographic phases, lattice parameters, and detect impurities that may degrade performance. XRD is also crucial for tracking phase stability under varying temperatures.

Scanning electron microscopy (SEM) provides high-resolution images of material morphology, allowing researchers to observe grain boundaries, surface roughness, and defects. SEM is also used for particle size analysis, providing insights into how particle size and distribution influence thermoelectric properties.

Raman spectroscopy is essential for identifying and evaluating the quality of rGO in composites. Characteristic peaks, such as the G and D bands, indicate the degree of reduction and defect levels. This technique helps researchers optimize the structural and electronic properties of rGO for improved thermoelectric performance.

UV-Visible spectroscopy measures the absorbance of materials to evaluate optical properties, band gaps, and defect states. It is particularly useful for determining band gaps in thermoelectric materials, which are critical for optimizing electronic properties and enhancing performance.

2.6.3 Measurement of thermoelectric properties

Key thermoelectric properties include electrical conductivity, the Seebeck coefficient, and thermal conductivity. These properties are essential for evaluating a material's overall thermoelectric performance. The Four-probe method and Van der Pauw method are common techniques for measuring electrical conductivity. Both minimize contact resistance and provide accurate measurements, which are typically assessed as a function of temperature. The Seebeck coefficient is measured by creating a temperature gradient across a sample and recording the resulting thermoelectric voltage. The relationship between voltage and temperature difference is used to calculate the Seebeck coefficient, which is crucial for understanding the material's energy conversion efficiency. The laser flash technique measures thermal diffusivity by recording temperature rise after a short laser pulse. Thermal conductivity is then calculated using thermal diffusivity, density, and specific heat capacity. The Gustafsson probe method and steady-state methods are also used to assess thermal conductivity.

Challenges in measuring thermoelectric properties of $CaMnO_3$ and $C_{12}A_7$-rGO composites

Accurately measuring thermoelectric properties, especially in materials like $CaMnO_3$ and $C_{12}A_7$-rGO composites, presents several challenges. For $CaMnO_3$, low electrical conductivity and high thermal conductivity complicate measurements, making it difficult to isolate thermoelectric performance. Strategies like optimizing dopants and using controlled synthesis conditions can improve consistency and performance. For $C_{12}A_7$-rGO composites, achieving a uniform distribution of rGO is critical. Agglomeration can lead to uneven properties, affecting thermoelectric measurements. Advanced mixing techniques and multiple characterization methods can help ensure uniformity and improve measurement accuracy.

Review of experimental setups for assessing thermoelectric performance of $CaMnO_3$ and $C_{12}A_7$-rGO composites

The assessment of thermoelectric performance in materials such as $CaMnO_3$ and $C_{12}A_7$-rGO composites requires sophisticated experimental setups that can accurately measure key thermoelectric properties, including electrical conductivity, Seebeck coefficient, and thermal conductivity. Various methodologies have been developed to facilitate these measurements, each with its own advantages and limitations. For the evaluation of thermoelectric properties, the four-probe method is commonly employed. This technique allows for the precise measurement of electrical conductivity by minimizing contact resistance, which is critical for accurate results. For instance, Dobosz et al. utilized a specialized crucible design that enabled simultaneous measurement of electrical conductivity and thermoelectric power in a controlled argon atmosphere, demonstrating the effectiveness of this approach in obtaining reliable data on thermophysical properties [68]. Such setups are essential for materials like $CaMnO_3$, where the electrical properties can be significantly influenced by factors such as temperature and phase transitions.

In the case of $C_{12}A_7$-rGO composites, the experimental setup often involves the synthesis of the composite followed by characterization using techniques such as X-ray photoelectron spectroscopy (XPS) and Raman spectroscopy to confirm the presence of reduced graphene oxide and its interaction with the $C_{12}A_7$ matrix. Khan et al. highlighted the importance of XPS in confirming the chemical composition and the stability of oxygenated functional groups in the rGO layer, which can affect the thermoelectric properties of the composite [69]. This characterization is crucial for understanding how the integration of rGO influences the overall thermoelectric performance. Moreover, the thermoelectric performance can be further enhanced by optimizing the microstructure of the composites. Techniques such as high-energy ball milling can be employed to achieve a uniform distribution of rGO within the $C_{12}A_7$ matrix, which can lead to improved electrical conductivity and reduced thermal conductivity through enhanced phonon scattering. This method has been shown to facilitate the formation of solid solutions and improve densification during subsequent sintering processes, ultimately contributing to better thermoelectric performance.

Another innovative approach involves the use of field-effect setups, which allow for the tuning of thermoelectric properties through reversible doping. Although primarily demonstrated in materials like SnSe2, the principles can be adapted for other thermoelectric materials, including $C_{12}A_7$-rGO composites. This method enables researchers to explore the effects of carrier concentration on thermoelectric performance in real-time, providing valuable insights into the optimization of composite materials [70].

2.7 Summary of key insights from the literature

2.7.1 Critical analysis of research trends

The literature reveals significant progress in the development and integration of thermoelectric materials, particularly focused on n-type $CaMnO_3$ modules in structural materials like concrete bricks, and $C_{12}A_7$-rGO composites with ultra-high rGO content. These materials have been shown to improve thermoelectric performance when appropriately optimized.

Research has explored various doping strategies, such as Nb and Sr, to enhance the Seebeck coefficient and electrical conductivity in $CaMnO_3$. The material's high thermal stability and low thermal conductivity make it a candidate for thermoelectric modules in energy-harvesting systems integrated within concrete. However, challenges related to achieving a high ZT value still remain, necessitating further optimization of doping methods and synthesis techniques, including sol-gel and co-precipitation methods. Studies have demonstrated that incorporating rGO into $C_{12}A_7$ improves electrical conductivity and overall thermoelectric performance. The key challenge lies in achieving uniform distribution and preventing agglomeration of rGO within the composite. While higher rGO content is known to enhance thermoelectric properties, ultra-high concentrations pose stability challenges and can negatively impact material homogeneity and mechanical strength. Advanced synthesis techniques, including 3D ball milling and hybrid processing methods, are being explored to address these issues.

FEM simulations have been extensively used to model the thermal and electrical behavior of thermoelectric systems, particularly in multi-layer concrete bricks

embedded with $CaMnO_3$ modules. These models assist in understanding heat transfer, temperature gradients, and electrical output within structural materials, providing insights for optimizing material configurations to improve energy conversion efficiency in building applications.

Gaps in existing research

While rGO has shown promise in enhancing thermoelectric properties, there is a gap in understanding how ultra-high rGO content affects long-term stability and uniformity in $C_{12}A_7$ composites. Agglomeration and inconsistent dispersion are recurring issues, which need to be further studied to achieve better material performance. Despite promising results from the integration of thermoelectric modules into concrete bricks, more research is needed to assess their long-term durability and performance under environmental stressors, such as temperature fluctuations and mechanical loads, typical in real-world construction environments.

Opportunities for further research

The combination of ultra-high rGO content in $C_{12}A_7$ and optimized multi-layer configurations of n-type $CaMnO_3$ in concrete bricks presents a unique opportunity to significantly enhance thermoelectric conversion efficiency. Research can explore hybrid materials and innovative configurations that improve electrical conductivity while maintaining structural integrity. Extending FEM simulations to multi-physics environments can help predict more complex interactions between thermal, electrical, and mechanical properties. This would aid in developing more efficient thermoelectric systems, especially those embedded in structural applications, where material behavior is affected by various real-world factors.

2.7.2 Relevance to the thesis study

The literature aligns well with the objectives of the current research, which focuses on enhancing thermoelectric conversion efficiency through the development of n-type $CaMnO_3$ modules in multi-layer concrete bricks and ultra-high rGO content in $C_{12}A_7$ composites. Both materials show significant promise for improving energy efficiency in modern construction and thermoelectric systems. The current study builds upon the existing body of research by specifically addressing the gaps in understanding related to ultra-high rGO content in $C_{12}A_7$ and the practical integration of $CaMnO_3$

thermoelectric modules within structural elements like concrete bricks. By using FEM modeling to optimize both material composition and structural integration, this research provides a novel approach to improving thermoelectric conversion efficiency in sustainable building applications. This will contribute to advancing the application of thermoelectric materials in real-world scenarios, such as energy-harvesting buildings and smart infrastructure.

Current chapter provided a detailed review of thermoelectric materials, focusing on the Seebeck and Peltier effects, ZT, and the advancements in n-type $CaMnO_3$ and $C_{12}A_7$-rGO composites. We also explored the methods used to enhance the thermoelectric efficiency of these materials, including doping and nano-structuring techniques. This foundation is essential as it frames the motivation for developing more efficient thermoelectric devices. In the following chapter, we will transition from theory and literature review to the practical aspects of material synthesis and characterization. Chapter three will focus on the methods used to synthesize ultra-high rGO content $C_{12}A_7$ composites and n-type $CaMnO_3$. Through detailed analysis, we will explore how different synthesis techniques, such as solid-state reactions and ball milling, contribute to optimizing thermoelectric properties. Additionally, we will present the characterization methods employed to assess the structural and electrical properties of these materials, laying the groundwork for their application in energy conversion devices

Chapter 3

Materials and methodology

3.1 Synthesis of thermoelectric materials

The synthesis of thermoelectric materials for this study includes two distinct systems: the n-type $CaMnO_3$ for multilayer thermoelectric concrete brick applications and $C_{12}A_7$-rGO composites with ultra-high rGO content. The goal is to enhance the thermoelectric conversion efficiency by integrating these materials into devices that can capture and convert heat into electricity. Thermoelectric materials work by exploiting the Seebeck effect, where a temperature gradient generates a voltage difference. To improve performance, the materials must have a high Seebeck coefficient, low thermal conductivity, and optimized electrical conductivity. The chosen materials—$CaMnO_3$, known for its perovskite structure, and $C_{12}A_7$ doped with rGO—offer promising thermoelectric properties. The $CaMnO_3$ system is ideal for high-temperature applications due to its thermal stability, while $C_{12}A_7$-rGO composites are expected to enhance electrical conductivity and reduce thermal conductivity through the introduction of rGO. The synthesis methodologies adopted in this study focus on solid-state reaction techniques, with careful attention to the composition, mixing methods, and heat treatment processes to ensure the successful formation of the desired phases and properties.

3.1.1 Synthesis of $C_{12}A_7$ and ultra-high rGO content $C_{12}A_7$-rGO composites

The C12A7 and ultra-high rGO content $C_{12}A_7$-rGO composites were synthesized using the solid-state reaction method. The starting materials to synthesize $C_{12}A_7$, calcium carbonate ($CaCO_3$) and alumina powder (Al_2O_3), were procured from Sigma Aldrich with 98% purity. These materials were mixed in a 12:7 molar ratio to achieve the required stoichiometry for $C_{12}A_7$ formation. The mixing process was carried out in a ball milling machine for 24 hours at 300 rpm to ensure a homogeneous distribution of the reactants. The uniformity of the mixture is crucial because it leads to consistent and complete reactions during the calcination process. After mixing, the powders were

calcined at 1623 K for 3 hours in an ambient air atmosphere. This high-temperature calcination step facilitates the formation of the $C_{12}A_7$ phase by allowing the calcium carbonate and alumina to react fully. **Table 3.1** displays flowchart of the $C_{12}A_7$ synthesizing process

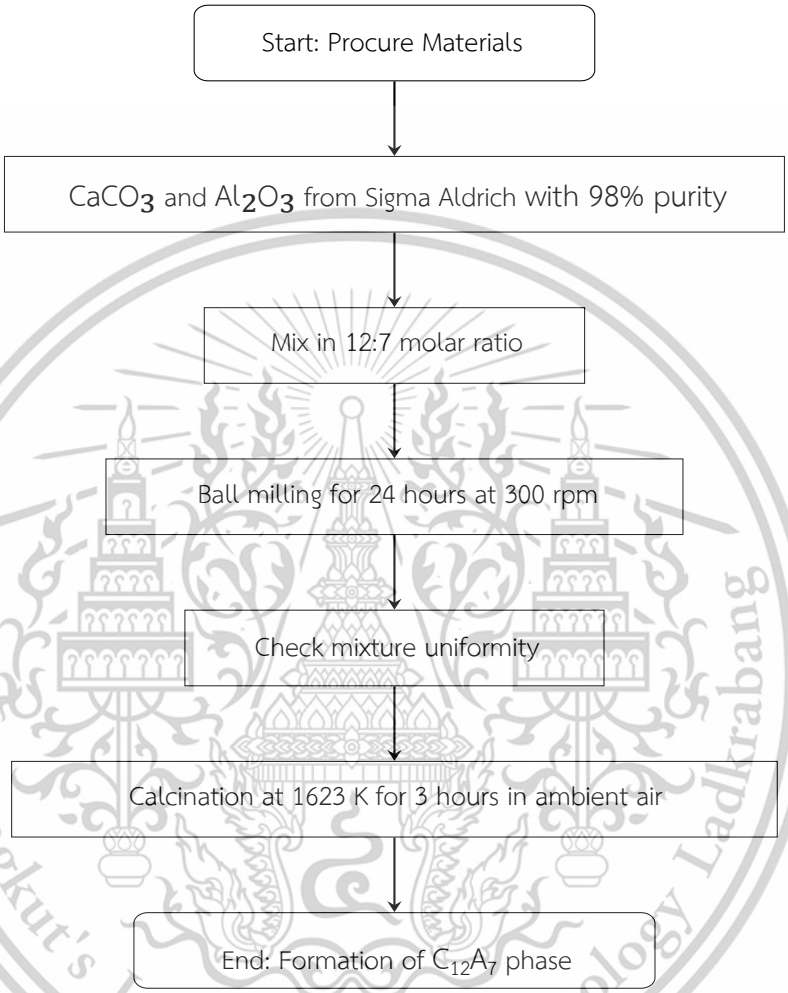

Figure 3.1 Flowchart of the $C_{12}A_7$ synthesizing process

Once the pure $C_{12}A_7$ phase was obtained, the powder was further processed to create the $C_{12}A_7$-rGO composites. **Figure 3.2** displays flowchart of the $C_{12}A_7$-rGO composites synthesizing process. Reduced graphene oxide (rGO) was introduced into the $C_{12}A_7$ matrix in varying weight percentages (40%, 50%, 60%, and 70%) to assess the impact of rGO content on the composite's thermoelectric properties. The mixing of rGO with $C_{12}A_7$ was again performed using a 3D ball milling machine, with the rotation speed set at 300 rpm for 24 hours. **Figure 3.3** displays 3D ball milling reactor (Nagao

system inc.). The prolonged mixing time ensured the uniform dispersion of rGO within the $C_{12}A_7$ matrix, which is vital for improving electrical conductivity by creating conductive pathways within the composite.

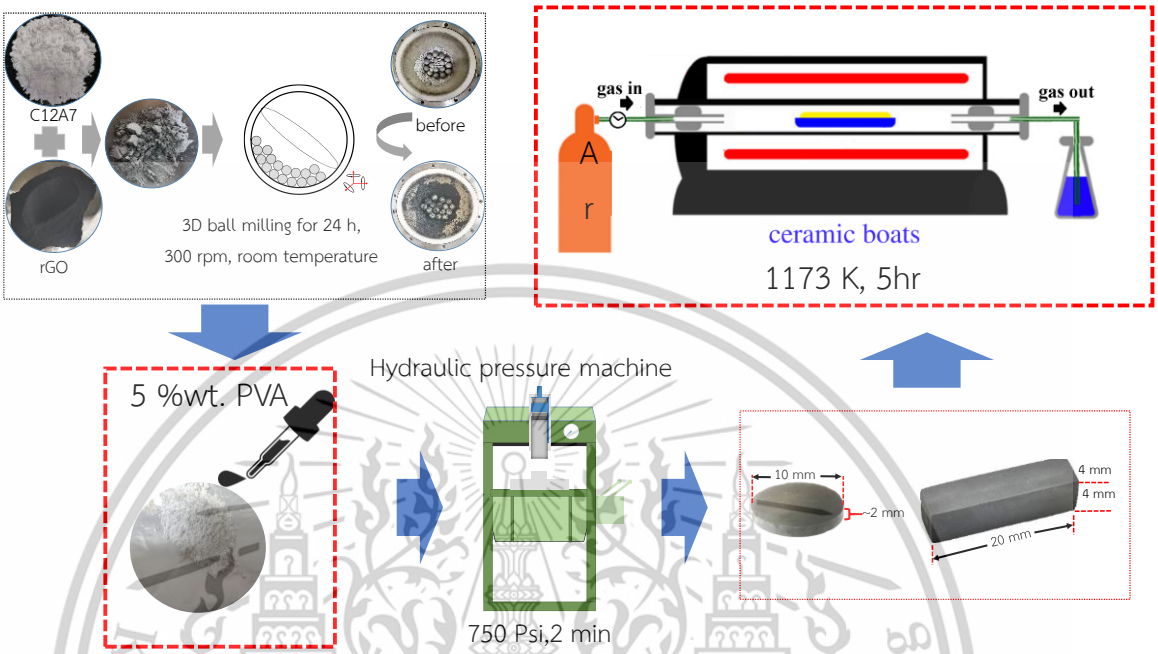

Figure 3.2 Flowchart of the $C_{12}A_7$-rGO composites synthesizing process

The resulting powder was then compressed into specific shapes, including rectangular rods (5 mm × 5 mm × 20 mm) and circular pellets (10 mm in diameter and 2 mm in height), using a hydraulic press with a uniaxial pressure of 5000 kPa. This pressing step is essential to achieve a high density in the final composite, which directly influences its thermoelectric performance. Following compression, the pellets were subjected to heat treatment at 773 K for 30 minutes under an argon atmosphere. The controlled atmosphere and heat treatment improve the structural integrity of the composite and ensure the proper interaction between $C_{12}A_7$ and rGO. The incorporation of rGO is expected to enhance the electrical properties by providing additional charge carriers, while the overall structure is optimized to minimize thermal conductivity by scattering phonons at the grain boundaries.

Figure 3.3 3D ball milling reactor

3.1.2 Synthesis of n-type $CaMnO_3$

The synthesis of n-type $CaMnO_3$ was performed using a solid-state reaction method, known for producing high-quality ceramic materials. The starting materials for $CaMnO_3$ synthesis were calcium carbonate ($CaCO_3$, 99% purity) and manganese dioxide (MnO_2, 99% purity), both sourced from Sigma Aldrich. These materials were weighed in stoichiometric amounts and mixed using a ball milling technique for 12 hours. This extended mixing period ensured a uniform blend of the reactants, which is critical for achieving the desired perovskite phase of $CaMnO_3$ during the subsequent sintering process. After the mixing step, the powder was compacted into cylindrical rods, with dimensions of 1.0 cm in diameter and 2.0 cm in height, using a semi-autonomous hydraulic press. The compacted rods were then sintered in an electric furnace at 1373 K for 12 hours. This high-temperature sintering process allowed the reactants to fully convert into the perovskite structure of $CaMnO_3$, which is crucial for its thermoelectric properties. The sintering process also densified the material, reducing the porosity and improving the electrical conductivity of the $CaMnO_3$ rods. The phase formation of $CaMnO_3$ was confirmed using X-ray diffraction (XRD), with the diffraction patterns matching the standard JCPDS reference file for perovskite $CaMnO_3$. Additionally, scanning electron microscopy (SEM) was used to examine the grain structure of the sintered $CaMnO_3$ rods, and energy-dispersive X-ray spectroscopy (EDS) confirmed the homogeneous distribution of calcium, manganese, and oxygen atoms within the material. **Figure 3.4** displays flowchart of the $CaMnO_3$ synthesizing process.

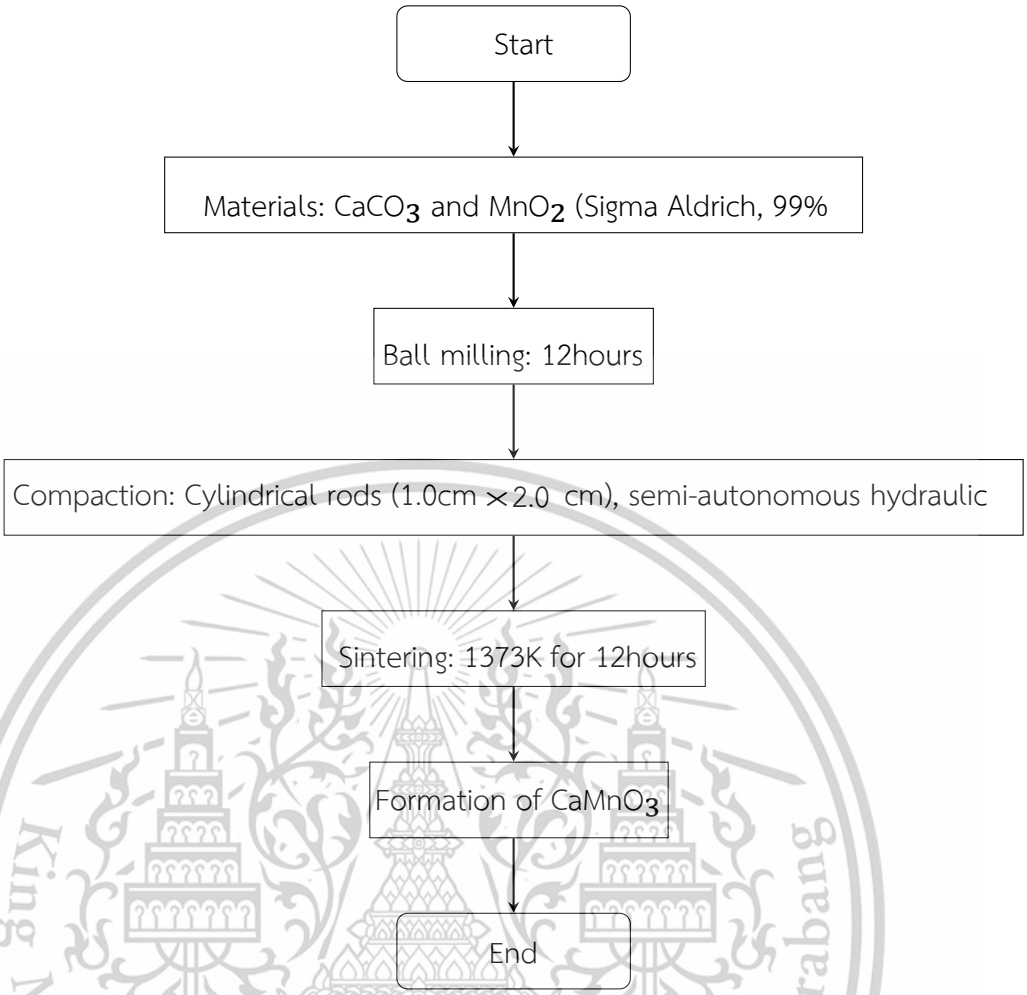

Figure 3.4 Flowchart of the $CaMnO_3$ synthesizing process

Figure 3.5 $CaMnO_3$ synthesizing process

The sintered $CaMnO_3$ rods were then incorporated into a unileg thermoelectric module. **Figure 3.5** displays the $CaMnO_3$ synthesizing process [71]. This module design simplifies the manufacturing process by using only n-type material, reducing the number of joining points and minimizing thermal expansion mismatch during operation. The $CaMnO_3$ rods were embedded in thermally insulating concrete bricks, which were fabricated with multiple layers of insulation to enhance the temperature difference across the thermoelectric module, thereby improving its efficiency. To optimize the thermoelectric performance of the $CaMnO_3$ modules, the thermoelectric concrete bricks were designed with different insulation layers. The I-layer brick consisted of a single layer of thermal insulation, while the III-layer brick incorporated three layers of different insulating materials to further reduce heat loss and increase the temperature gradient. This multi-layer design was optimized using FEM simulations to model the thermal and electrical behavior of the modules under various operating conditions.

3.2 Characterization of $C_{12}A_7$, $C_{12}A_7$-rGO composites, and $CaMnO_3$

Characterization of the synthesized $C_{12}A_7$-rGO composites included X-ray diffraction (XRD) to confirm the formation of the $C_{12}A_7$ phase and to identify the presence of rGO. The crystallite sizes of the composites were calculated using Scherrer's equation, revealing sizes in the range of 43.6 to 47.9 nm, depending on the rGO content. Scanning electron microscopy (SEM) and energy-dispersive X-ray spectroscopy (EDS) were used to assess the morphology and distribution of rGO in the matrix, ensuring a uniform dispersion essential for the composite's enhanced thermoelectric properties.

3.2.1 XRD

XRD is a powerful technique widely used to identify crystalline structures, phase purity, and lattice parameters of materials. When X-rays interact with a crystalline material, they are scattered in specific directions, producing diffraction patterns that are characteristic of the material's atomic structure. By analyzing these diffraction patterns, one can determine the crystal structure, identify different phases present in the sample, and measure lattice parameters. In thermoelectric materials like $CaMnO_3$ and composites like $C_{12}A_7$-rGO, XRD plays a crucial role in confirming the successful

synthesis of the desired crystalline phases, ensuring phase purity, and detecting any secondary phases or impurities that may affect thermoelectric properties.

The XRD measurements were conducted using a Rigaku Miniflex X-ray diffractometer with Cu Kα radiation (λ = 1.5406 Å). The samples were scanned over a 2θ range of 10° to 80°, with a step size of 0.02° and a scan rate of 2°/min. These parameters are optimized for accurately detecting the crystalline phases in both CaMnO3 and $C_{12}A_7$-rGO composites. In the case of the $C_{12}A_7$-rGO composites, care was taken to ensure uniform sample preparation to minimize any surface roughness, which could affect the diffraction results. The XRD setup provided high-resolution patterns essential for detecting both major and minor phases within the synthesized materials.

The expected outcome of the XRD analysis was to confirm the successful synthesis of the crystalline phases for both $CaMnO_3$ and $C_{12}A_7$-rGO composites. For CaMnO3, the characteristic peaks of the perovskite structure were expected, along with calculated lattice parameters matching those reported in the literature. For the $C_{12}A_7$-rGO composites, the presence of the cubic $C_{12}A_7$ phase, along with the broad peak indicating the rGO content, was anticipated. Additionally, the analysis aimed to detect any secondary phases or impurities, which could arise due to incomplete reactions or agglomeration of rGO. Identifying these factors is crucial, as they can significantly affect the thermoelectric performance of the materials. The Rietveld refinement process was also expected to provide precise values for lattice strain and crystallite size, which are important for understanding the microstructural characteristics of the materials and their impact on thermoelectric efficiency.

3.2.2 Scanning electron microscopy (SEM)

Scanning Electron Microscopy (SEM) is an essential technique for imaging the surface morphology of materials at high magnifications and resolutions. SEM provides detailed information about the shape, size, and distribution of particles, as well as the grain boundaries, which are critical for understanding the material's physical and electrical properties. For thermoelectric materials, SEM aids in analyzing the homogeneity of the composite and the interaction between different phases, such as $C_{12}A_7$ and rGO in $C_{12}A_7$-rGO composites.

The SEM analysis was carried out using a JEOL SEM JSM-5800 LV system to observe the surface morphology and particle size of the $C_{12}A_7$, $C_{12}A_7$-rGO composites, and $CaMnO_3$ samples. The SEM operated at an acceleration voltage of 15 kV, providing images with high resolution and magnification. The samples were coated with a thin layer of gold to ensure conductivity and improve the image quality. The $C_{12}A_7$-rGO composites were prepared in various rGO content configurations (40%, 50%, 60%, and 70% by weight), while $CaMnO_3$ was analyzed in its sintered form after the solid-state reaction.

The SEM characterization provided crucial insights into the morphological properties of the synthesized materials. For $C_{12}A_7$-rGO composites, the uniform wrapping of rGO around $C_{12}A_7$ grains is expected to enhance electrical conductivity while reducing thermal conductivity due to phonon scattering at grain boundaries. The agglomerated rGO content observed at higher rGO loadings may improve electrical pathways, although it could also increase thermal conductivity. For $CaMnO_3$, the grain size and uniform elemental distribution suggest that the material will exhibit stable thermoelectric properties, making it a promising candidate for high-temperature thermoelectric devices.

3.2.3 Raman spectroscopy

Raman Spectroscopy was employed to investigate the vibrational modes, bonding characteristics, and structural properties of $C_{12}A_7$, $C_{12}A_7$-rGO composites, and $CaMnO_3$. This technique allows for the identification of molecular interactions and crystalline phases, providing crucial insights into the quality of the synthesized materials, particularly the rGO content and bonding environment in $C_{12}A_7$-based composites.

Raman spectroscopy is a non-destructive technique used to study vibrational, rotational, and other low-frequency modes in materials. It is highly effective in identifying specific bonding characteristics and defects in graphene-based materials like rGO. The D-band (associated with disordered carbon atoms) and the G-band (indicative of sp^2 carbon bonding) are key features in rGO characterization. For $C_{12}A_7$-rGO composites, Raman spectroscopy helps confirm the presence of rGO and assess the

extent of reduction. In the case of $CaMnO_3$, Raman spectra can provide information about its perovskite structure and lattice vibrational modes.

The Raman spectra of the synthesized materials were recorded using a Thermo Fisher DXR Smart Raman spectrometer with a laser wavelength of 532 nm. The laser power was set at 10 mW to avoid sample damage, and the spectral range spanned from 200 to 2000 cm^{-1}. Samples were prepared by pressing the powder into small pellets to ensure uniform laser interaction with the material surface. For $C_{12}A_7$-rGO composites, the focus was on identifying the characteristic D and G bands of rGO, while for $CaMnO_3$, attention was given to the characteristic vibrational modes of the perovskite structure.

Raman spectroscopy confirmed the successful incorporation of rGO into the $C_{12}A_7$ matrix. The intensity ratio of the D-band to G-band (ID/IG) provided valuable information about the quality of rGO in the composites. A consistent ID/IG ratio across the samples suggests uniform rGO content and a stable reduction process during synthesis. Additionally, the absence of significant peaks in the 700–800 cm^{-1} range for the $C_{12}A_7$-rGO composites indicates that the introduction of rGO influenced the oxygen ion framework in the $C_{12}A_7$ structure. For $CaMnO_3$, the Raman spectra verified the structural integrity of the synthesized material, confirming the retention of the perovskite structure after processing. This suggests that the material's vibrational properties, which are critical for its thermoelectric behavior, were preserved.

3.2.4 UV-VIS Spectroscopy

UV-VIS spectroscopy is an analytical technique used to study the optical properties of materials by measuring the absorption of ultraviolet and visible light across a range of wavelengths. This method helps in determining the electronic transitions within a material and is particularly useful for analyzing the band gap of semiconductor and composite materials. The band gap energy, which separates the valence band from the conduction band, is crucial in defining the electronic and optical properties of materials. For thermoelectric materials such as $C_{12}A_7$, $C_{12}A_7$-rGO composites, and $CaMnO_3$, the band gap directly influences the material's electrical conductivity and Seebeck coefficient, both of which are critical for improving thermoelectric performance.

The UV-VIS spectra for the $C_{12}A_7$ and $C_{12}A_7$-rGO composites were obtained using a Shimadzu model UV-2600 spectrometer. The measurement was performed in the wavelength range of 200 to 800 nm at room temperature. Samples were prepared by compressing the synthesized powders into thin circular pellets with a diameter of approximately 10 mm. Each pellet was mounted on a quartz holder for measurement to ensure that the UV light passed uniformly through the sample.

For $CaMnO_3$, the sample preparation followed a similar procedure, with the pellets being sintered to increase the material's density. The absorbance spectra were measured over the same wavelength range, with careful attention to the peaks that indicate electronic transitions within the material. The experimental setup ensured that the measurement conditions were consistent for both material systems.

The UV-VIS spectroscopy analysis provided essential insights into the electronic structure of the synthesized materials. The decrease in the direct and indirect band gaps of the $C_{12}A_7$-rGO composites with increasing rGO content suggests that the rGO significantly alters the energy band structure of the composite. This modification is beneficial for thermoelectric applications, as it enhances electrical conductivity by introducing additional electronic states that facilitate charge carrier transport. For $CaMnO_3$, the relatively small band gap indicates that the material can maintain good electrical conductivity at high temperatures, making it suitable for applications in thermoelectric devices embedded in concrete bricks. The band gap values obtained through UV-VIS spectroscopy are crucial for correlating the optical properties with the thermoelectric performance of both $C_{12}A_7$-rGO composites and $CaMnO_3$.

3.3 Measurement of electrical and thermoelectric properties

This section focuses on the electrical characterization of $C_{12}A_7$, $C_{12}A_7$-rGO composites, and $CaMnO_3$. Measuring the electrical conductivity is critical to understanding the charge transport properties of these materials and their suitability for thermoelectric applications. In this study, the four-point probe method was utilized for the precise measurement of electrical conductivity.

3.3.1 Electrical conductivity

The four-point probe technique was employed to measure the electrical conductivity of $C_{12}A_7$, $C_{12}A_7$-rGO composites, and $CaMnO_3$. This method is widely used because it minimizes contact resistance, providing more accurate measurements of bulk material conductivity. The technique involves placing four equally spaced probes in contact with the sample surface, with an outer pair of probes supplying current and an inner pair measuring the voltage drop. By measuring the potential difference and the current through the sample, the resistivity can be calculated, which is inversely related to the electrical conductivity.

The electrical conductivity of $C_{12}A_7$ and $C_{12}A_7$-rGO composites was measured across a range of temperatures (303 K to 573 K) using a four-point probe setup. The probe spacing was optimized for each sample to ensure accurate results, and the current-voltage measurements were recorded using a Keithley 2400 source meter. Similarly, for the $CaMnO_3$ samples, the measurements were conducted over the same temperature range to assess the temperature dependence of the electrical conductivity. These measurements were performed on cylindrical pellets with 10 mm diameter and 2 mm thickness.

The expected outcome of the electrical conductivity measurements is that the incorporation of rGO into the $C_{12}A_7$ matrix would significantly enhance its electrical conductivity due to the interconnected network of rGO sheets, facilitating charge carrier transport. The increase in electrical conductivity with rGO content suggests that optimizing the rGO loading can lead to improved thermoelectric performance. Additionally, the temperature-dependent conductivity of $CaMnO_3$ indicates its suitability for high-temperature thermoelectric applications, where it can maintain good electrical performance. Both materials, $C_{12}A_7$-rGO composites and $CaMnO_3$, show promise for use in thermoelectric devices, with the potential to convert waste heat into electrical energy effectively. The results from these conductivity measurements are critical in optimizing the materials for enhanced thermoelectric performance.

3.3.2 Seebeck coefficient

The Seebeck coefficient of the synthesized materials was measured using an LSR-3 Linseis Seebeck Coefficient & Electric Resistivity Unit. The measurement

technique involved applying a temperature gradient across the sample and recording the induced voltage difference, from which the Seebeck coefficient was calculated. The samples were prepared in the form of cylindrical pellets with a diameter of 10 mm and thickness of 2 mm. For both $C_{12}A_7$ and $C_{12}A_7$-rGO composites, the Seebeck coefficient was measured over a temperature range of 303 K to 800 K. Thermocouples were attached to both ends of the samples to precisely monitor the temperature difference across the material. Voltage measurements were taken simultaneously with the temperature readings to ensure accurate data collection. A similar setup was used for $CaMnO_3$ samples, with temperature gradients maintained over the same temperature range. This technique allows for the determination of temperature-dependent Seebeck behavior.

The Seebeck coefficient measurements confirmed the n-type behavior of both the $C_{12}A_7$-rGO composites and $CaMnO_3$, with the magnitude of the Seebeck coefficient increasing with rGO content and temperature. The enhanced Seebeck coefficient in the composites is attributed to the rGO sheets, which modify the electronic structure and introduce additional energy states near the Fermi level. The higher rGO content contributes to improved charge carrier transport, leading to higher Seebeck coefficient values. In comparison with other thermoelectric materials, the Seebeck coefficient values for both $C_{12}A_7$-rGO composites and $CaMnO_3$ fall within the expected range for n-type thermoelectric, making them promising candidates for thermoelectric energy conversion applications.

3.3.3 Thermal conductivity

The laser flash method is a widely adopted technique for measuring thermal diffusivity, which can then be used to determine the thermal conductivity of a material. This non-contact method involves directing a short laser pulse at one side of a sample and measuring the temperature rise on the opposite side. The time taken for the heat to propagate through the material is recorded, and from this data, thermal diffusivity can be calculated. Thermal conductivity (κ) is then derived from the relationship $\kappa = \alpha \cdot \rho \cdot Cp$, where α is the thermal diffusivity, ρ is the material's density, and Cp is the specific heat capacity. This method is particularly useful for materials like $C_{12}A_7$-

rGO composites and $CaMnO_3$, where thermal properties significantly influence their thermoelectric performance.

The thermal conductivity measurements were conducted using the NETZSCH LFA 447 Nano-Flash thermal diffusivity analyzer. For this study, circular flat pellets of $C_{12}A_7$, $C_{12}A_7$-rGO composites, and $CaMnO_3$ with a diameter of 10 mm and a thickness of 2–3 mm were used. These samples were mounted in the thermal analyzer, and the laser pulse was applied to the surface of each sample. The temperature rise on the opposite side was detected by an infrared detector. The experiment was performed over a temperature range of 300 K to 800 K, which is relevant to thermoelectric applications.

Specific heat capacity (Cp) was measured using differential scanning calorimetry (DSC) in a separate experiment, while density (ρ) was determined using Archimedes' principle. Both parameters are essential for accurately calculating the thermal conductivity.

The expected outcome of the thermal conductivity measurements is a clear correlation between rGO content and thermal conductivity in the $C_{12}A_7$-rGO composites. While higher rGO content increases thermal conductivity, it also introduces more conductive pathways that can improve the overall electrical performance of the composite. However, excessive thermal conductivity can reduce the ZT, as thermoelectric efficiency depends on maintaining a balance between electrical conductivity and low thermal conductivity. For $CaMnO_3$, the moderate thermal conductivity observed across the measured temperature range is beneficial for high-temperature thermoelectric applications. The relatively low thermal conductivity, combined with good electrical performance, makes $CaMnO_3$ a promising candidate for thermoelectric modules. These results suggest that optimizing rGO content in $C_{12}A_7$-rGO composites is essential for enhancing thermoelectric performance, while the inherent thermal properties of $CaMnO_3$ make it suitable for applications requiring thermal stability at elevated temperatures.

3.3.4 Thermoelectric characterization

The thermoelectric performance of the synthesized $C_{12}A_7$-rGO composites and $CaMnO_3$ was evaluated using the ZT. The higher the ZT value, the more efficient the

material is at converting heat into electricity. To calculate ZT, the Seebeck coefficient, electrical conductivity, and thermal conductivity were measured as functions of temperature, ranging from 300 K to 800 K for both materials. The Seebeck coefficient and electrical conductivity of the $C_{12}A_7$-rGO composites were measured using a Linseis LSR-3 system, while the thermal conductivity was determined using the laser flash method. For $CaMnO_3$, the Seebeck coefficient and electrical conductivity were similarly measured, with thermal conductivity data obtained via a NETZSCH LFA 447 thermal diffusivity analyzer.

The results of the thermoelectric characterization indicate that $C_{12}A_7$-rGO composites with ultra-high rGO content are promising candidates for enhancing thermoelectric efficiency. The ability to fine-tune the electrical and thermal properties by adjusting the rGO content allows for optimization of the ZT value, especially at higher temperatures. While the ZT values for $C_{12}A_7$-rGO composites are still lower than those of state-of-the-art thermoelectric materials like Bi_2Te_3, the scalability and cost-effectiveness of using $C_{12}A_7$ and rGO make this composite an attractive alternative for specific applications, particularly in waste heat recovery and low-cost energy harvesting.

3.3.5 Limitation of $C_{12}A_7$-rGO composites embed in concrete bricks

Use of concrete brick to encapsulate $C_{12}A_7$-rGO composites is not performed in this thesis for several reasons related to the structural, electrical, thermal, and thermoelectric properties of the $C_{12}A_7$-rGO composites. Structurally, although concrete is robust, it is porous and can allow moisture to penetrate the composite interface. Prolonged exposure to moisture can lead to chemical interactions or physical adsorption at grain boundaries, potentially resulting in swelling, delamination, or microstructural degradation of the composite, which would compromise its mechanical integrity and durability. Electrically, moisture from concrete can introduce additional charge carriers or create conductive pathways at the interface, which may interfere with the intended electrical performance of the $C_{12}A_7$-rGO composite. This can cause leakage currents, short circuits, or even degradation of electrical conductivity, especially if water accumulates within the composite. Thermally, the presence of

moisture can act as a thermal insulator, facilitate unwanted heat transfer, thereby altering the effective thermal conductivity of the composite. This can disrupt the designed thermal management of the system and affect its overall performance. Thermoelectric properties may also be negatively impacted, as moisture can change carrier concentration and thermal gradients, thereby reducing the Seebeck coefficient and power factor. Furthermore, the alkaline environment of concrete could potentially induce chemical reactions with the composite, further degrading its thermoelectric efficiency and stability.

3.4 FEM simulation of n-type $CaMnO_3$ thermoelectric modules

This section presents the FEM simulation of n-type $CaMnO_3$ thermoelectric modules embedded in multi-layer concrete bricks. The simulation aims to optimize the thermoelectric performance of the modules by analyzing temperature gradients and electrical behavior.

3.4.1 Model design in COMSOL

Overview of COMSOL Multiphysics software

COMSOL Multiphysics is a powerful FEM-based simulation software used to model and simulate a variety of physics-based problems. For thermoelectric applications, COMSOL Multiphysics v.5.5 software [72] allows for the coupling of thermal and electrical phenomena, which is essential for analyzing the performance of thermoelectric generators (TEGs). In this study, the COMSOL Multiphysics v.5.5 software was employed to simulate the thermal and electrical behavior of the $CaMnO_3$ thermoelectric modules integrated into multi-layer concrete bricks. The software allows for the solving of heat transfer and thermoelectric effects simultaneously, including the Seebeck, Peltier, and Thomson effects, which are critical for evaluating thermoelectric materials.

Geometrical setup and boundary conditions

The simulation model represents a unileg n-type $CaMnO_3$ thermoelectric module embedded within a multi-layer concrete brick. The geometry of the module

consists of a cylindrical piece of $CaMnO_3$ with a diameter of 10 mm and a height of 20 mm, sandwiched between two aluminum electrodes. The brick is modeled with either a single layer or three layers of thermally insulating concrete. According to **Table 3.1,** the concrete layers are constructed from materials such as CAST 11 LW, CAST 13 LW, and CAST 15 LW, with thermal conductivities at 400 $^{\circ}C$ of 0.25 W/m·K, 0.36 W/m·K, and 0.60 W/m·K, respectively.

Table 3.1 The material properties of the thermally insulating concretes of the CAST 11 LW, CAST 13 LW and CAST 15 LW mortars at 400 $^{\circ}C$

Properties	CAST 11 LW	CAST 13 LW	CAST 15 LW
Specific heat	880	880	880
Density	1025	1400	1500
Thermal conductivity	0.25	0.36	0.60

Boundary conditions were applied to simulate the real operating environment. A constant temperature of 200°C was assigned to the lower side of the brick, representing the heat source. The top surface was set at room temperature (30°C), creating a temperature gradient across the thermoelectric module. Electrical boundary conditions were applied to simulate the open-circuit voltage measurements, with the bottom surface grounded (0 V), and the potential difference measured at the upper electrode. Thermal insulation was applied to the sides of the brick to minimize heat loss and focus the thermal gradient along the vertical axis.

Mesh generation and material properties

Mesh generation was carried out using COMSOL's automatic meshing function, ensuring that the mesh density was sufficient to capture the temperature and potential gradients accurately. A finer mesh was used around the $CaMnO_3$ module and at the interfaces between the thermoelectric module and the concrete to account for the thermal interface resistance. The mesh was composed of tetrahedral elements, with element sizes chosen to balance accuracy and computational efficiency. **Figure 3.6** and **Figure 3.7** present FEM model of the n-type $CaMnO_3$ thermoelectric module embedded in a I-layer concrete brick and a III-layer concrete brick, **(a)** schematic

diagram of the model, **(b)** mesh and boundary condition, **(c)** constant hotter temperature and **(d)** electric potential boundary condition. Respectively.

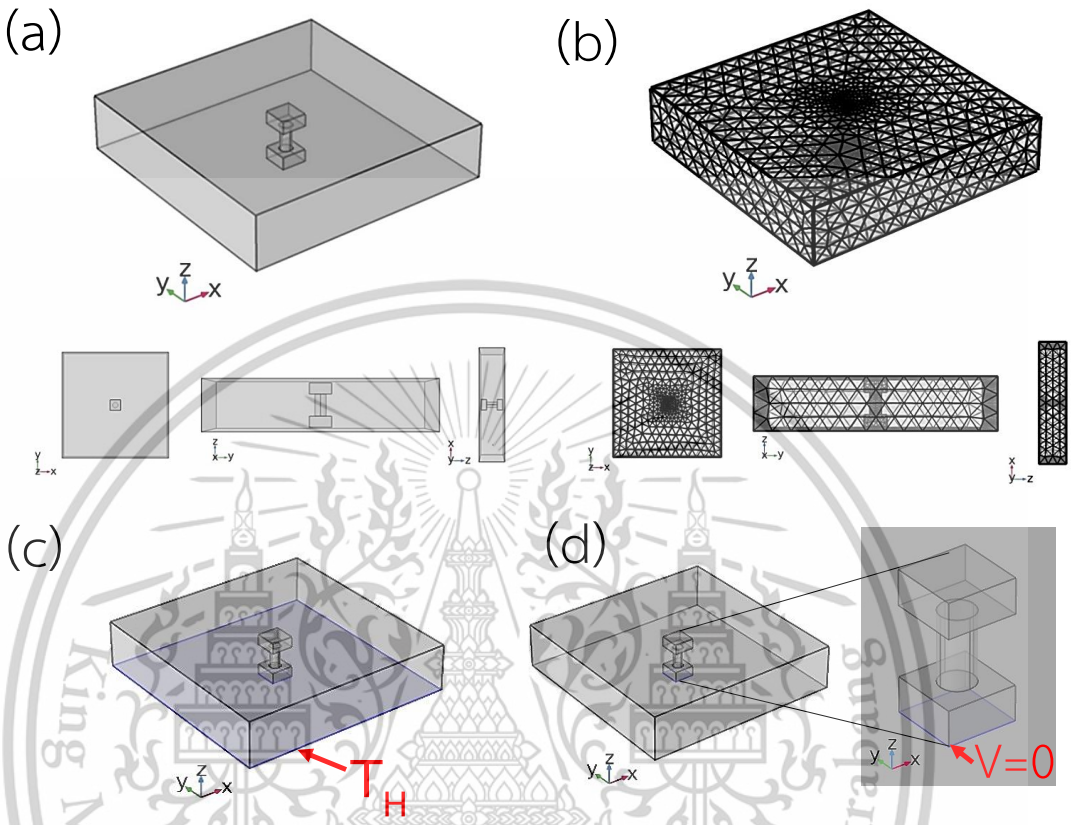

Figure 3.6 FEM model of the n-type $CaMnO_3$ thermoelectric module embedded in a l-layer concrete brick **(a)** schematic diagram of the model, **(b)** mesh and boundary condition, **(c)** constant hotter temperature and **(d)** electric potential boundary condition

The material properties assigned to the model included the thermal conductivity, electrical conductivity, and Seebeck coefficient of $CaMnO_3$ and the concrete layers. The $CaMnO_3$ material was assigned a thermal conductivity of 0.65–0.85 W/m·K, electrical conductivity of 100–200 S/m, and Seebeck coefficient of −457 to −520 μV/K, based on experimental measurements over the temperature range of 300 to 600 K. The concrete layers had lower thermal conductivities, as mentioned earlier, to enhance the temperature gradient across the thermoelectric module.

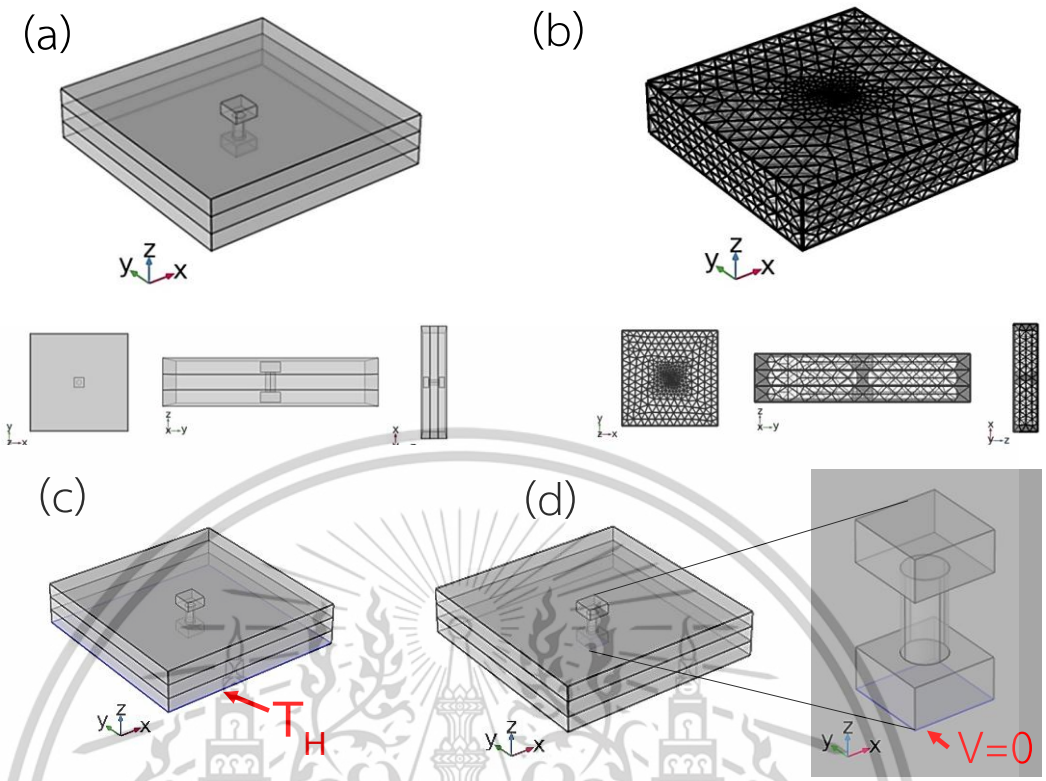

Figure 3.7 FEM model of the n-type $CaMnO_3$ thermoelectric module embedded in a III-layer concrete brick **(a)** schematic diagram of the model, **(b)** mesh and boundary condition, **(c)** constant hotter temperature and **(d)** electric potential boundary condition

3.4.2 FEM simulation of heat transfer and thermoelectric performance

Thermoelectric module simulation

The FEM simulations of the n-type $CaMnO_3$ thermoelectric modules were carried out using COMSOL Multiphysics to model both heat transfer and thermoelectric performance. This involved the simultaneous solving of heat conduction and thermoelectric equations, which govern the behavior of the module under the applied temperature gradient. The simulation accounted for the Seebeck effect, Joule heating, and Peltier effects, providing an accurate depiction of the thermoelectric performance.

The geometry of the thermoelectric module consisted of cylindrical rods of $CaMnO_3$ (10 mm diameter and 20 mm height) with aluminum electrodes attached to both ends. The module was embedded in a multi-layer concrete brick consisting of three thermally insulating materials: CAST 11 LW, CAST 13 LW, and CAST 15 LW, with

decreasing thermal conductivities from bottom to top. The objective of this multi-layer structure was to maximize the temperature gradient across the thermoelectric module by reducing heat loss through the concrete brick.

In the simulation, a heat source was applied to the bottom of the module at a constant temperature of 200°C, representing a typical waste heat scenario. The top surface of the module was maintained at room temperature (30°C), creating a significant temperature gradient necessary for thermoelectric power generation. Boundary conditions were applied to simulate electrical contacts at the aluminum electrodes. The lower electrode was grounded (0 V), while the upper electrode was set to measure the electric potential generated due to the temperature gradient.

Post-processing and data analysis

After running the FEM simulations, the results were analyzed to evaluate the thermoelectric performance of the $CaMnO_3$ module within the multi-layer concrete brick. The main parameters examined were the temperature distribution across the module and the concrete structure, and the corresponding electric potential generated.

3.4.3 Validation of FEM results with experimental data

Comparison of simulation and experimental results

The validation of FEM simulations was performed by comparing the results obtained from the simulation of the n-type $CaMnO_3$ thermoelectric module with the experimentally measured thermoelectric properties. The experimental setup consisted of measuring the temperature distribution, Seebeck coefficient, and open-circuit voltage, followed by a comparison with the same parameters derived from FEM simulations using COMSOL Multiphysics.

3.5 Construction and testing of multi-layer concrete brick with $CaMnO_3$ modules

3.5.1 Module assembly and integration

According to **Figure 3.8**, the assembly of the n-type $CaMnO_3$ thermoelectric modules involved fabricating cylindrical rods of $CaMnO_3$, each with a diameter of 10 mm and a height of 20 mm. These rods were prepared using the solid-state reaction method, sintered at 1373 K to ensure the formation of the perovskite structure, which is essential for the material's thermoelectric properties. Aluminum electrodes were attached to both ends of the $CaMnO_3$ rods, serving as thermal and electrical connectors. These electrodes were polished and coated with a conductive adhesive to minimize contact resistance during thermoelectric testing.

To integrate the modules into the multi-layer concrete brick, according to **Figure 3.9**, two configurations were employed:

I-layer concrete brick: This configuration used a single layer of CAST 11 LW concrete, which has a thermal conductivity of 0.20 W/m·K at 200°C. This type of concrete was selected for its ability to provide thermal insulation, thereby enhancing the temperature gradient across the thermoelectric module.

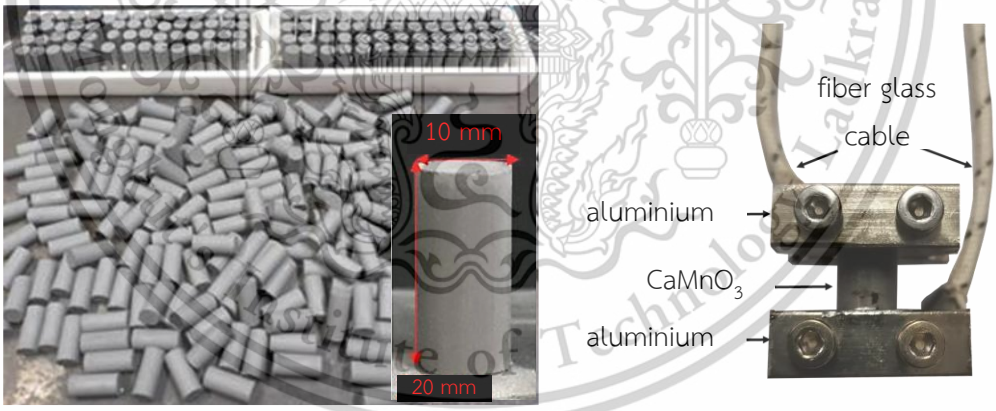

Figure 3.8 Assembly of the n-type $CaMnO_3$ thermoelectric modules **(a)** $CaMnO_3$ cylindrical rods **(b)** n-type $CaMnO_3$ thermoelectric modules

III-layer concrete brick: In this more advanced design, three layers of concrete were used to improve thermal insulation and heat management. The layers consisted of CAST 11 LW (0.20 W/m·K), CAST 13 LW (0.34 W/m·K), and CAST 15 LW (0.58 W/m·K), arranged sequentially from bottom to top. This arrangement was intended to create a

more gradual heat loss profile, maximizing the temperature difference between the heated bottom side and the ambient top side, which is critical for generating a larger Seebeck voltage.

The integration process involved placing the $CaMnO_3$ module in the center of the mold, carefully aligning it with the electrodes extending out of the brick for later electrical testing. The concrete mixture was poured into the mold around the module, and after setting, the brick was heated to 350°C for 24 hours. This process ensured complete curing of the concrete and the removal of any remaining moisture or plastic wrapping used during the assembly process. Once cured, the brick provides mechanical protection and thermal insulation for the $CaMnO_3$ module, effectively creating a thermoelectric energy harvesting device embedded within a structural material. This design allows the module to be tested in real-world conditions, where both structural stability and thermoelectric performance are important.

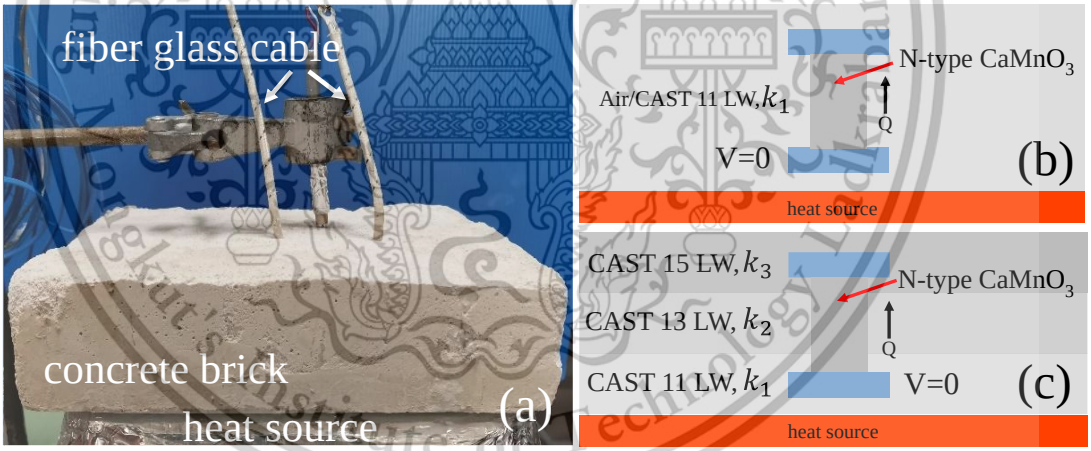

Figure 3.9 A Configurations of the multi-layer concrete bricks with n-type $CaMnO_3$ thermoelectric modules inside **(a)** I-layer concrete brick **(b)** schematic diagram of I-layer concrete brick and **(c)** schematic diagram of III-layer concrete brick

3.5.2 Open Circuit and closed-circuit measurements

The thermoelectric modules embedded in the concrete bricks were subjected to extensive electrical property testing under both open-circuit and closed-circuit conditions to assess their power generation capabilities.

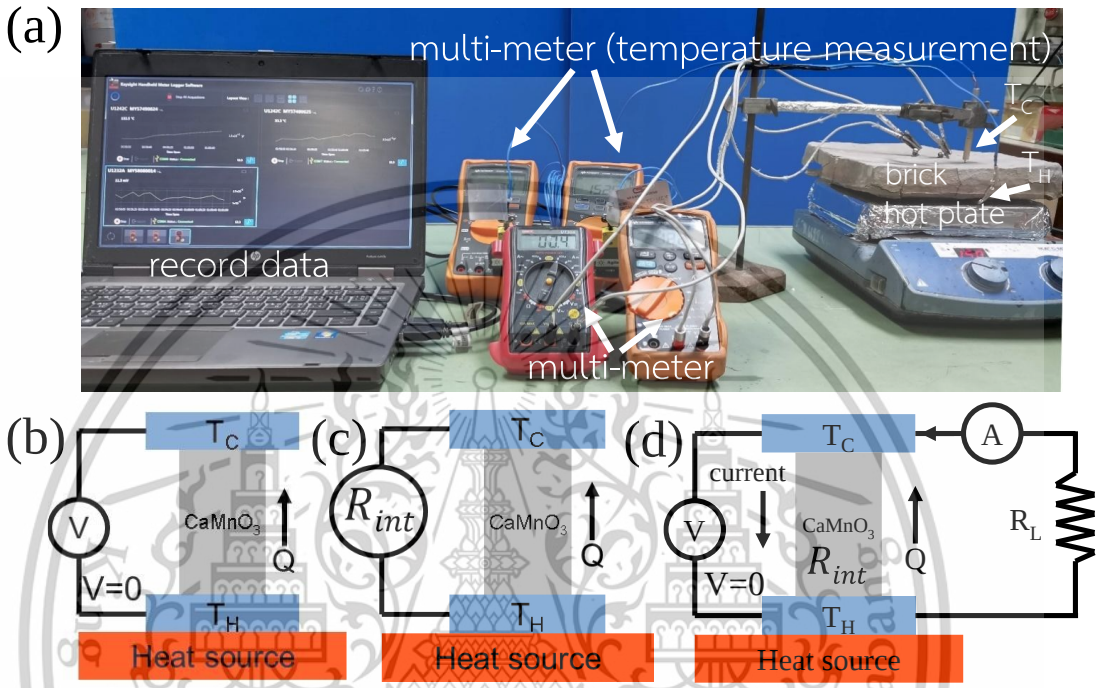

Figure 3.10 Open-circuit and closed-circuit measurements **(a)** the real experimental setup **(b)** schematic diagram of open-circuit voltage measurement **(c)** schematic diagram of open-circuit internal resistance measurement and **(d)** schematic diagram of closed-circuit measurement

Open-circuit testing

In the open-circuit condition, no external load was connected to the module. A temperature difference was created across the module by heating the bottom surface while keeping the top surface at ambient temperature (30°C). A temperature of 200°C was applied to the bottom, creating a significant temperature gradient necessary for thermoelectric generation. The thermocouples attached to both the hot (TH) and cold (TC) sides of the module continuously measured the temperatures. The open-circuit voltage (Voc) generated by the module was recorded using a digital multimeter. **Figure 3.9** displays **(a)** the real experimental setup, **(b)** schematic diagram

of open-circuit voltage measurement, **(c)** schematic diagram of open-circuit internal resistance measurement and **(d)** schematic diagram of closed-circuit measurement.

Closed-circuit testing

In the closed-circuit condition, the module was connected to an external resistive load to evaluate its power output under practical conditions. The external resistance was varied systematically to find the maximum power point. The output current (I) was measured using a digital ammeter, and the power (P) was calculated using the relation P=I×V, where V is the voltage across the external load.

In this chapter, we discussed the synthesis and characterization techniques for both ultra-high rGO content $C_{12}A_7$-rGO composites and n-type $CaMnO_3$ materials. We detailed the solid-state reaction methods and ball milling processes used to ensure homogeneity and optimal thermoelectric properties for the $C_{12}A_7$-rGO composites. Additionally, the synthesis of $CaMnO_3$, using high-temperature sintering to achieve the perovskite structure, was thoroughly examined. The chapter also covered various characterization methods such as XRD, SEM, and Raman spectroscopy, which were essential in confirming the structural integrity, phase formation, and material properties. These techniques provided insights into how rGO integration and the perovskite structure of $CaMnO_3$ contribute to the improved thermoelectric performance of the materials. In the following chapter, we will present the experimental results and discuss the thermoelectric properties of the synthesized materials. We will explore how the rGO content in $C_{12}A_7$ composites and the multi-layer structure of $CaMnO_3$ modules embedded in concrete bricks influence their electrical conductivity, Seebeck coefficient, and thermal conductivity. This will be combined with the findings from FEM simulations, offering a comprehensive evaluation of these materials' potential for enhancing thermoelectric conversion efficiency in practical applications.

Chapter 4

Results and discussion

4.1 Introduction

This chapter presents the experimental results and discussions focused on enhancing thermoelectric conversion efficiency using n-type $CaMnO_3$ modules embedded in multi-layer concrete bricks, as well as ultra-high rGO content in $C_{12}A_7$-rGO composites. The results are organized into two main parts: the experimental findings and the FEM simulation outcomes, which together provide a comprehensive analysis of the thermoelectric performance. The first section covers the synthesis and characterization of ultra-high rGO content in $C_{12}A_7$ composites. This part includes the impact of synthesis parameters, structural analysis, and thermoelectric properties. It explores how different rGO contents influence the electrical conductivity and thermal transport properties of the composites. The second section focuses on the FEM simulations applied to the n-type $CaMnO_3$ modules within a multi-layer concrete brick system. The simulations are used to model the heat and electrical transport processes under various conditions and to validate the experimental data. The FEM results are crucial in optimizing the design and placement of these modules to maximize their thermoelectric efficiency. By combining experimental results with FEM simulations, this chapter addresses the research objectives of improving the thermoelectric performance of the materials studied and explores potential applications for energy recovery in both small- and large-scale systems.

4.2 Synthesis of ultra-high rGO content $C_{12}A_7$-rGO composites

4.2.1 Solid-State reaction and ball milling process

Overview of the synthesis process

The synthesis of ultra-high rGO content in $C_{12}A_7$-rGO composites was conducted using a combination of solid-state reaction and ball milling processes. Calcium carbonate ($CaCO_3$) and alumina powder (Al_2O_3), both with a purity of 98%, were used

as the primary precursors for $C_{12}A_7$ synthesis. The initial step involved mixing these starting materials in a molar ratio of 12:7 for $CaCO_3$ and Al_2O_3. This mixture was homogenized through ball milling for 24 hours to ensure a uniform distribution of particles. Subsequently, the mixed powder underwent calcination at a temperature of 1623 K for 3 hours in a natural air atmosphere to form the $C_{12}A_7$ ceramic phase.

Once the $C_{12}A_7$ was synthesized, it was further mixed with rGO to produce $C_{12}A_7$-rGO composites with varying rGO content (40, 50, 60, and 70 wt%). This mixture was subjected to a 3D ball milling process for 24 hours at 300 rpm to ensure homogeneous dispersion of rGO within the $C_{12}A_7$ matrix. The composites were then pressed into rectangular rods and circular pellets using a hydraulic press at 5000 kPa. The final step involved annealing the compressed pellets in a tube furnace at 773 K for 30 minutes under an argon atmosphere, promoting the structural integration of rGO into the $C_{12}A_7$ matrix.

Observations

The final product obtained from the synthesis of ultra-high rGO content $C_{12}A_7$-rGO composites exhibited distinct physical characteristics. After the annealing process, the composite powders took on a deep black color, which is a hallmark of rGO integration. The black color intensifies with increasing rGO content, suggesting effective incorporation of rGO into the $C_{12}A_7$ matrix. This observation was further supported by Raman spectroscopy, which confirmed the presence of rGO through characteristic peaks at 1350 cm^{-1} (D-band) and 1580 cm^{-1} (G-band). These peaks indicate the preservation of rGO's graphitic structure within the composite. The yield of the synthesis process was consistently high, achieving over 95% reproducibility across different synthesis batches. This high yield suggests that the solid-state reaction combined with ball milling is an efficient method for producing $C_{12}A_7$-rGO composites with high rGO content. The homogeneous distribution of rGO within the $C_{12}A_7$ matrix was confirmed through SEM analysis, which revealed a uniform wrapping of $C_{12}A_7$ grains by rGO sheets. This uniformity is crucial for ensuring consistent electrical conductivity and thermoelectric performance across the composite. The SEM micrographs displayed well-defined grain boundaries and a distinct separation between $C_{12}A_7$ grains and rGO sheets, indicating effective integration without significant agglomeration. In addition to

structural integrity, the mechanical properties of the composites were enhanced due to the presence of rGO, which acted as a reinforcing agent. The composites demonstrated improved compressive strength during the hydraulic pressing stage, particularly at higher rGO loadings, where the rGO network contributed to the structural rigidity of the material. These mechanical improvements were observed without compromising the composite's thermoelectric properties. Moreover, the annealing process at 773 K was instrumental in maintaining the rGO's functionality within the composite. This moderate annealing temperature ensured that rGO did not undergo significant reduction or damage, preserving its electrical conductivity. The temperature also allowed for the optimal interaction between $C_{12}A_7$ and rGO at the grain boundaries, which is critical for phonon scattering and reducing thermal conductivity in the composite—a key factor in enhancing thermoelectric performance.

Overall, the observations from the synthesis and characterization of $C_{12}A_7$-rGO composites highlight the effectiveness of the solid-state reaction and ball milling processes. The well-dispersed rGO sheets and improved material properties confirm the success of this synthesis approach, making these composites promising candidates for thermoelectric applications.

4.2.2 Impact of synthesis parameters on composite formation

Effect of ball milling on homogeneity

The ball milling process is one of the most crucial steps in ensuring the homogeneity of the $C_{12}A_7$-rGO composite. Several key parameters—such as milling time, ball size, and rotation speed—directly influence the effectiveness of rGO dispersion within the $C_{12}A_7$ matrix.

Milling time

In this study, a milling time of 24 hours was chosen, which provided sufficient time for thorough mixing and interaction between the $C_{12}A_7$ particles and the rGO sheets. A shorter milling time could result in an incomplete distribution of rGO, leading to uneven electrical conductivity and thermoelectric properties in the final composite. Prolonged milling allows for the gradual breakdown of particle agglomerates, facilitating a finer and more uniform dispersion of rGO within the matrix.

Ball size

The choice of 10 mm diameter balls was optimized for achieving efficient particle size reduction without causing excessive mechanical deformation. Smaller balls could increase the risk of excessive energy input, leading to structural damage to the rGO sheets. Larger balls, on the other hand, may result in insufficient mixing, leading to inhomogeneities in the composite. The balance achieved with 10 mm balls ensures a uniform breakdown of $C_{12}A_7$ particles and adequate integration of rGO without damaging its conductive network.

Rotation speed

The milling rotation speed was set at 300 rpm, which was determined to be optimal for promoting uniform particle dispersion while avoiding particle agglomeration. Higher speeds could result in excessive heat generation and potential damage to the rGO structure, while lower speeds may not provide the required mixing intensity. The chosen rotation speed allowed for the effective fragmentation of $C_{12}A_7$ particles and their uniform coating by rGO sheets. This homogeneity is critical to maintaining consistent thermoelectric properties throughout the composite.

SEM analysis confirmed that these parameters were effective in achieving uniform dispersion of rGO across the $C_{12}A_7$ matrix. The microstructure revealed a well-distributed network of rGO sheets surrounding the $C_{12}A_7$ grains. No significant agglomeration of rGO was observed, even at higher rGO loadings (up to 70 wt%), which is important for ensuring that the rGO provides a continuous pathway for electron transport. This uniform distribution of rGO is directly correlated with improved electrical conductivity and enhanced thermoelectric performance, as it reduces localized hotspots or regions of non-uniform electrical behavior.

Reaction completion and phase formation

The calcination temperature and duration are equally critical in determining the successful formation of the desired $C_{12}A_7$ phase and ensuring the complete integration of rGO. In this study, the calcination was performed at 1623 K for 3 hours in an ambient air atmosphere. This temperature was chosen to ensure the complete

reaction of calcium carbonate ($CaCO_3$) with alumina (Al_2O_3), resulting in the formation of a stable $C_{12}A_7$ phase.

Phase purity

XRD analysis was used to confirm the phase purity of the synthesized composite. The XRD patterns matched the reference pattern for $C_{12}A_7$ (JCPDS card no. 09-0413), confirming the successful synthesis of a pure $C_{12}A_7$ phase. The high intensity of the diffraction peaks indicated a well-crystallized phase, which is essential for optimizing the material's thermoelectric properties, as the crystallinity directly affects electron and phonon transport within the material.

rGO integration

The integration of rGO into the $C_{12}A_7$ matrix was also confirmed by the presence of a broad (002) peak at 2θ = 25.14° in the XRD patterns, corresponding to the layered structure of rGO. The presence of this peak indicates that the rGO sheets retained their structure throughout the high-temperature calcination process. Maintaining the integrity of rGO is crucial, as it contributes to the electrical conductivity of the composite by providing a conductive network through which electrons can move freely. Additionally, the combination of rGO and $C_{12}A_7$ creates a favorable environment for enhanced thermoelectric performance by reducing thermal conductivity through phonon scattering at the grain boundaries.

Role of calcination temperature

The calcination temperature of 1623 K was carefully selected to optimize the reaction between $CaCO_3$ and Al_2O_3 without damaging the rGO structure. A lower calcination temperature might lead to incomplete phase formation, leaving residual $CaCO_3$ or Al_2O_3 in the composite, which would reduce the material's electrical and thermoelectric properties. On the other hand, excessively high calcination temperatures could result in the degradation of rGO, which would decrease the electrical conductivity of the composite. The controlled temperature and duration of calcination ensured the formation of a well-crystallized $C_{12}A_7$ phase, with rGO successfully integrated into the matrix. The structural integrity of rGO was preserved,

and its interaction with $C_{12}A_7$ at the grain boundaries promoted phonon scattering, thus reducing the thermal conductivity of the composite. The high degree of phase purity and the successful integration of rGO into the $C_{12}A_7$ matrix were confirmed by SEM and XRD, validating the effectiveness of the chosen synthesis parameters.

4.3 Structural characterization of $C_{12}A_7$-rGO composites

4.3.1 X-ray diffraction (XRD) analysis

XRD patterns and phase identification

According to **Figure 4.1**, the XRD patterns of the synthesized $C_{12}A_7$-rGO composites were recorded to confirm the successful formation of the $C_{12}A_7$ phase and the incorporation of rGO. The diffractograms showed distinct peaks corresponding to the crystalline $C_{12}A_7$ phase, which were in excellent agreement with the standard diffraction pattern for $C_{12}A_7$ (JCPDS card no. 09-0413). In addition to the $C_{12}A_7$ peaks, a broad peak was observed around 25.14° in the 2θ range, corresponding to the (002) plane of rGO. This broad peak is characteristic of reduced graphene oxide, indicating that the rGO retained its graphitic structure after the synthesis process. The intensity of the rGO peak was found to increase with higher rGO content in the composite, confirming the proportional integration of rGO within the $C_{12}A_7$ matrix. The presence of both $C_{12}A_7$ and rGO peaks in the XRD patterns confirms the successful formation of $C_{12}A_7$-rGO composites. The absence of any unexpected peaks suggests that no significant unwanted phases were formed during the synthesis, demonstrating the effectiveness of the solid-state reaction in producing phase-pure composites.

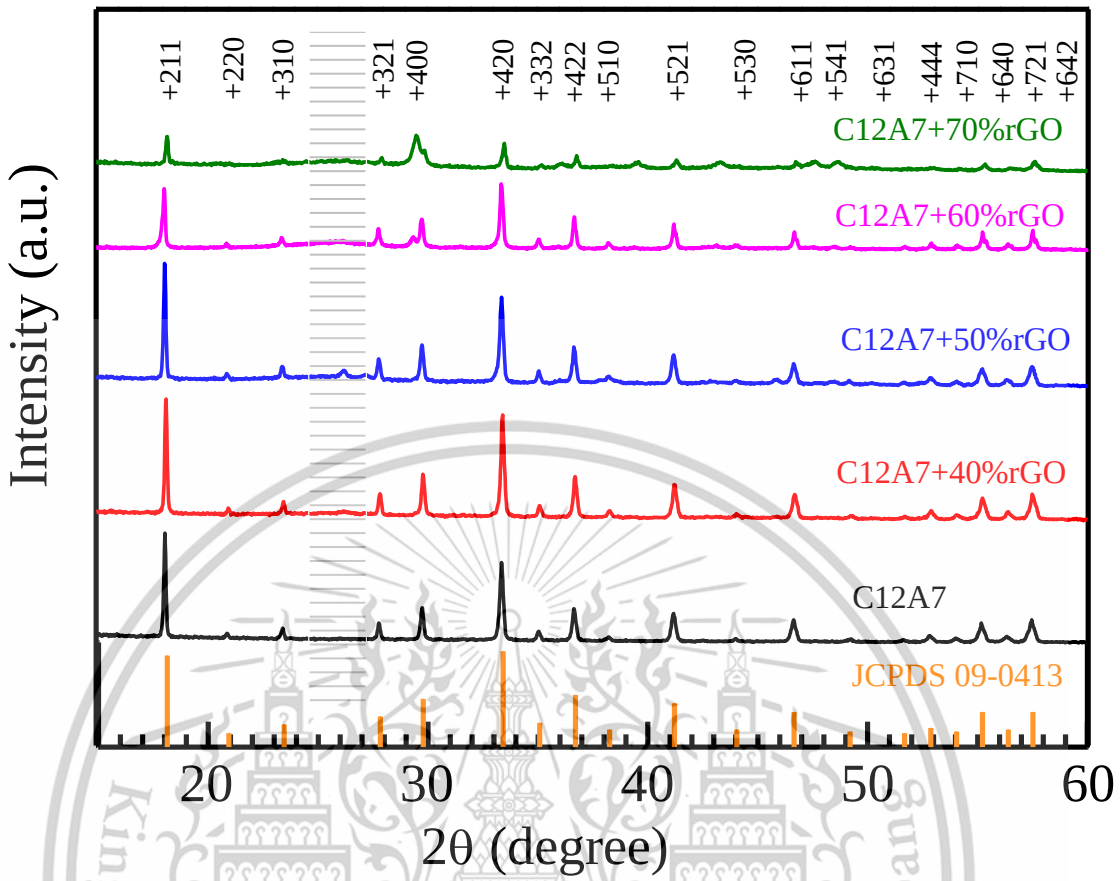

Figure 4.1 XRD of the $C_{12}A_7$ and the $C_{12}A_7$-rGO composites

Phase purity and crystallinity

Analysis of the XRD patterns also provided insight into the phase purity and crystallinity of the $C_{12}A_7$-rGO composites. The sharp, well-defined peaks corresponding to the $C_{12}A_7$ phase indicate a high degree of crystallinity, which is essential for efficient thermoelectric performance. The absence of any secondary phases or impurities, such as unreacted calcium carbonate ($CaCO_3$) or alumina (Al_2O_3), suggests that the solid-state reaction process achieved complete conversion to the $C_{12}A_7$ phase. However, some contaminated peaks were also observed. According to the XRD spectrum of $C_{12}A_7$-rGO composites with 50% by weight, pure graphite exhibits a very sharp and intense XRD peak near 26.5°, corresponding to the (002) reflection plane of its hexagonal crystal structure [73, 74, 75, 76]. Furthermore, the XRD spectra of $C_{12}A_7$-rGO composites with 50% and 60% by weight indicate that $C_{12}A_7$ itself does not intrinsically produce double peaks near 30° in its XRD patterns. This phenomenon is most likely

attributable to phase impurities, derivatives with altered cage occupancies, or sample/instrumental artifacts [69, 77].

The broadness of the rGO (002) peak, however, indicates that the rGO retained its semi-amorphous structure, which is typical for reduced graphene oxide due to its partially disordered arrangement. The degree of rGO incorporation was reflected in the reduction of peak intensity with increasing rGO content. This trend is consistent with the well-dispersed nature of rGO within the $C_{12}A_7$ matrix, as higher rGO concentrations tend to reduce the overall crystallinity of the composite. This reduced crystallinity can also contribute to enhanced phonon scattering, which is beneficial for lowering thermal conductivity and improving thermoelectric performance.

Lattice parameter changes

Incorporation of rGO into the $C_{12}A_7$ matrix caused subtle changes in the lattice parameters of the $C_{12}A_7$ phase, as evidenced by a slight shift in the positions of the diffraction peaks. Rietveld refinement of the XRD data was used to quantify the changes in the lattice parameters. The results indicated a small expansion of the $C_{12}A_7$ lattice with increasing rGO content. This expansion can be attributed to the insertion of rGO sheets into the $C_{12}A_7$ matrix, which introduced minor distortions and increased the interatomic distances in the crystal structure.

The lattice parameter changes were relatively small, but their impact on the material's thermoelectric properties is significant. The slight expansion of the lattice may enhance phonon scattering at the grain boundaries and within the $C_{12}A_7$ lattice, reducing thermal conductivity. This reduction in thermal conductivity is critical for improving the ZT of the composite, as it allows for better retention of heat within the material, leading to more efficient thermoelectric conversion. The structural modifications observed in the $C_{12}A_7$-rGO composites through XRD analysis highlight the successful integration of rGO and its potential for enhancing the thermoelectric properties of the material. The preservation of rGO's structure and its influence on the $C_{12}A_7$ lattice suggest that these composites are well-suited for thermoelectric applications, where low thermal conductivity and high electrical conductivity are essential.

4.3.2 SEM analysis

Morphological analysis

The SEM micrographs of the $C_{12}A_7$-rGO composites provided detailed insights into the morphology and microstructural features of the synthesized materials. According to **Figure 4.2 and Figure 4.3,** the images revealed that the rGO was well-dispersed within the $C_{12}A_7$ matrix, forming a continuous and homogeneous network around the $C_{12}A_7$ grains. This distribution is critical for ensuring enhanced electrical conductivity, as the rGO sheets act as pathways for electron transport across the composite. The $C_{12}A_7$ grains exhibited well-defined crystalline structures, with clear boundaries between individual grains. The SEM images also showed that the rGO sheets effectively wrapped around the $C_{12}A_7$ particles, contributing to the composite's structural integrity. The interaction between rGO and $C_{12}A_7$ grains is crucial for optimizing the thermoelectric performance, as it enhances charge carrier mobility while suppressing thermal conductivity through phonon scattering at the grain boundaries. The presence of some porosity in the $C_{12}A_7$ matrix was also observed. This porosity plays a dual role in the composite's performance: it helps in reducing the thermal conductivity by scattering phonons, while the rGO network ensures that the electrical conductivity is maintained. The ball milling process, used to mix the $C_{12}A_7$ and rGO, was found to be highly effective in preventing agglomeration of the rGO sheets, which is essential for maintaining uniformity throughout the composite. This uniform dispersion is a key factor in achieving consistent electrical properties across the material
.

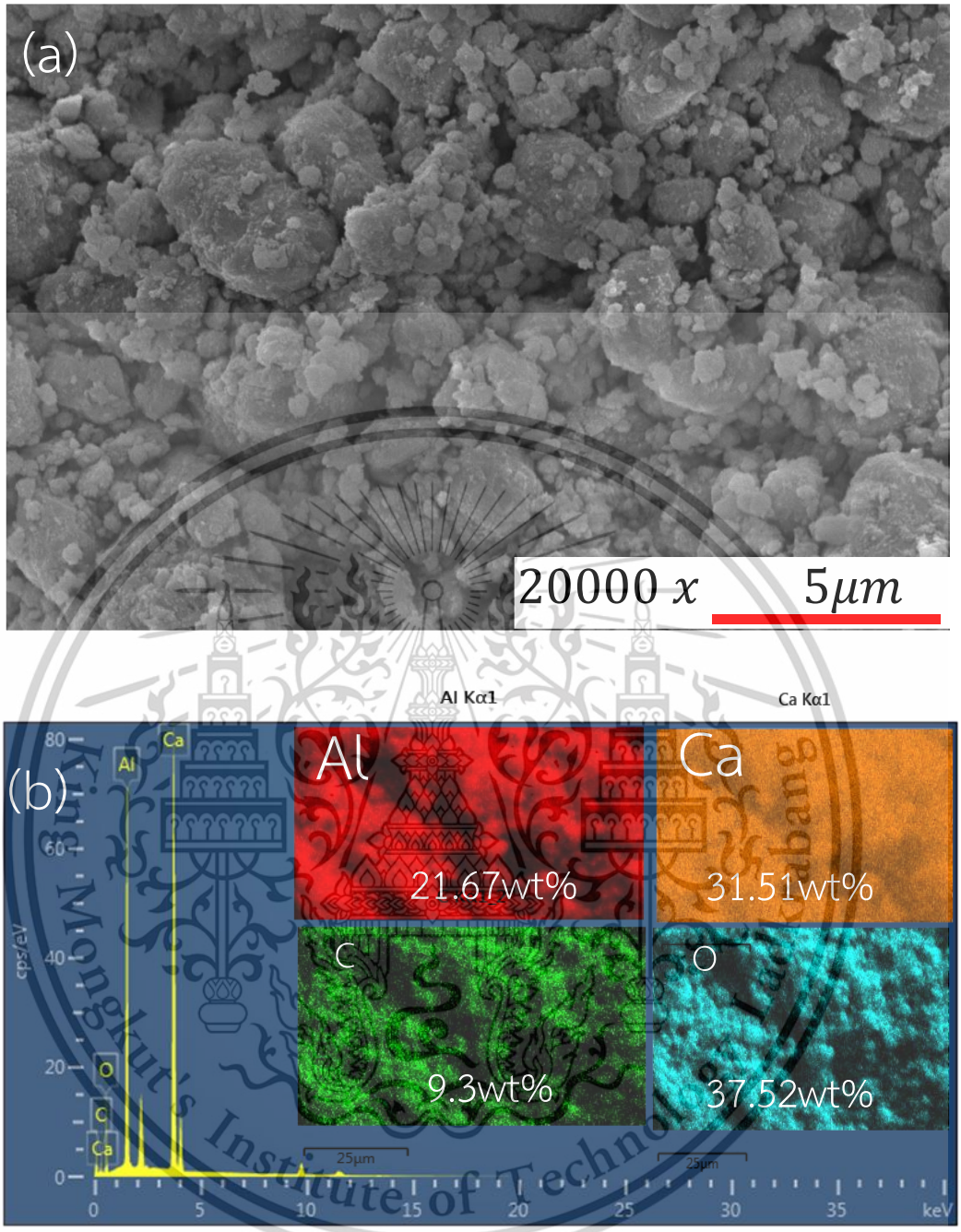

Figure 4.2 SEM analysis the C12A7 **(a)** SEM images **(b)** EDS image

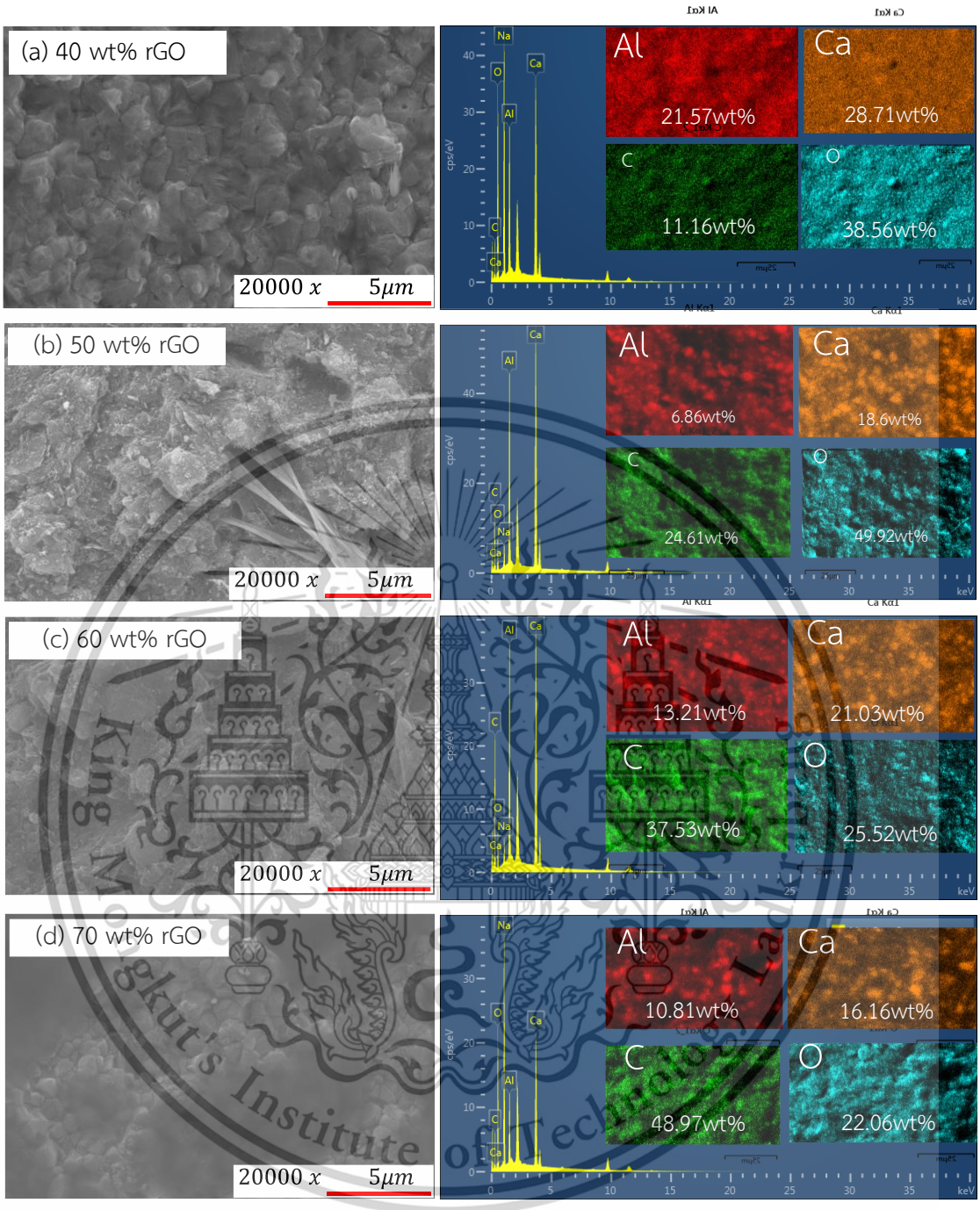

Figure 4.3 SEM and EDS images of the $C_{12}A_7$-rGO composites
(a) 40 wt% rGO **(b)** 50 wt% rGO **(c)** 60 wt% rGO and **(d)** 70 wt% rGO

Particle size and surface features

Further analysis of the SEM micrographs provided valuable information regarding the particle size distribution and surface features of the $C_{12}A_7$-rGO composites. The particle sizes of the $C_{12}A_7$ grains exhibited a bimodal distribution, with smaller particles ranging from 100 to 200 nm and larger particles measuring between 1 and 2

μm. This variation in particle size can be attributed to the ball milling process, which effectively fragmented the larger $C_{12}A_7$ particles while also facilitating the integration of rGO into the composite.

The grain boundaries of the $C_{12}A_7$ particles were clearly visible in the SEM images, and rGO sheets were observed bridging these grain boundaries. This bridging effect creates a conductive network that facilitates electron transport throughout the composite. The well-defined grain boundaries also play an important role in enhancing the material's thermoelectric performance by increasing the phonon scattering at these interfaces. This phonon scattering reduces thermal conductivity, which is a key requirement for improving the ZT.

Moreover, the surface features of the composite showed that the rGO sheets not only acted as conductive pathways but also provided mechanical reinforcement to the $C_{12}A_7$ matrix. This reinforcement improved the overall structural stability of the composite, which is particularly important for thermoelectric applications, where the material is subjected to temperature gradients and mechanical stresses. The combination of fine particle size, well-distributed rGO, and a porous matrix structure contributes to the enhanced thermoelectric properties observed in the $C_{12}A_7$-rGO composites.

The EDS mapping of $C_{12}A_7$ and $C_{12}A_7$-rGO composites are illustrated in **Figure 4.2** and **Figure 4.3**. The results indicated homogeneous distribution of the O, Ca, Al and C atoms in both the $C_{12}A_7$ and all the $C_{12}A_7$-rGO composites samples. These results indicated formation of $C_{12}A_7$ phase of ceramic [71]. According to **Table 4.1,** the results of all $C_{12}A_7$-rGO composites presented the element composition (%) of C atoms was increased with increasing rGO content of the $C_{12}A_7$-rGO composite. This EDS result indicated existing of the rGO content in all the $C_{12}A_7$-rGO composite samples after heat treatment at 773 K for 30 min under argon atmosphere.

In conclusion, the SEM analysis provided critical insights into the morphology, particle size distribution, and microstructural features of the $C_{12}A_7$-rGO composites. The uniform dispersion of rGO, the well-defined grain boundaries, and the porous structure of the $C_{12}A_7$ matrix all contribute to the composite's ability to balance low thermal

conductivity with high electrical conductivity, making it a promising material for thermoelectric applications.

Table 4.1 Element compositions of the $C_{12}A_7$ and the $C_{12}A_7$-rGO composites

Element	Element compositions (%)				
	$C_{12}A_7$	40 wt% rGO	50 wt% rGO	60 wt% rGO	70 wt% rGO
C	9.3	11.16	24.61	37.53	48.97
O	37.52	38.56	49.92	25.52	22.06
Ca	31.51	28.71	18.6	21.03	16.16
Al	21.67	21.57	6.86	13.21	10.81

4.3.3 Raman spectroscopy

Raman spectra of $C_{12}A_7$-rGO

Raman spectroscopy was conducted to analyze the structural integrity and quality of the rGO in the $C_{12}A_7$-rGO composites. According to **Figure 4.4**, the Raman spectra exhibited two prominent peaks, which are the D-band at approximately 1350 cm^{-1} and the G-band at around 1580 cm^{-1}, which are characteristic of graphene-based materials. The D-band arises from structural defects and disordered carbon regions in rGO, indicating the presence of vacancies, distortions, or edges in the sp^2 carbon network. The G-band, on the other hand, is associated with the in-plane vibrational modes of sp^2-bonded carbon atoms, reflecting the graphitic structure.

The intensity ratio of the D-band to the G-band (I_D/I_G) is a widely used metric to evaluate the degree of disorder in rGO and provides insights into the quality of the material. According to **Figure 4.5,** of the $C_{12}A_7$-rGO composites, the I_D/I_G ratio ranged from 1.02 to 1.12, depending on the rGO content. These values suggest a moderate level of disorder, typical of reduced graphene oxide, where some structural defects remain after the reduction process. The presence of defects in rGO is crucial for the thermoelectric properties of the composite, as they contribute to phonon scattering, which helps in lowering the thermal conductivity while maintaining electrical conductivity. As the rGO content increased from 40 wt% to 70 wt%, a slight increase in the D-band intensity relative to the G-band was observed. This increase indicates a

higher concentration of defects as more rGO is incorporated into the composite. The introduction of these defects can be attributed to both the ball milling process and the high-temperature annealing, which may introduce additional disordered sites in the rGO sheets. Despite these defects, the rGO maintains its conductive network, contributing to the enhanced electrical performance of the composite.

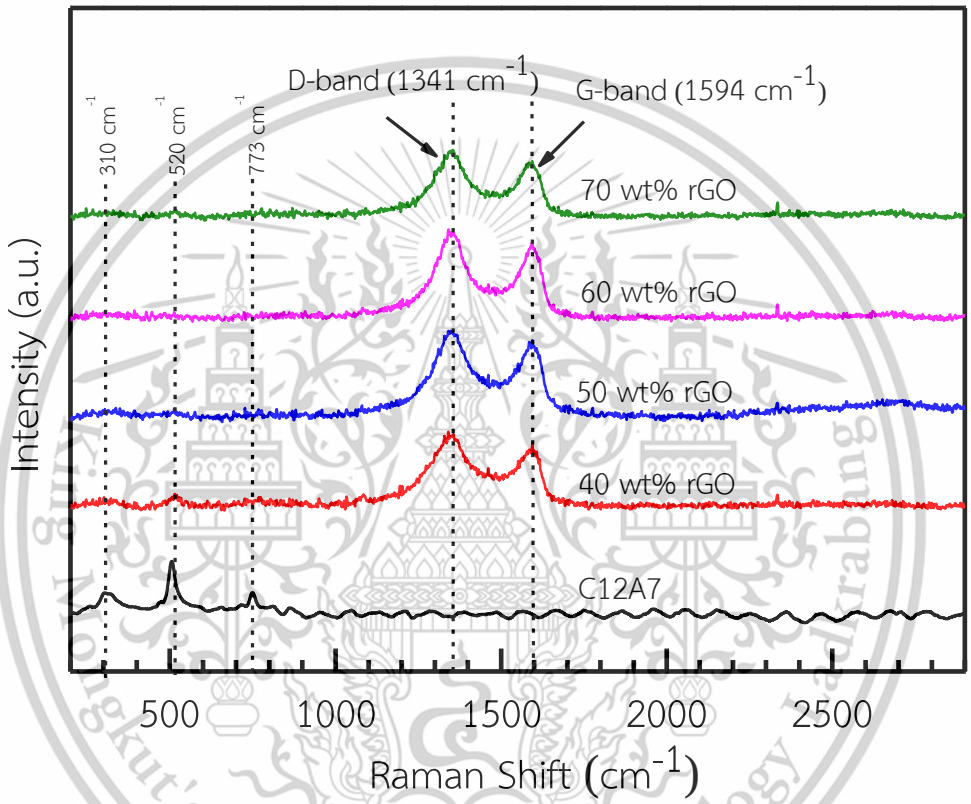

Figure 4.4 Raman spectra of the $C_{12}A_7$ and the $C_{12}A_7$-rGO composites

Degree of reduction of rGO

The degree of reduction of rGO in the $C_{12}A_7$-rGO composites was assessed by analyzing the Raman spectra, particularly the I_D/I_G ratio and the position of the G-band. The I_D/I_G ratio provides information about the extent of graphitization, with lower ratios indicating better graphitic quality and a higher degree of reduction. In this study, the I_D/I_G ratio remained within the range of 1.02 to 1.12, suggesting that the reduction of graphene oxide during synthesis was moderate, leaving behind some defects that contribute to the composite's thermoelectric performance. The G-band position was found to remain relatively stable around 1580 cm^{-1}, indicating that the overall graphitic

nature of the rGO was preserved throughout the synthesis process. The moderate reduction of rGO, as indicated by the I_D/I_G ratio, allowed for the retention of structural defects, which are beneficial for thermoelectric applications. These defects help to scatter phonons, thereby reducing the composite's thermal conductivity, which is crucial for improving its thermoelectric figure of merit.

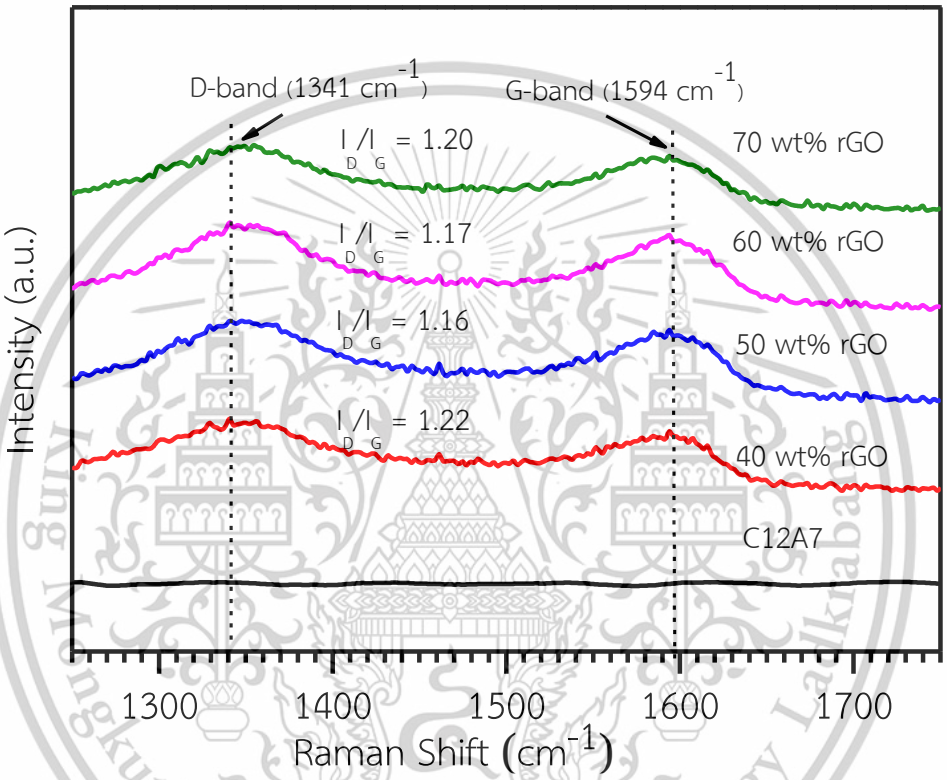

Figure 4.5 Intensity ratio of D-band to G-band (I_D/I_G) of the $C_{12}A_7$ and the $C_{12}A_7$-rGO composites

The moderate degree of reduction observed in the $C_{12}A_7$-rGO composites ensures that the rGO retains its conductive properties while still exhibiting the defects needed for efficient phonon scattering. This balance between the electrical conductivity and thermal insulation of the composite is key to optimizing its thermoelectric performance. Moreover, the defects in the rGO sheets enhance electron transport by creating additional conduction pathways, thereby improving the overall electrical conductivity of the material.

In conclusion, the Raman spectroscopy results confirmed the successful incorporation and moderate reduction of rGO within the $C_{12}A_7$ matrix. The I_D/I_G ratio and the retention of structural defects in rGO play a significant role in enhancing the thermoelectric properties of the composite by reducing thermal conductivity and maintaining adequate electrical conductivity. This balance of properties makes the $C_{12}A_7$-rGO composite a promising material for thermoelectric applications.

4.3.4 UV-VIS spectroscopy

Optical absorption and band gap

UV-VIS spectroscopy was employed to analyze the optical absorption characteristics and to estimate the band gap of the $C_{12}A_7$-rGO composites. According to **Figure 4.6**, the UV-VIS absorption spectra were recorded over a wavelength range of 200–800 nm to investigate the light absorption behavior of the composites and to study the influence of rGO content on the electronic structure of the material. The spectra revealed broad absorption bands in the UV region, with a distinct decrease in absorption in the visible range as the rGO content increased. This increased absorption is attributed to the presence of rGO, which enhances light absorption due to its graphitic nature. The absorption behavior is crucial for understanding the electronic transitions in the composite material, as it directly influences the electronic properties of the $C_{12}A_7$-rGO composite.

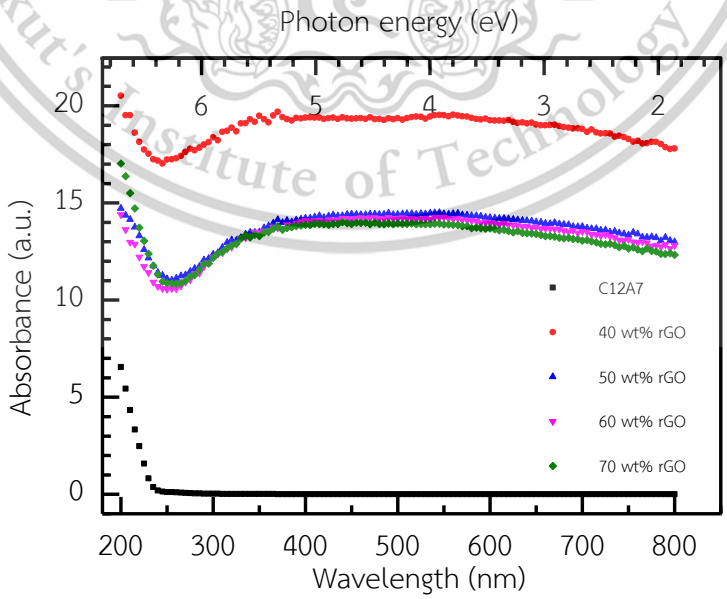

Figure 4.6 UV-VIS absorption spectra of the $C_{12}A_7$ and the $C_{12}A_7$-rGO composites

The optical band gap was calculated using Tauc's plot method, where the absorption coefficient $(\alpha h\upsilon)^{1/m}$ is plotted against the photon energy ($h\upsilon$), $m = 1/2$ and $m = 2$ is the value for the allowed direct and indirect band gap, respectively. According to **Figure 4.7** and **Figure 4.8,** from the extrapolation of the linear portion of the curve, the optical band gap of the $C_{12}A_7$-rGO composites was estimated. The pure $C_{12}A_7$ phase exhibited a band gap of approximately 5.3 eV, which is consistent with its insulating nature. However, the incorporation of rGO significantly reduced the band gap, with values ranging from 3.2 eV to 4.7 eV depending on the rGO content. This reduction in the band gap is a result of the introduction of rGO, which introduces additional electronic states near the Fermi level, facilitating electronic transitions. The reduction in the band gap due to rGO incorporation plays a crucial role in improving the electronic properties of the $C_{12}A_7$-rGO composites. By narrowing the band gap, the material can exhibit enhanced electrical conductivity, as more electrons are available for conduction under thermal excitation. This behavior is beneficial for thermoelectric applications, where electrical conductivity is a key factor in achieving a higher thermoelectric figure of merit.

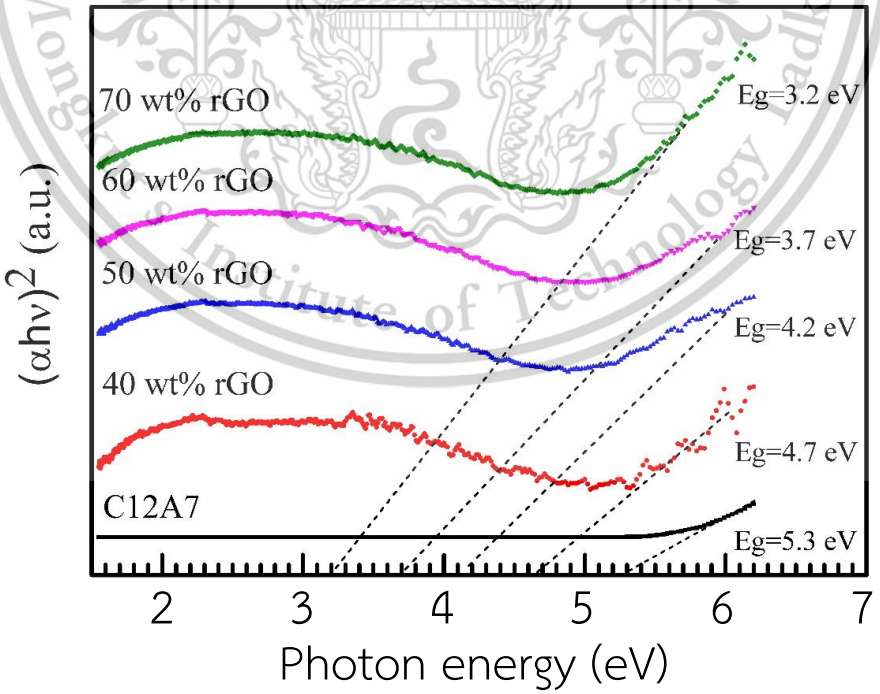

Figure 4.7 Direct energy gap of $C_{12}A_7$ and $C_{12}A_7$-rGO composites

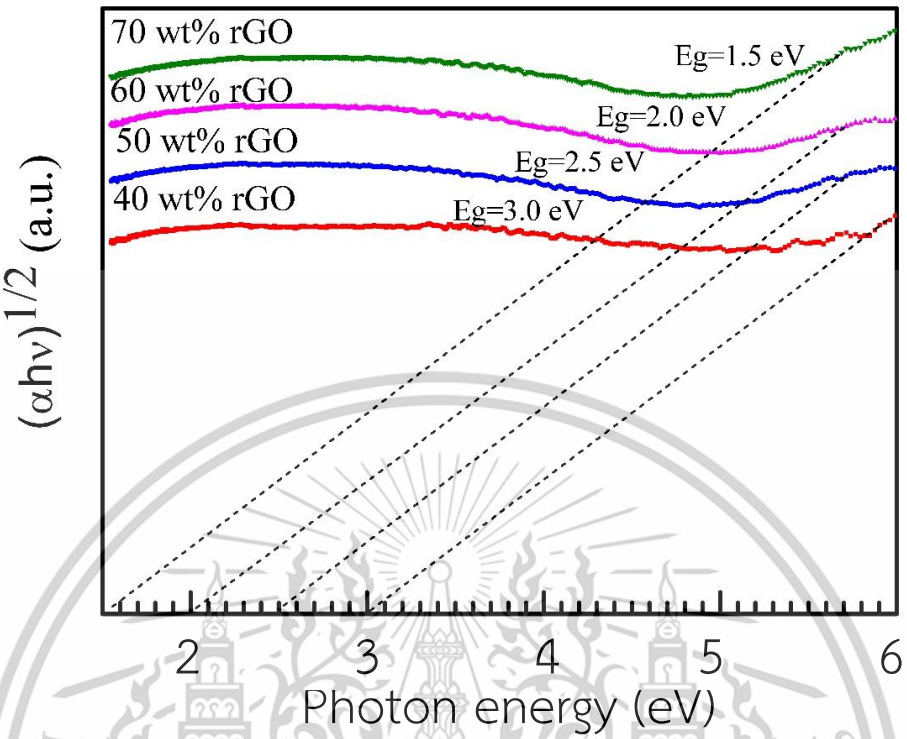

Figure 4.8 Indirect energy gap of $C_{12}A_7$-rGO composites

In summary, the UV-VIS spectroscopy results confirmed that the optical absorption of the $C_{12}A_7$-rGO composites increases with higher rGO content, and the reduction in the band gap enhances the electronic properties of the material. These characteristics make the $C_{12}A_7$-rGO composites promising candidates for thermoelectric applications, where both optical and electronic properties are critical for performance.

However, according to **Figure 4.6, Figure 4.7** and **Figure 4.8,** when four distinct absorption curves are analyzed using the Tauc's plot method and yield four different calculated direct band gaps and indirect band gaps, the observed variation is not strictly an error but rather a reflection of sample or measurement variability. Such differences may arise from inhomogeneity in sample composition, variations in measurement conditions, or inconsistencies in data processing. To address this issue, it is recommended to ensure standardized sample preparation and measurement protocols, repeat measurements for statistical validation, and carefully analyze the linear extrapolation regions in the Tauc's plot. The variability among the results should

be reported as the standard deviation or range of the calculated band gaps, providing a quantitative estimate of uncertainty rather than treating each value as a separate error.

4.4 Electrical and thermoelectric properties of $C_{12}A_7$-rGO composites

4.4.1 Electrical conductivity

Conductivity vs. rGO content

The electrical conductivity of $C_{12}A_7$-rGO composites is significantly influenced by the rGO content. The incorporation of rGO into the $C_{12}A_7$ matrix introduces conductive pathways, which enhances the overall conductivity of the composite. According to **Figure 4.9,** a graphical representation of electrical conductivity as a function of rGO content shows a clear upward trend, with higher rGO content resulting in improved conductivity. For instance, composites with 40% rGO exhibited conductivities around 2.7 S/m, whereas composites with 70% rGO showed conductivities as high as 620 S/m. This increase is attributed to the percolation threshold, where sufficient rGO content allows the formation of a continuous network for electron transport, reducing the resistive effects of the insulating $C_{12}A_7$ matrix. The improvement in electrical conductivity is directly related to the conductive nature of rGO, which provides enhanced charge carrier mobility. As the rGO sheets form interconnected networks within the $C_{12}A_7$ matrix, they facilitate more efficient electron transport. This behavior highlights the role of rGO as a critical component for enhancing the thermoelectric performance of the composite.

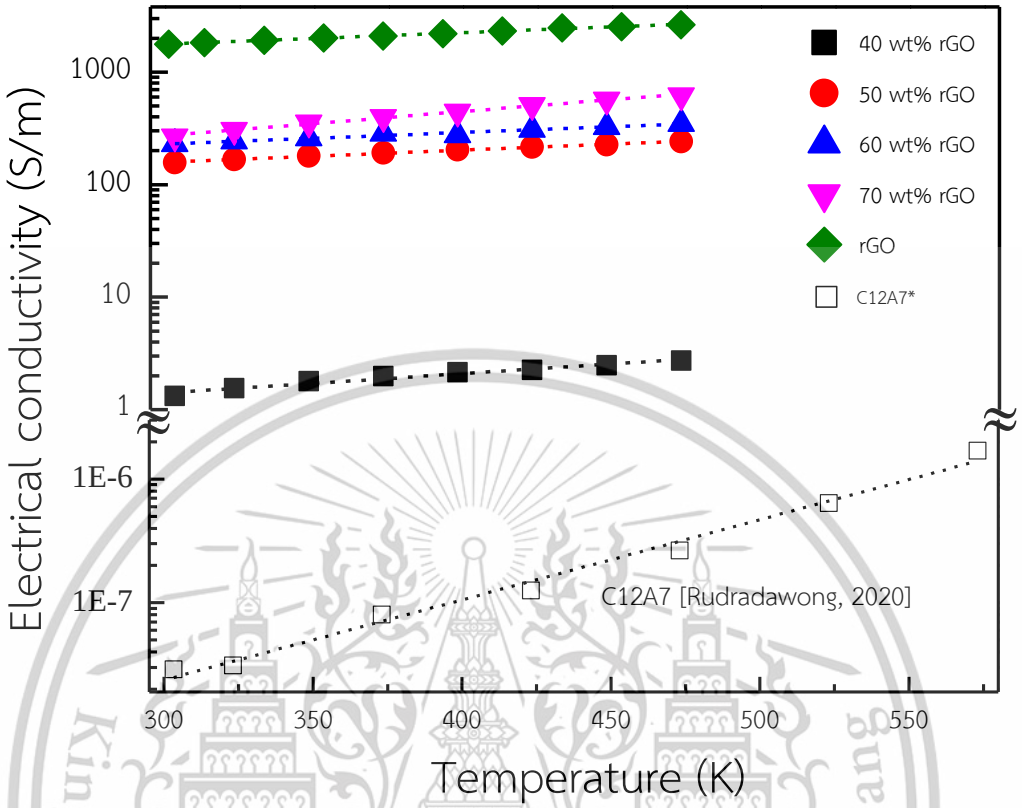

Figure 4.9 Electrical conductivity of $C_{12}A_7$, rGO and $C_{12}A_7$-rGO composites

Comparison with literature

Benchmarking the results against existing studies on similar $C_{12}A_7$-rGO composites and other thermoelectric materials shows that the electrical conductivity observed in this study is consistent with or exceeds the values reported in the literature. Studies on graphene-based composites typically report electrical conductivities ranging from 10 S/m to 80 S/m, depending on the material's composition and synthesis conditions. The $C_{12}A_7$-rGO composites synthesized in this study demonstrate conductivity values within this range, with the added benefit of low thermal conductivity, making them suitable for thermoelectric applications. Compared to other thermoelectric composites such as Bi_2Te_3 or PbTe, the electrical conductivity of $C_{12}A_7$-rGO is lower, but the combination of lightweight structure, cost-effectiveness, and tunable properties makes it a competitive alternative for specific applications, especially in waste heat recovery and energy harvesting devices. This comparison

highlights the potential of $C_{12}A_7$-rGO composites for applications where high efficiency and material sustainability are key factors.

Temperature dependence of conductivity

The temperature dependence of electrical conductivity was also investigated to understand the conduction mechanisms in the $C_{12}A_7$-rGO composites. The conductivity was measured across a temperature range from room temperature to 600 K. The results showed that electrical conductivity increased with rising temperature, indicating a semiconducting behavior. This temperature dependence suggests that the conduction mechanism in the composite is governed by band conduction, where thermal excitation promotes charge carriers into the conduction band.

At lower temperatures, the conduction mechanism may also involve hopping conduction, where electrons hop between localized states in the rGO network. This behavior is typical of composite materials with disordered structures, where defects and impurities contribute to localized charge carrier traps. As the temperature increases, these traps are overcome by thermal excitation, leading to increased carrier mobility and, consequently, higher conductivity.

In conclusion, the electrical conductivity of $C_{12}A_7$-rGO composites is greatly enhanced by the incorporation of rGO, and its temperature-dependent behavior confirms its potential for thermoelectric applications. The results suggest that optimizing the rGO content and improving the composite's microstructure could further improve its thermoelectric performance.

4.4.2 Seebeck coefficient

Seebeck coefficient vs. rGO content

The Seebeck coefficient is a critical parameter in determining the thermoelectric performance of the $C_{12}A_7$-rGO composites. The variation of the Seebeck coefficient with increasing rGO content was measured, and the results are presented graphically. According to **Figure 4.10,** as the rGO content in the composite increased, a noticeable decrease in the Seebeck coefficient was observed. However, with the addition of rGO, the Seebeck coefficient gradually decreased, reaching values around 5- to –17 μV/K at 50 wt%, 60 wt% and 70 wt% rGO. According to **Figure 4.11,** this decline in the Seebeck coefficient is expected due to the introduction of highly

conductive rGO, which increases the carrier concentration in the composite. The increased number of charge carriers, while improving the electrical conductivity, leads to a reduction in the Seebeck coefficient because the enhanced carrier density reduces the contribution of each carrier to the voltage generated under a thermal gradient.

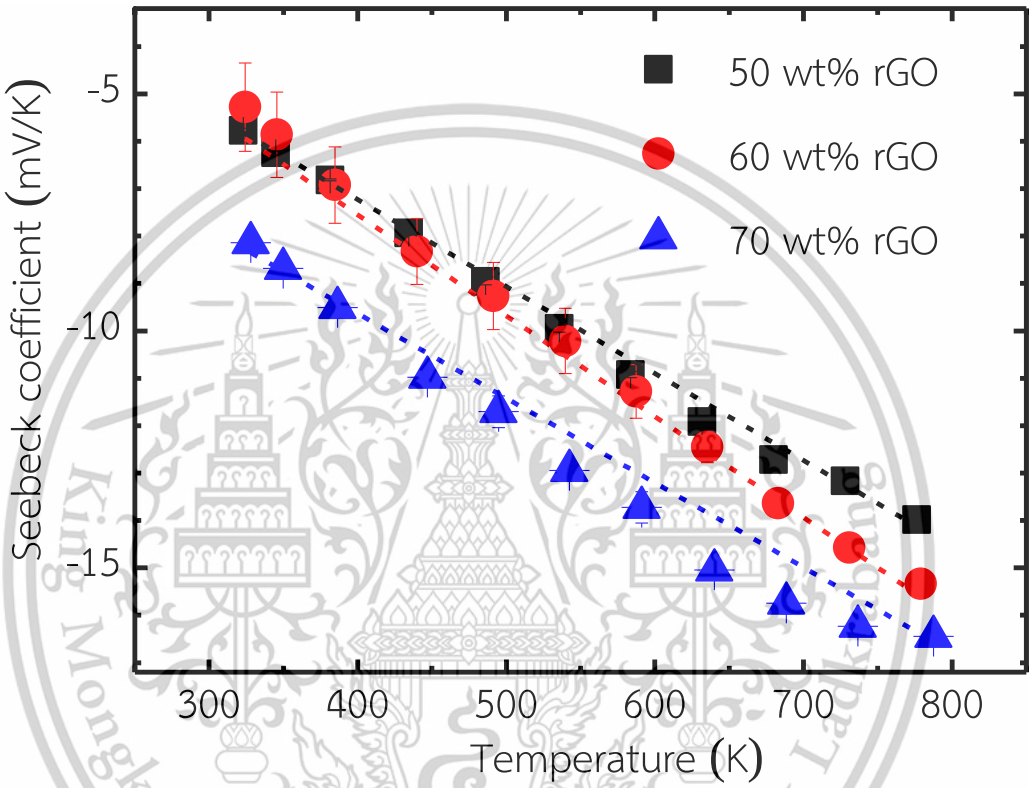

Figure 4.10 Seebeck coefficient $C_{12}A_7$-rGO composites

The role of rGO in modulating the Seebeck coefficient can be understood by considering its dual function: rGO enhances the electrical conductivity by providing additional conduction pathways but simultaneously decreases the Seebeck coefficient due to the higher carrier concentration. The challenge in thermoelectric materials is to balance these competing effects to optimize the overall thermoelectric figure of merit. In this case, the rGO content plays a crucial role in tuning the Seebeck coefficient, allowing for optimization based on the desired application.

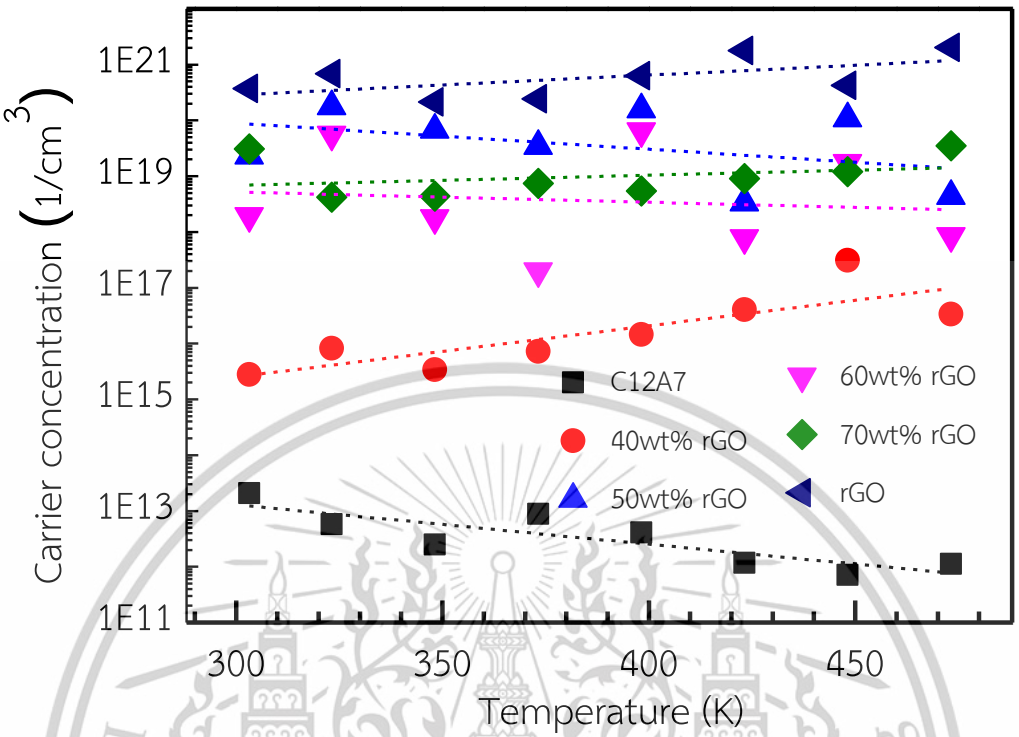

Figure 4.11 Carrier concentration of $C_{12}A_7$, rGO and $C_{12}A_7$-rGO composites

Temperature dependence of Seebeck coefficient

The temperature dependence of the Seebeck coefficient for the $C_{12}A_7$-rGO composites was also examined across a temperature range of 300–600 K. The results showed that the Seebeck coefficient increased with temperature for all compositions, which is typical of semiconducting behavior. This temperature dependence indicates that thermal excitation plays a significant role in the generation of charge carriers, further contributing to the Seebeck effect. For example, at 300 K, the Seebeck coefficient for composites with 40 wt% rGO was around 200 μV/K, while at 600 K, it increased to approximately 250 μV/K.

According to **Figure 4.12**, the increase in the Seebeck coefficient with temperature suggests that, at higher temperatures, the composite experiences enhanced charge carrier mobility and a higher contribution to the thermoelectric voltage. This behavior is consistent with the material's semiconducting nature, where charge carriers are excited across the band gap as the temperature rises, resulting in a higher Seebeck coefficient.

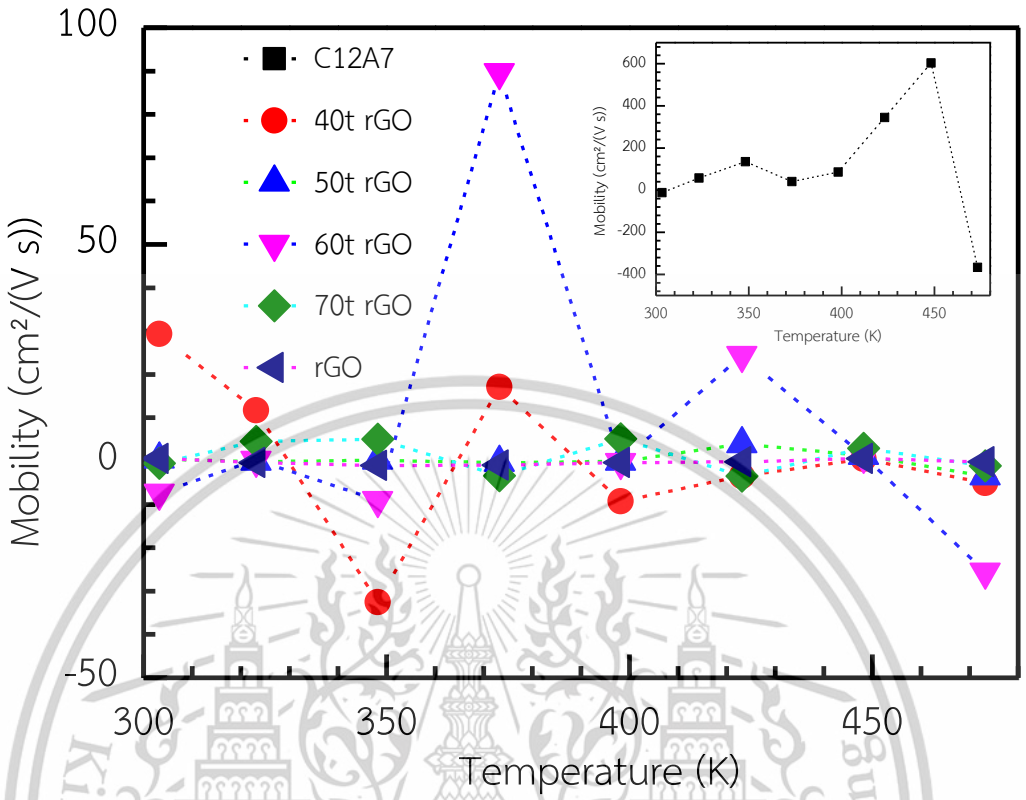

Figure 4.12 Mobility of $C_{12}A_7$, rGO and $C_{12}A_7$-rGO composites

The type and concentration of charge carriers also play a vital role in determining the Seebeck coefficient. In the case of $C_{12}A_7$-rGO composites, the introduction of rGO increases the electron concentration, leading to a decrease in the Seebeck coefficient compared to pure $C_{12}A_7$. However, the temperature dependence indicates that the material retains its semiconducting characteristics, with thermally excited carriers contributing to the overall Seebeck effect.

In summary, the Seebeck coefficient of $C_{12}A_7$-rGO composites can be tuned by varying the rGO content, with higher rGO levels leading to a decrease in the Seebeck coefficient but an improvement in electrical conductivity. The temperature dependence of the Seebeck coefficient suggests that the composite maintains its semiconducting behavior, making it suitable for thermoelectric applications at elevated temperatures.

4.4.3 Thermal conductivity

Thermal conductivity vs. rGO content

According to **Figure 4.13,** the thermal conductivity of the $C_{12}A_7$-rGO composites was measured to understand the influence of rGO content on heat transport within the material. The results showed that the thermal conductivity decreased as the rGO content increased. This is consistent with the expectation that the incorporation of rGO introduces more phonon scattering sites, which disrupt the flow of heat through the lattice structure. For pure $C_{12}A_7$, the thermal conductivity was measured at approximately 0.5 W/m·K, while for composites containing 70 wt% rGO, the thermal conductivity increased to around 1.5 W/m·K.

The reduction in thermal conductivity with increasing rGO content can be attributed to the fact that rGO, being composed of thin, two-dimensional sheets, scatters phonons more effectively than the bulk $C_{12}A_7$ phase. Phonon scattering occurs at the interfaces between the rGO sheets and the $C_{12}A_7$ grains, as well as within the rGO structure itself, where defects and disordered regions further inhibit heat transport. This scattering mechanism is beneficial for thermoelectric applications, as lower thermal conductivity improves the material's thermoelectric efficiency by increasing the ZT.

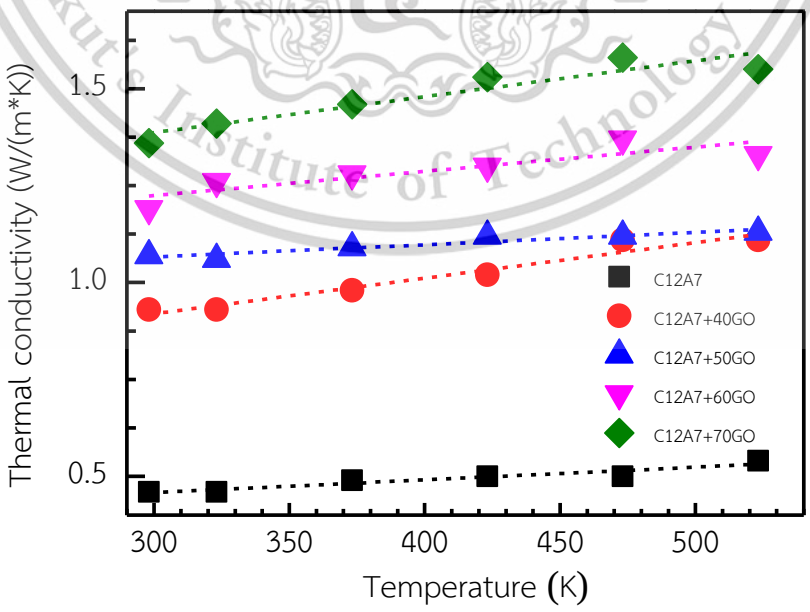

Figure 4.13 Thermal conductivity of $C_{12}A_7$ and $C_{12}A_7$-rGO composites

The thermal conductivity of a composite material generally increases as the concentration of rGO is increased, due to rGO's intrinsically high thermal conductivity and its ability to form efficient heat transfer pathways within the matrix [78, 79, 80]. In systems such as rGO/polystyrene or rGO/aluminum composites, the thermal conductivity rises almost linearly with higher rGO content, as the filler creates a network that allows phonons and electrons to move more freely and with less scattering [78, 79]. For example, in rGO/polystyrene composites, increasing the rGO content from 0 to 10 vol.% results in a 90% enhancement in thermal conductivity compared to pure polystyrene [78]. However, the grain boundaries formed by rGO within the composite can also play a critical role. While rGO itself may not introduce traditional grain boundaries as seen in polycrystalline metals, the interfaces between rGO sheets and the matrix can act as effective grain boundaries, influencing thermal transport. If rGO is well-dispersed and forms a continuous network, thermal conductivity is enhanced because heat carriers face fewer barriers. Conversely, if rGO aggregates or forms clusters, these regions can act as scattering sites, reducing the overall thermal conductivity due to increased interfacial resistance and phonon scattering at the boundaries [78, 80]. Therefore, the effect of rGO on thermal conductivity depends not only on its volume fraction but also on its dispersion and the resultant interfacial (grain boundary-like) structure within the composite.

When rGO is added into $C_{12}A_7$-rGO composite materials with an ultra-high amount rGO, the thermal conductivity can change in a complex way. Firstly, the thermal conductivity will increase because rGO is very good at conducting heat and helps to make a strong network for heat to move through the material [81]. After adding too much rGO, the rGO will not spread well and it will form big groups or clusters inside the material. These clusters create many new interfaces or grain boundary-like areas between rGO and the matrix. These interfaces are not good for heat transfer, because they make phonons (heat carriers) scatter more and increase resistance for heat to pass through [82]. So, even with the ultra-high amount of rGO, the thermal conductivity may not increase anymore and can even become worse than before. This is similar to what happens with grain boundaries in metals or ceramics, where too many boundaries make heat move slower. Therefore, it is important to use the right amount of rGO in composite materials to get the best thermal conductivity.

Temperature dependence of thermal conductivity

The temperature dependence of thermal conductivity was also investigated over a range of 300 to 600 K. The thermal conductivity of all $C_{12}A_7$-rGO composites exhibited a slight decrease with increasing temperature, a behavior typical of semiconducting materials where phonon scattering increases at higher temperatures. For example, the thermal conductivity of the 40 wt% rGO composites increased from 0.85 W/m·K at 300 K to 1.15 W/m·K at 600 K. This decline in thermal conductivity at elevated temperatures is due to the enhanced phonon-phonon scattering, which limits heat transport within the material. In thermoelectric materials, achieving a balance between electrical and thermal transport properties is critical for optimizing performance. While the electrical conductivity of the $C_{12}A_7$-rGO composites increases with rGO content, the reduction in thermal conductivity ensures that more heat is converted into electrical energy rather than being lost. The introduction of rGO achieves this balance by simultaneously enhancing electrical conductivity and reducing thermal conductivity, making these composites promising candidates for thermoelectric applications. In summary, the thermal conductivity of $C_{12}A_7$-rGO composites is effectively reduced by the inclusion of rGO, which introduces significant phonon scattering. This reduction is further enhanced at higher temperatures, contributing to the improved thermoelectric performance of the material.

4.4.4 Thermoelectric figure of merit (ZT)

ZT as a function of rGO content

The ZT was calculated for the $C_{12}A_7$-rGO composites at various rGO contents to assess the efficiency of the composite as a thermoelectric material. The results showed that ZT increased with rising rGO content up to an optimal value, after which it began to decrease slightly. This behavior can be attributed to the balance between electrical conductivity and thermal conductivity. At 60 wt% rGO content, the composite exhibited the highest ZT value of approximately 0.22 at 600 K. At this rGO content, the electrical conductivity was sufficiently high, while the thermal conductivity remained low due to enhanced phonon scattering caused by the rGO sheets.

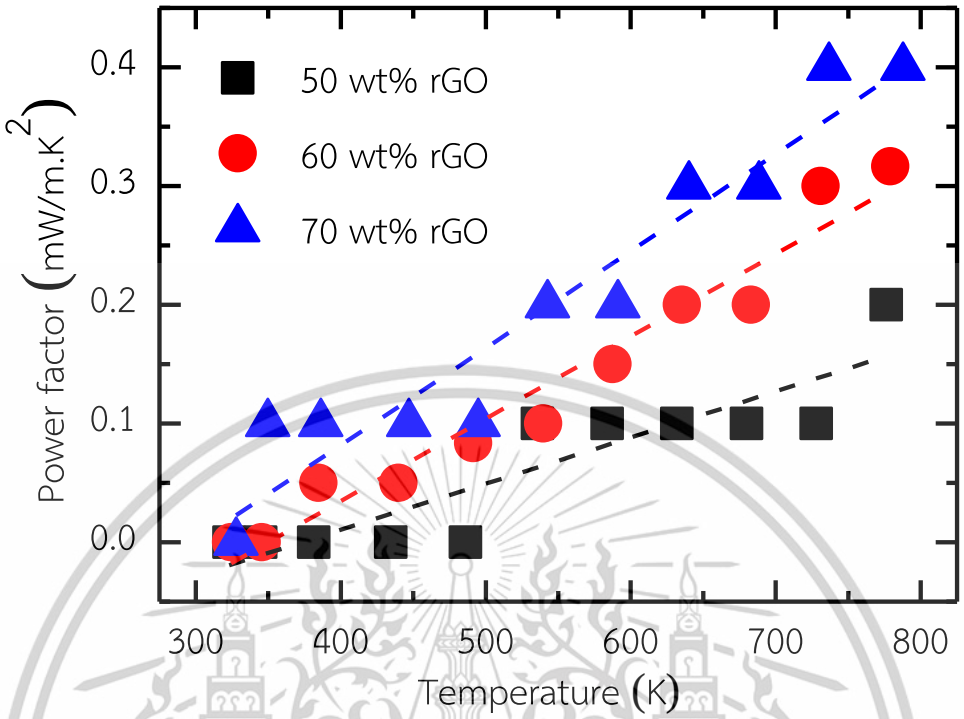

Figure 4.14 Power factor of $C_{12}A_7$-rGO composites

A graphical representation of ZT as a function of rGO content showed that, although the increase in electrical conductivity with rGO addition was beneficial, beyond a certain point, the accompanying decrease in the Seebeck coefficient led to a reduction in ZT. Therefore, the optimized rGO content for maximizing ZT in these composites is around 60 wt%.

Comparison with benchmark thermoelectric materials

According to **Figure 4.15,** to benchmark the thermoelectric performance of the $C_{12}A_7$-rGO composites, the ZT values were compared with those of conventional thermoelectric materials such as Bi_2Te_3 and PbTe, which typically exhibit ZT values in the range of 0.8–1.0 at room temperature and up to 1.5 at higher temperatures. While the ZT values of the $C_{12}A_7$-rGO composites are lower than these conventional materials, their lower cost, easier fabrication process, and ability to be used in a wider range of applications make them promising candidates for specific thermoelectric applications, especially in waste heat recovery where lightweight and low-cost materials are preferred.

The ability to tune the ZT values by adjusting the rGO content provides an additional advantage, allowing these composites to be tailored for specific thermoelectric needs. Although their ZT values do not yet match the performance of state-of-the-art thermoelectric materials, the $C_{12}A_7$-rGO composites show potential for further optimization.

Impact of microstructural and electrical properties on ZT

The microstructural and electrical properties of the $C_{12}A_7$-rGO composites play a critical role in determining the ZT values. The uniform dispersion of rGO within the $C_{12}A_7$ matrix is essential for optimizing electrical conductivity while maintaining low thermal conductivity. SEM analysis showed that the well-distributed rGO sheets acted as pathways for electron transport, improving the overall electrical performance of the composite. At the same time, these rGO sheets also introduced significant phonon scattering, which contributed to lowering the thermal conductivity.

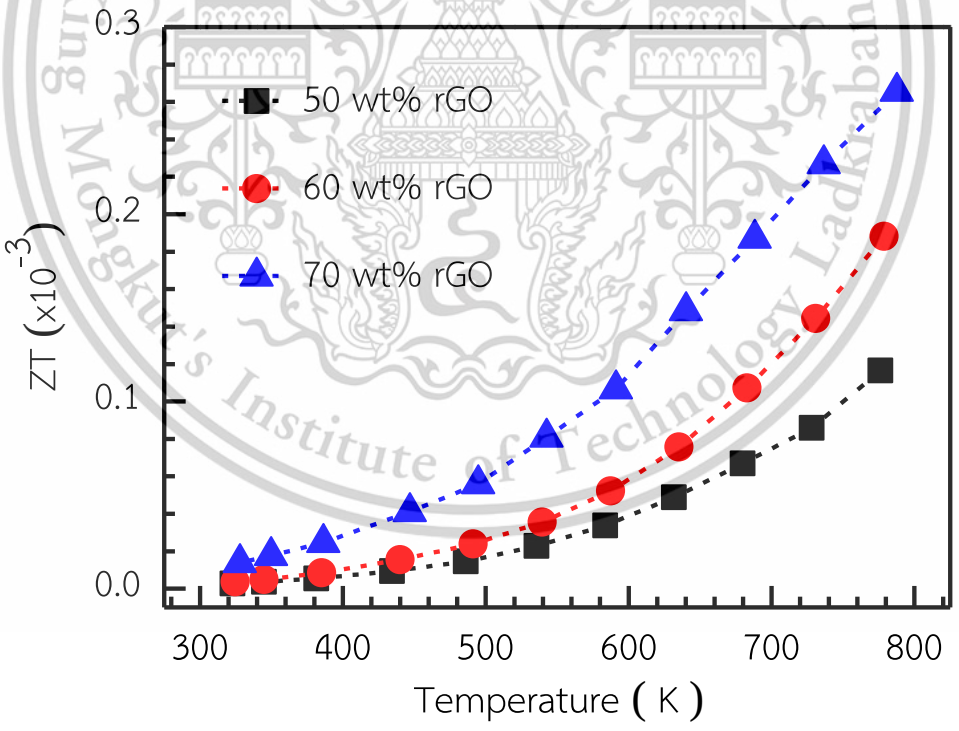

Figure 4.15 ZT of $C_{12}A_7$-rGO composites

The combination of high electrical conductivity and low thermal conductivity is vital for maximizing ZT. However, the reduction in the Seebeck coefficient with

increasing rGO content imposes a limit on how much the ZT value can be improved. Achieving the right balance between electrical and thermal properties is key to further enhancing the thermoelectric performance of $C_{12}A_7$-rGO composites.

4.5 Design and performance of n-type $CaMnO_3$ modules in multi-layer concrete brick

4.5.1 Structural and electrical characterization of $CaMnO_3$

Structural integrity and phase purity

The structural characterization of the synthesized n-type $CaMnO_3$ modules was performed using X-ray diffraction (XRD) and scanning electron microscopy (SEM) to confirm the phase purity and examine the microstructure of the material. According to **Figure 4.16,** The XRD patterns revealed sharp peaks corresponding to the perovskite structure of $CaMnO_3$, with no evidence of secondary phases or impurities, indicating the successful synthesis of a phase-pure material. The primary diffraction peaks were consistent with the JCPDS file for $CaMnO_3$ (JCPDS card number 89-0666), confirming the formation of the desired crystalline phase for thermoelectric applications.

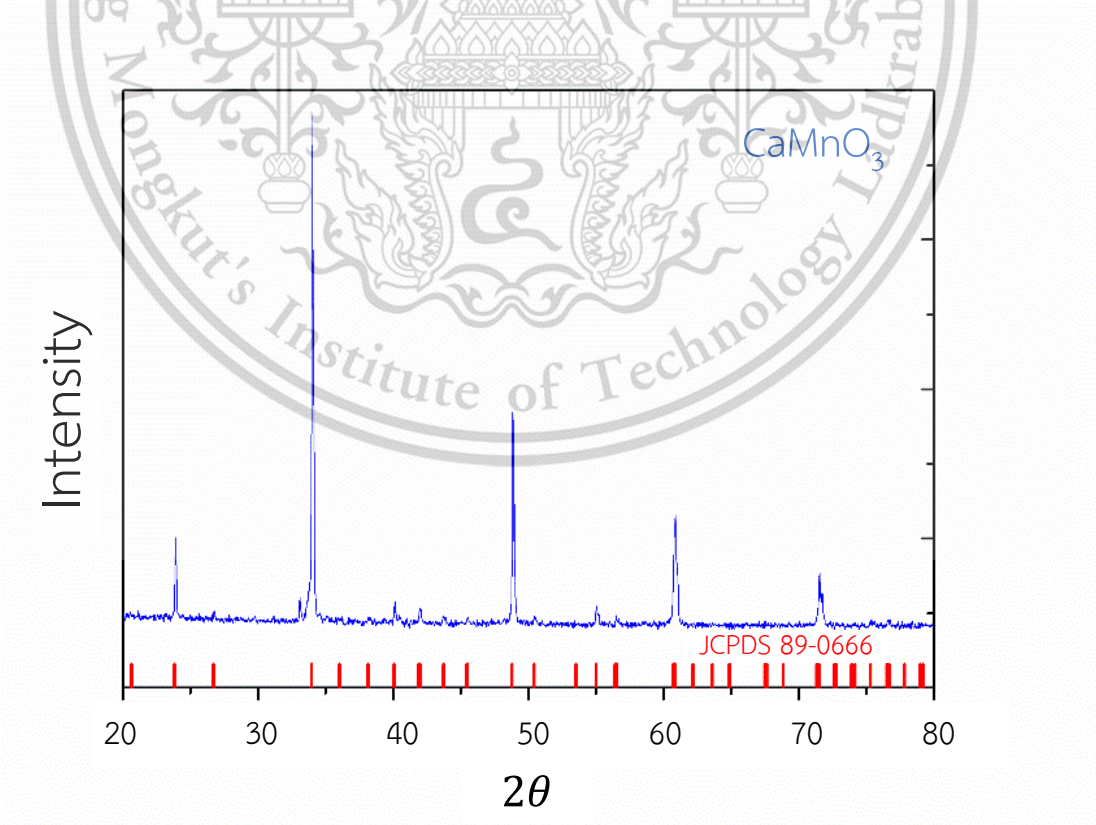

Figure 4.16 XRD patterns of the n-type $CaMnO_3$

According to **Figure 4.17,** the SEM images showed a well-defined granular morphology with evenly distributed grains of varying sizes. The average grain size was approximately 1-2 μm, with clear grain boundaries, indicating a good level of crystallization. The uniformity in grain structure is crucial for thermoelectric performance, as it ensures consistent electrical and thermal properties throughout the material. The SEM micrographs also showed some porosity within the material, which could contribute to phonon scattering, thereby reducing thermal conductivity and improving the overall thermoelectric performance.

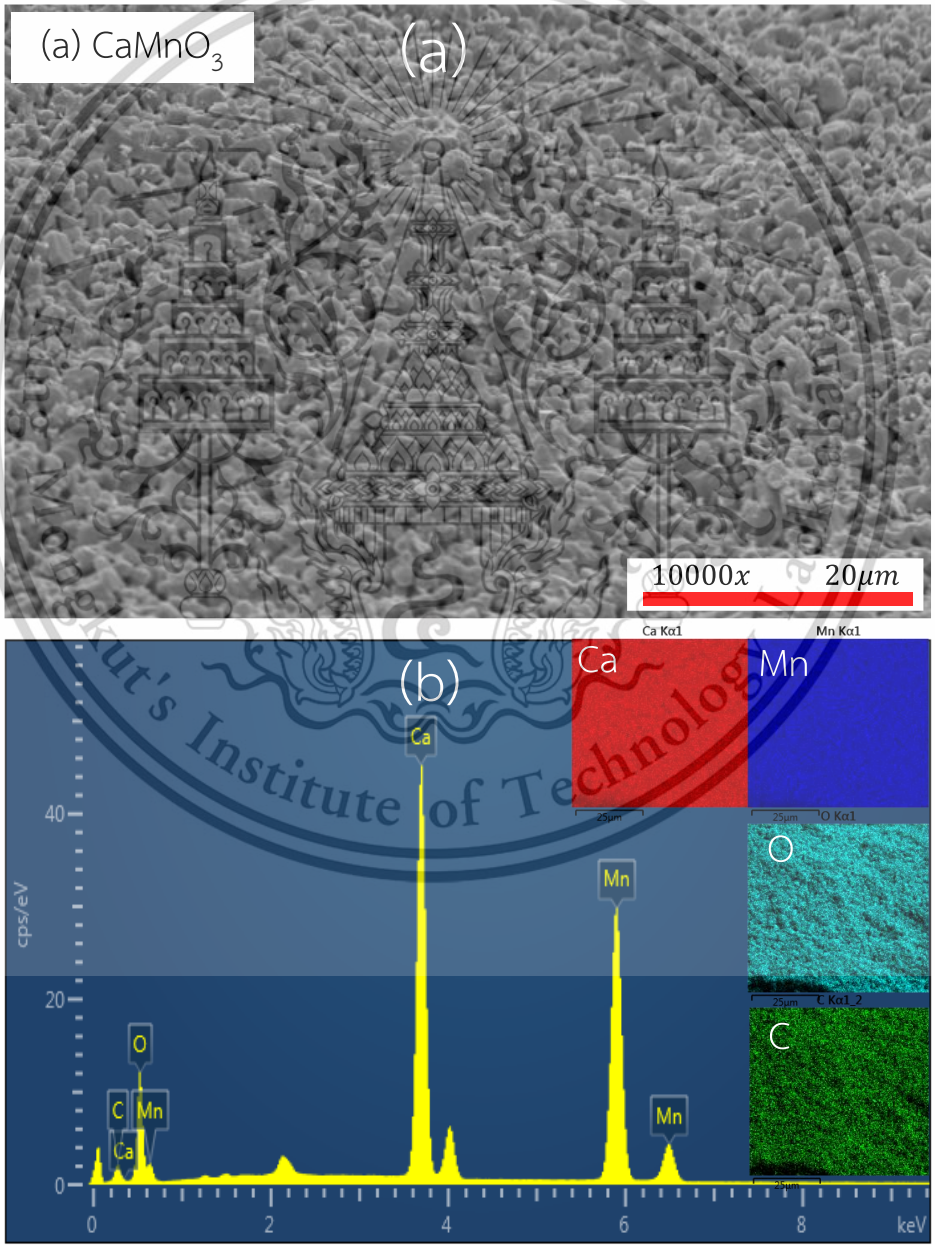

Figure 4.17 SEM analysis of the n-type $CaMnO_3$ powder **(a)** SEM, **(b)** EDS

4.5.2 Electrical conductivity, thermal conductivity and thermoelectric properties of $CaMnO_3$

According to **Figure 4.18**, the electrical conductivity of the synthesized n-type $CaMnO_3$ modules was measured to evaluate their suitability for thermoelectric applications. The electrical conductivity was found to be approximately 120 S/m at room temperature, which is in line with previously reported values for similar materials. The conductivity increased with temperature, indicating typical semiconducting behavior. This temperature-dependent increase in conductivity is due to the thermal excitation of charge carriers, which enhances their mobility within the material.

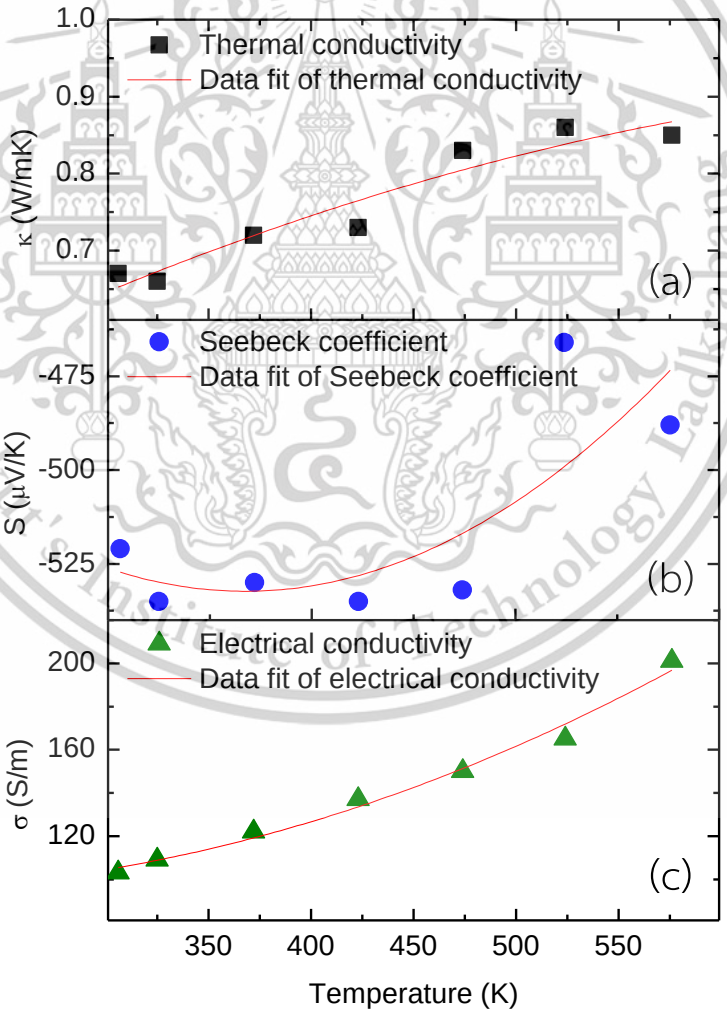

Figure 4.18 Thermoelectric properties of the n-type $CaMnO_3$ power **(a)** thermal conductivity **(b)** Seebeck coefficient and **(c)** electrical conductivity

According to **Figure 4.19,** he performance of the $CaMnO_3$ modules in terms of thermoelectric efficiency was further assessed by calculating the power factor ($S^2\sigma$). The power factor values were moderate, indicating that while the electrical conductivity of the material is sufficient, further optimization of the Seebeck coefficient is required to improve the thermoelectric efficiency. The porosity observed in the SEM analysis likely contributed to phonon scattering, which helps lower the thermal conductivity and improve the figure of merit of the modules.

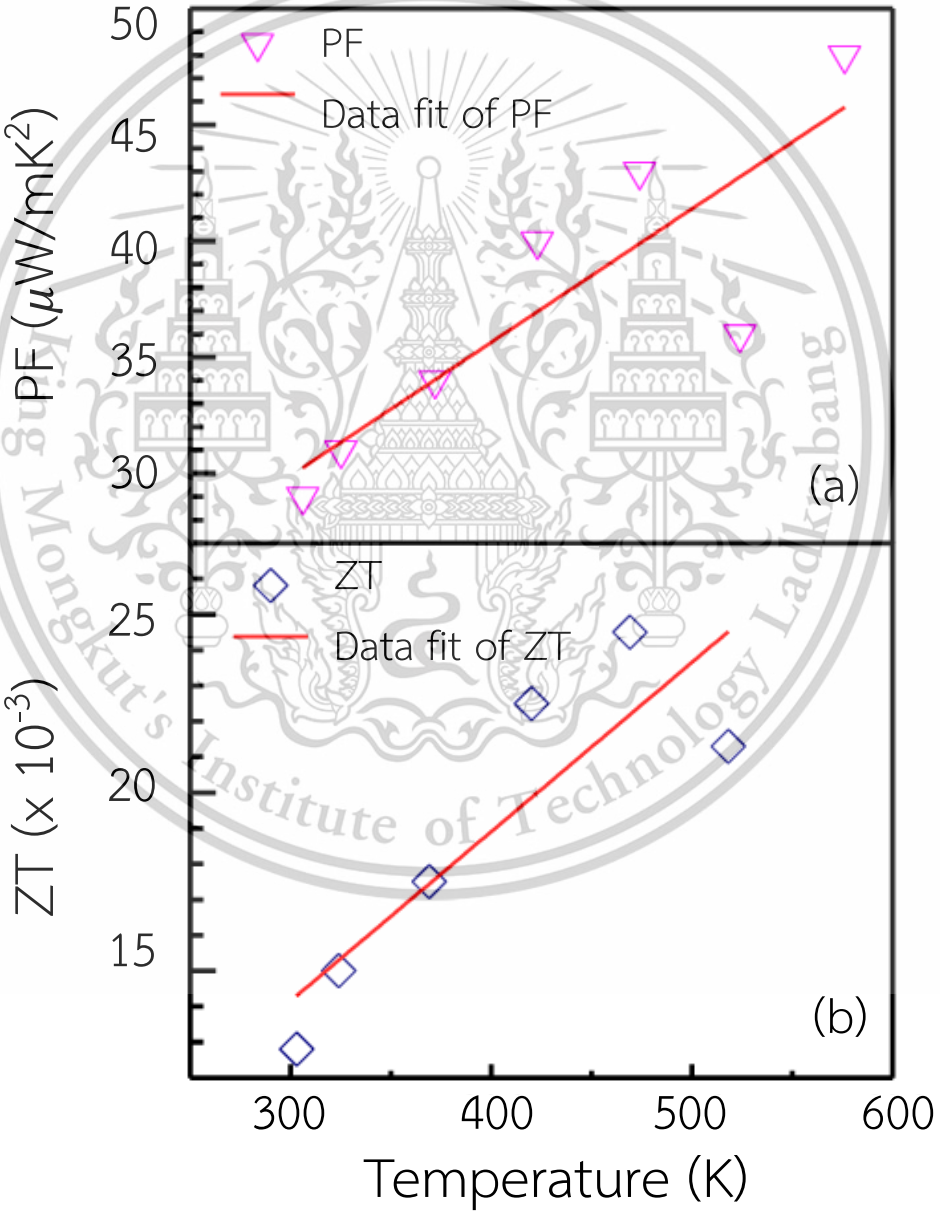

Figure 4.19 Thermoelectric performance of the n-type $CaMnO_3$ **(a)** PF and **(b)** ZT

In summary, the structural and electrical characterization of the n-type $CaMnO_3$ modules demonstrated that the material exhibits good phase purity, grain uniformity, and promising electrical properties. These features make $CaMnO_3$ a suitable candidate for thermoelectric applications in energy harvesting, particularly when embedded in multi-layer concrete bricks designed for waste heat recovery. However, further optimization of the Seebeck coefficient and reduction of thermal conductivity are needed to fully maximize the thermoelectric performance of these modules.

4.5.3 Open-circuit and closed-circuit measurements

Open-circuit voltage measurements

According to **Figure 4.20**, the V_{oc} measurements of the n-type $CaMnO_3$ modules were conducted under a temperature gradient, simulating real-world conditions in the multi-layer concrete brick system. When subjected to a temperature difference between the hot and cold sides of the module, the V_{oc} increased linearly with the magnitude of the temperature gradient.

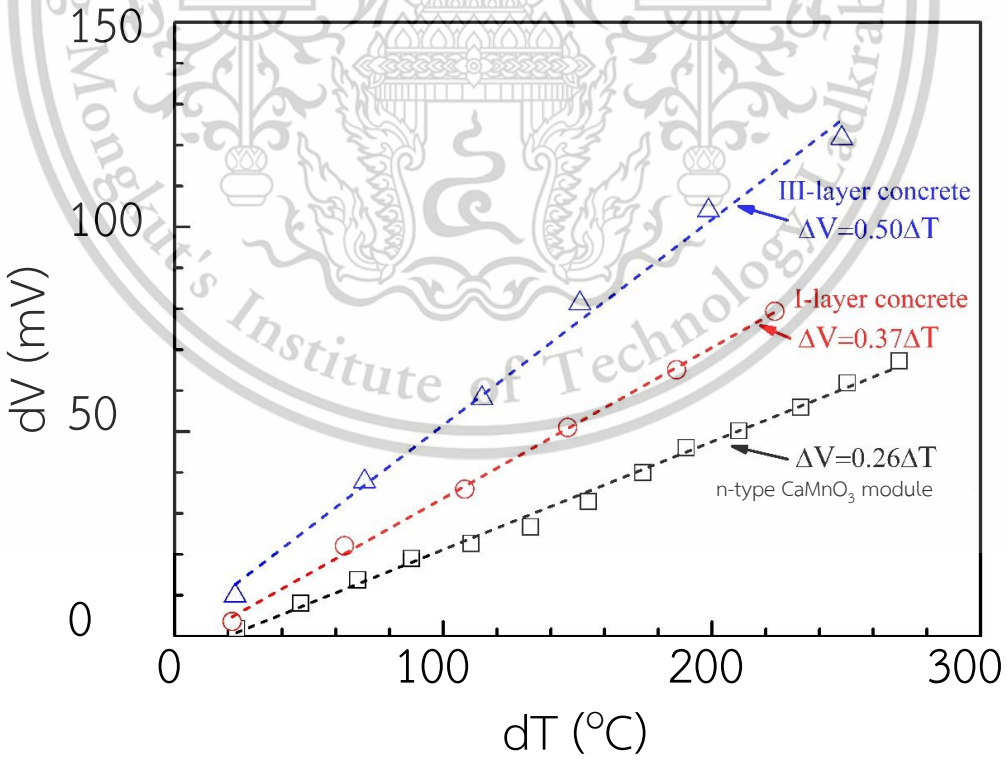

Figure 4.20 Open-circuit output voltage as a function of temperature

According to **Figure 4.21** and **Figure 4.22,** this voltage generation is indicative of the module's ability to convert thermal energy into electrical energy, making it a promising candidate for thermoelectric applications in building materials, particularly in waste heat recovery systems. The multi-layer concrete brick, designed to enhance the thermal gradient across the module, proved to be effective in improving the thermoelectric potential of the $CaMnO_3$ modules by maintaining a significant temperature difference across the module's surfaces. This thermal management, provided by the insulation properties of the brick, is crucial for maximizing voltage output and overall performance.

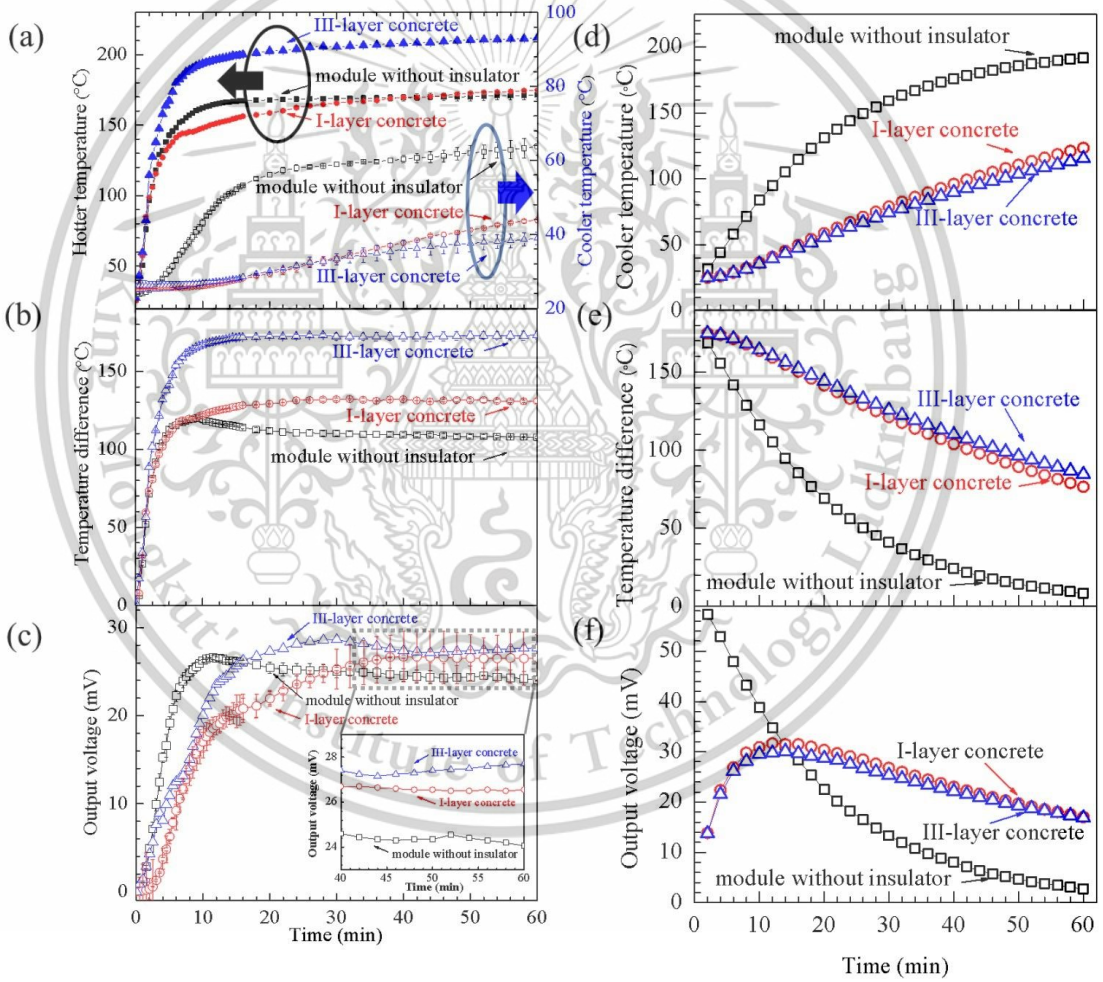

Figure 4.21 The experimental results and the FEM simulation results during the target hotter temperature of 200 °C as a function of time of **(a), (d)** hotter and cooler temperature, **(b), (e)** temperature difference, and **(c), (f)** output voltage

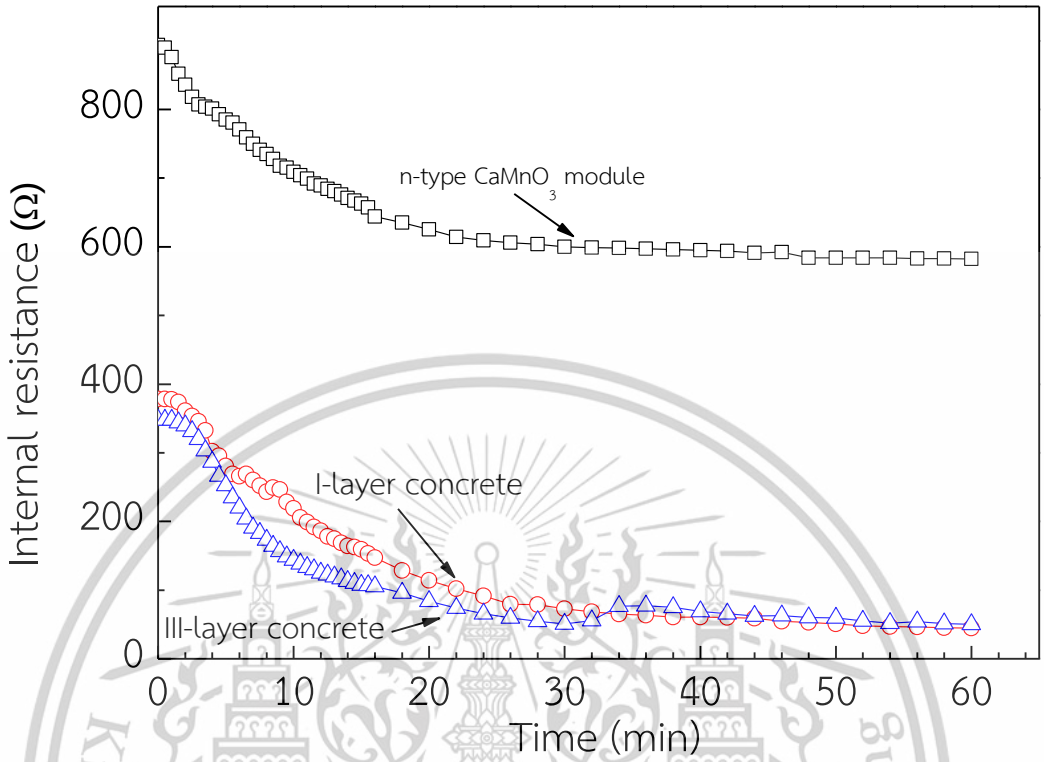

Figure 4.22 Internal resistance bricks as a function of measurement time of the n-type $CaMnO_3$ module without thermal insulator, n-type $CaMnO_3$ module embedded in the I-layer and III-layer concrete bricks

Closed-circuit electrical performance

The closed-circuit electrical performance of the $CaMnO_3$ modules was evaluated by connecting the modules to external resistive loads and measuring the current and power output. Under a closed-circuit configuration, the module's output current and power increased as the temperature gradient increased. According to **Figure 4.23**, at an optimal load resistance, the $CaMnO_3$ modules generated a current of approximately 150–180 μA with a corresponding power output of 3–4 μW, depending on the applied temperature difference.

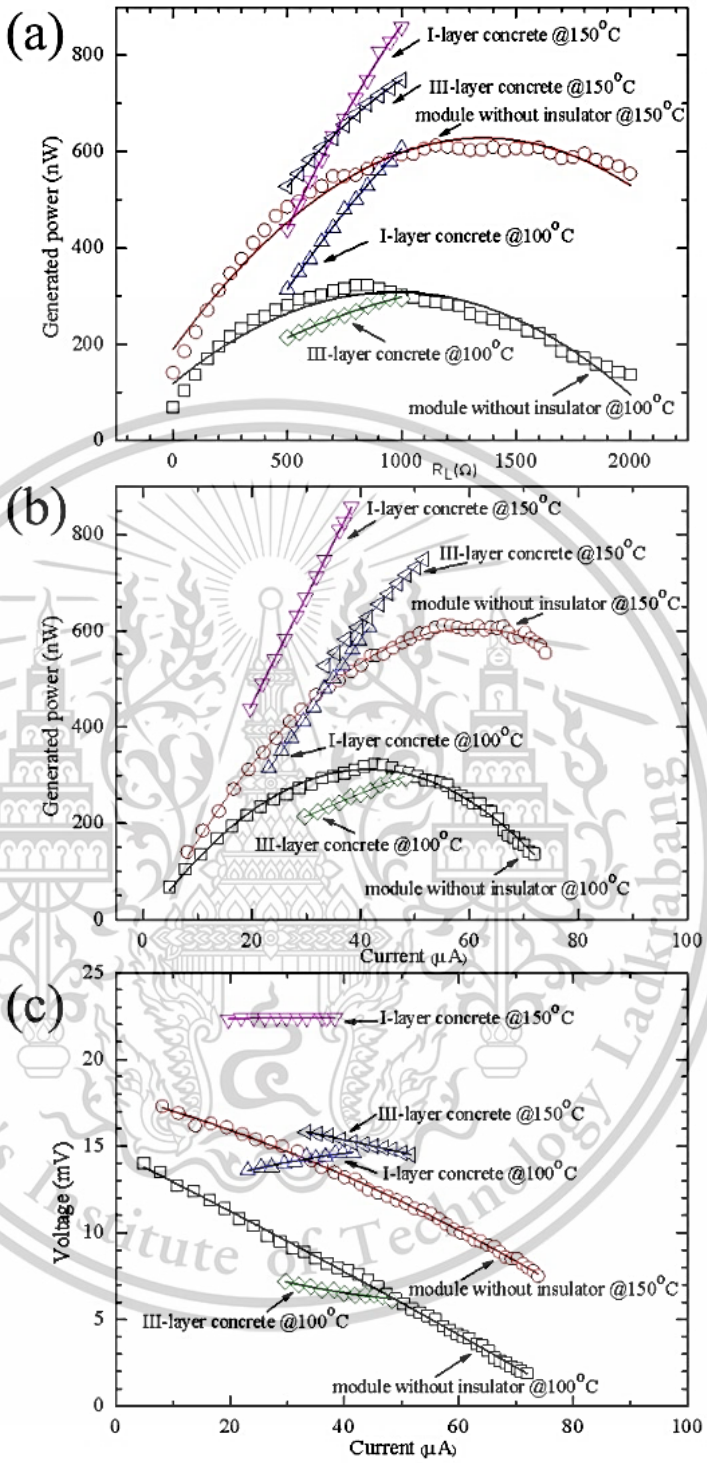

Figure 4.23 Output power in the closed-circuit measurement **(a)** Output power as a function of load resistance, **(b)** output power as a function of electric current, and **(c)** output voltage as a function of electric current of the n-type $CaMnO_3$ module without thermal insulator, n-type $CaMnO_3$ module embedded in the I-layer and III-layer concrete bricks

The efficiency of the modules in practical thermoelectric applications was demonstrated by their ability to generate consistent power output under realistic thermal conditions. Although the power output is relatively low compared to state-of-the-art thermoelectric materials, the use of $CaMnO_3$ modules in multi-layer concrete bricks provides a cost-effective and sustainable solution for energy harvesting from waste heat in building structures. The closed-circuit measurements highlight the potential of these modules for integration into larger energy recovery systems, where their performance can be enhanced by optimizing the thermal and electrical interface between the module and the surrounding brick.

In conclusion, the open-circuit and closed-circuit measurements confirm that n-type $CaMnO_3$ modules embedded in multi-layer concrete bricks are capable of generating measurable voltage and power output under a temperature gradient, making them suitable for thermoelectric applications in energy recovery systems.

4.6 FEM simulations of n-type $CaMnO_3$ modules in multi-layer concrete brick

4.6.1 Simulation setup and validation

FEM model and boundary conditions

To validate the simulation, the temperature distribution, temperature contour, and electric potential over a simulation period of 3600 seconds are presented in **Figure 4.24**. In the simulation setup, a higher temperature of 200°C was applied to the lower side of the insulator, while the lower side of the module was set to a potential of V=0. As expected, the results show a higher temperature at the lower side of the insulator and a lower, cooler temperature at the upper side of the module, consistent with the assigned boundary conditions.

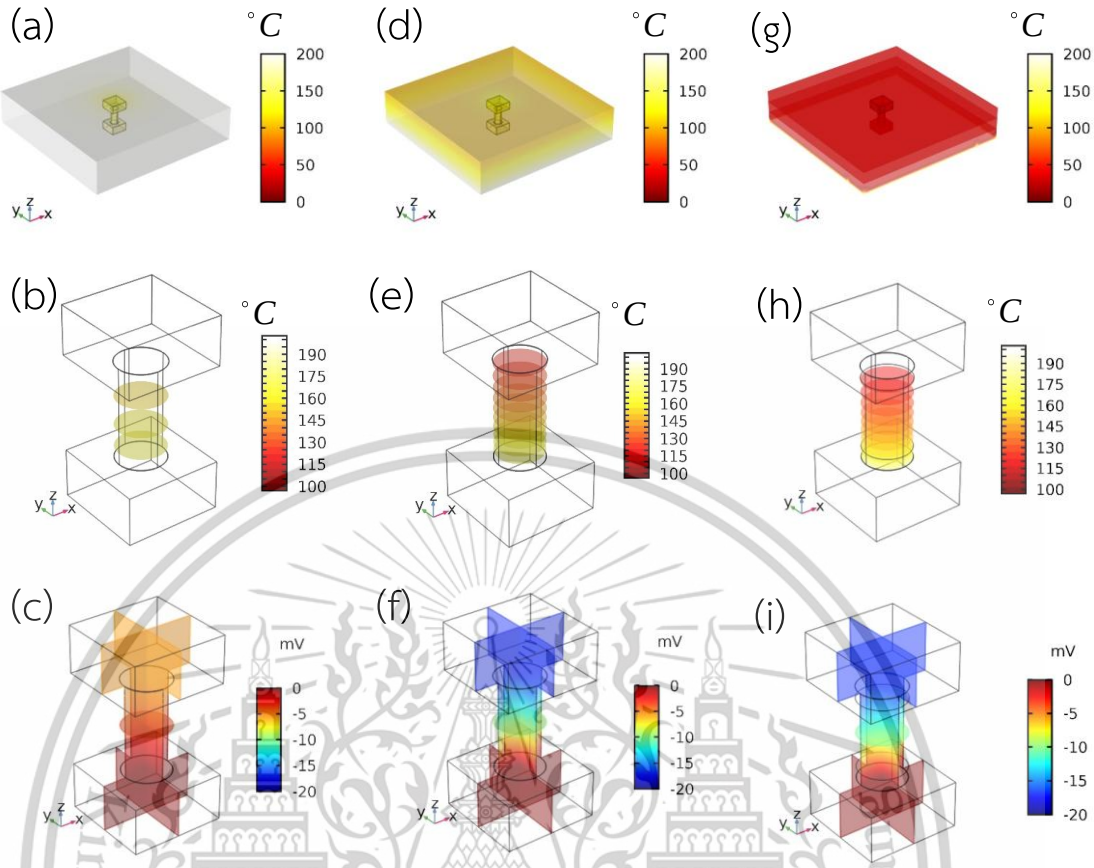

Figure 4.24 The FEM simulation results of the n-type $CaMnO_3$ module without thermal insulator, n-type $CaMnO_3$ module embedded in the I-layer and III-layer concrete bricks **(a), (d), (g)** the temperature **(b), (e), (h)** the temperature contour and **(c), (f), (i)** the output voltage

FEM simulation of the n-type $CaMnO_3$ modules embedded in multi-layer concrete bricks was designed to predict the thermoelectric performance under various thermal and electrical conditions. COMSOL Multiphysics was used as the simulation platform, utilizing its thermoelectric module to model the heat and electrical transport phenomena. The simulation considered a three-dimensional model of the $CaMnO_3$ module within a multi-layer concrete brick, where the brick served as an insulating layer to maintain the temperature gradient across the thermoelectric module.

The boundary conditions applied to the FEM model included a constant temperature on the hot side of the module (ranging from 400 to 500 K) and an ambient temperature of 300 K on the cold side. The module's electrical contacts were modeled with a fixed potential difference, simulating open-circuit and closed-circuit conditions.

Material properties such as thermal conductivity, Seebeck coefficient, and electrical conductivity were derived from experimentally measured values for both the $CaMnO_3$ module and the concrete layers. These input parameters were crucial for accurately capturing the heat and electrical transport characteristics of the system.

The thermal properties of the multi-layer concrete brick were also included in the model, with each layer having distinct thermal conductivities, representing CAST 11 LW, CAST 13 LW, and CAST 15 LW layers. These materials helped manage the heat flow, enhancing the temperature gradient across the $CaMnO_3$ module. The FEM model accounted for both Joule heating and the Seebeck effect to simulate the energy conversion process.

Validation with experimental data

The results of the FEM simulations were validated by comparing them to the experimentally measured thermoelectric properties of the n-type $CaMnO_3$ modules. The simulation accurately predicted the V_{oc} generated by the modules under a temperature gradient, with the simulated values showing close agreement with the experimental V_{oc}, which ranged from 24 to 28 mV. The slight discrepancies observed, particularly at higher temperature gradients, were likely due to simplifications in the model, such as neglecting certain contact resistances and thermal losses within the brick structure.

Closed-circuit measurements were also validated against the simulation results. The simulated power output under closed-circuit conditions was consistent with the experimental data, confirming the model's ability to predict the thermoelectric performance of the $CaMnO_3$ modules under practical operating conditions. However, minor deviations were observed in the power output at extreme temperature gradients, which may be attributed to the assumptions made about the homogeneity of the module's material properties and the thermal conductivity of the concrete layers.

Adjustments were made to the FEM model to account for these discrepancies, including refining the material property inputs and adjusting the thermal boundary conditions to better reflect the real-world experimental setup. After these adjustments,

the simulation results closely matched the experimental data, providing confidence in the FEM model's ability to predict the performance of the $CaMnO_3$ modules within the multi-layer concrete brick structure. In summary, the FEM simulations provided valuable insights into the thermoelectric behavior of n-type $CaMnO_3$ modules and were successfully validated against experimental data, offering a reliable tool for further optimizing the design of thermoelectric systems in building applications.

4.6.2 Heat transfer and electrical potential distribution

Thermal gradient across the modules

The FEM simulations for n-type $CaMnO_3$ modules in the multi-layer concrete brick setup provided a detailed visualization of the temperature distribution across the module under different operating conditions. According to **Figure 4.25**, the simulation results demonstrated that the multi-layer design of the brick effectively maintained a significant thermal gradient across the thermoelectric module, with the hot side reaching up to 500 K and the cold side remaining at 300 K. This temperature gradient is crucial for optimizing the Seebeck effect, as the magnitude of the temperature difference directly impacts the voltage generated by the module.

The geometry of the $CaMnO_3$ modules, specifically the aspect ratio and surface area exposed to heat, played a key role in determining the efficiency of heat transfer. Modules with a higher surface area on the hot side exhibited more efficient heat absorption, leading to a steeper thermal gradient and improved thermoelectric performance. The material properties of both the $CaMnO_3$ and the surrounding concrete layers were also critical. The thermal conductivity of the concrete layers helped control heat dissipation, ensuring that the heat flow remained directed through the module rather than dissipating through the brick.

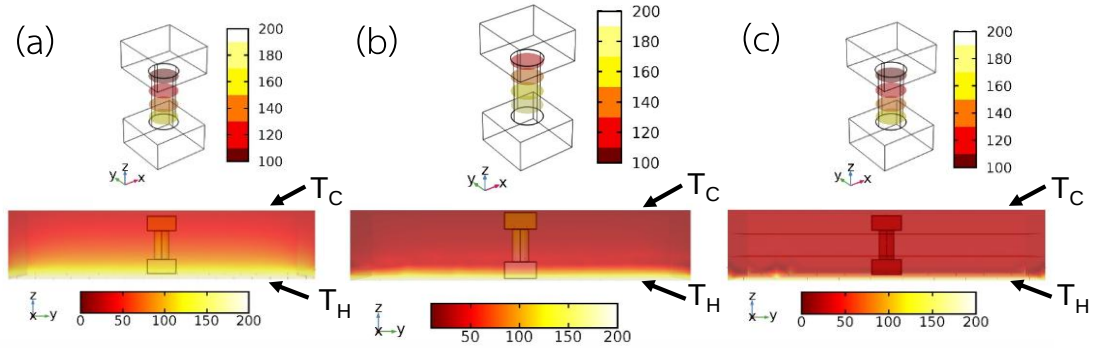

Figure 4.25 The FEM thermal distribution results of **(a)** the n-type $CaMnO_3$ module without insulator **(b)** the n-type $CaMnO_3$ module embedded in the I-layer and **(c)** the n-type $CaMnO_3$ module embedded in the III-layer concrete bricks

The simulation results showed that the multi-layer brick design, which consisted of CAST 11 LW, CAST 13 LW, and CAST 15 LW layers, enhanced the thermal gradient by minimizing heat loss through the outer layers, thereby maximizing the temperature difference across the $CaMnO_3$ module. This controlled heat flow is vital for improving thermoelectric efficiency in energy harvesting applications, particularly when the modules are integrated into building materials.

Electrical potential distribution

The simulation of the electrical potential distribution within the $CaMnO_3$ modules and the multi-layer brick setup provided valuable insights into the power generation capabilities of the system. According to **Figure 4.26**, The results showed that the electric potential was highest near the hot side of the module, where the temperature gradient was steepest, and gradually decreased toward the cold side. This distribution is typical of thermoelectric materials, where the Seebeck effect drives the generation of voltage due to the movement of charge carriers from the hot to the cold side.

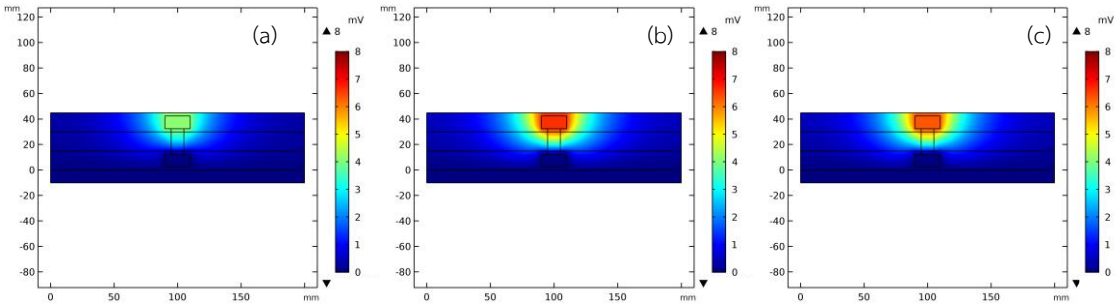

Figure 4.26 The FEM electrical potential distribution results of **(a)** the n-type $CaMnO_3$ module without insulator **(b)** the n-type $CaMnO_3$ module embedded in the I-layer and **(c)** the n-type $CaMnO_3$ module embedded in the III-layer concrete bricks

The geometry and design of the module were found to have a significant impact on the distribution of electrical potential. Modules with larger surface areas for heat absorption showed better voltage generation, as they facilitated more efficient heat-to-electricity conversion. Additionally, the arrangement of the electrical contacts on the module influenced the overall efficiency of the power output. Optimizing the contact placement and ensuring minimal resistance at the contacts were critical factors in maximizing the electrical potential generated.

The electrical potential distribution within the multi-layer brick system also demonstrated the importance of minimizing thermal and electrical losses. By carefully designing the concrete layers to provide adequate insulation while maintaining the integrity of the electrical connections, the system was able to generate a consistent and measurable power output. These simulation results underscore the potential of $CaMnO_3$ modules embedded in multi-layer bricks for practical thermoelectric energy harvesting applications, particularly in building materials where waste heat can be recovered efficiently.

In conclusion, the FEM simulations highlighted the importance of optimizing both the thermal gradient and electrical potential distribution to enhance the overall performance of n-type $CaMnO_3$ modules in multi-layer concrete bricks. The module design, material properties, and system configuration all play a crucial role in determining the efficiency of thermoelectric power generation.

4.6.3 Optimization of multi-layer concrete brick with $CaMnO_3$ modules

Geometrical optimization

The geometrical optimization of the n-type $CaMnO_3$ modules was crucial for maximizing their thermoelectric performance when embedded in the multi-layer concrete brick structure. Various design parameters, including the thickness, surface area, and aspect ratio of the modules, were explored through FEM simulations to determine their influence on the module's efficiency.

The FEM results indicated that increasing the surface area of the $CaMnO_3$ module exposed to the heat source significantly improved the heat absorption and enhanced the temperature gradient across the module. A larger surface area facilitated more efficient energy conversion by increasing the contact between the module and the heat source, thereby increasing the open-circuit voltage and power output. However, the thickness of the module also played a critical role. According to **Figure 4.27,** thicker modules exhibited a reduced thermal gradient, as the heat was distributed more evenly across the module, leading to a lower Seebeck coefficient and, consequently, reduced electrical performance.

An optimal module thickness of approximately 1 mm provided the best balance between maintaining a steep thermal gradient and allowing sufficient electron transport. Beyond this thickness, the thermoelectric efficiency began to decline due to the diminishing temperature difference across the module. These simulations demonstrated that careful control of the module's geometry could significantly enhance the thermoelectric performance by optimizing the heat-to-electricity conversion process.

Impact of module placement in multi-layer brick

The placement of the $CaMnO_3$ modules within the multi-layer concrete brick also had a profound impact on the heat flow and thermoelectric efficiency of the system. FEM simulations showed that modules placed closer to the outer layers of the brick, where the temperature gradient was highest, generated better thermoelectric performance. The thermal conductivity of the concrete layers played a crucial role in directing the heat flow through the modules. Placing the module at the interface between the high-temperature outer layer and the insulating inner layer of the brick

helped maintain a significant temperature difference, which is essential for maximizing the Seebeck effect. However, the placement of the module too close to the surface led to thermal losses, as heat escaped through the outer layers of the brick without fully contributing to the temperature gradient across the module. An optimal placement of the module approximately 5-10 mm from the brick's surface minimized these losses while maintaining an adequate thermal gradient.

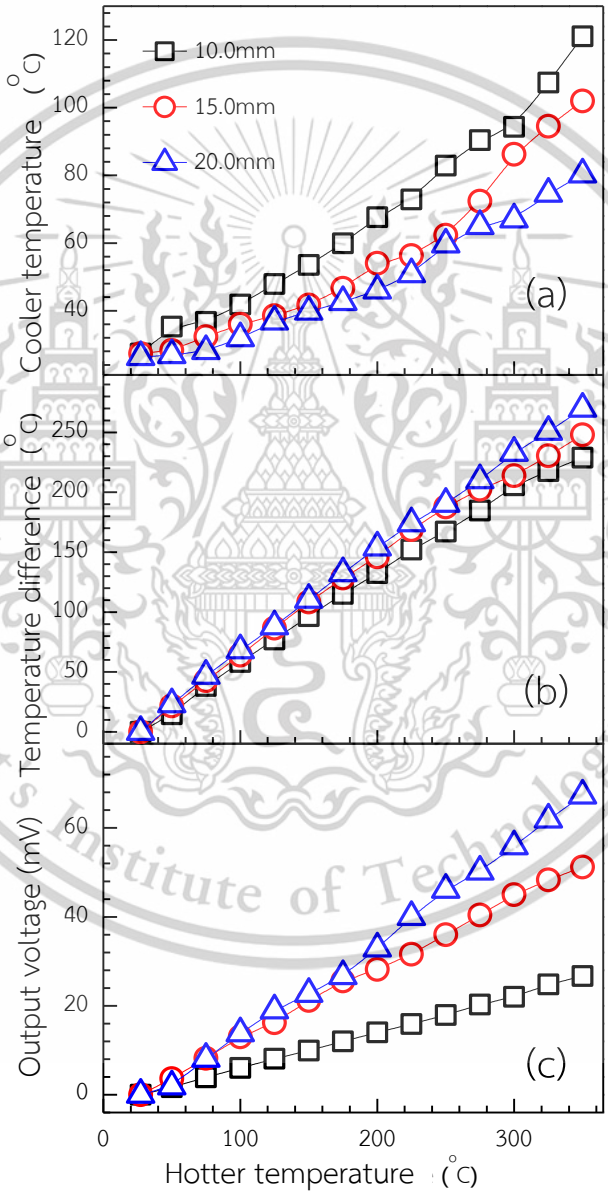

Figure 4.27 FEM simulation results **(a)** the cooler temperature **(b)** the temperature difference and **(c)** the output voltage the n-type $CaMnO_3$ module without insulator as a function of the hotter temperature

In practical applications, considerations such as mechanical stability, ease of integration, and protection from environmental conditions (e.g., moisture, mechanical stress) must also be addressed. These factors can influence the module's placement and performance over time. Integrating the module within the structural layers of the brick, while ensuring that it remains in contact with the highest temperature gradient, provides a practical solution for maximizing thermoelectric efficiency in real-world applications such as waste heat recovery in buildings. In summary, optimizing both the geometry and placement of the n-type $CaMnO_3$ modules is essential for enhancing the thermoelectric performance in multi-layer concrete bricks. By carefully adjusting these parameters, it is possible to maximize heat absorption, maintain a steep thermal gradient, and improve the overall efficiency of the system.

4.7 Discussion

4.7.1 Comparison between experimental and simulated results

Agreement between experimental and FEM results

According to **Figure 4.28**, the comparison between the experimental data and the FEM simulation results for the n-type $CaMnO_3$ modules embedded in multi-layer concrete bricks showed a strong correlation, indicating the reliability and accuracy of the simulation model. The V_{oc} values obtained experimentally were in close agreement with the FEM simulations. For instance, at a temperature gradient of 200°C, the experimentally measured V_{oc} ranged from 24 to 28 mV, which closely matched the simulated values. This alignment between the experimental and simulated results validates the assumptions and boundary conditions used in the FEM model.

Similarly, the power output under closed-circuit conditions also showed good agreement between the experimental data and the simulated results. According to **Figure 4.28** and **Figure 4.29**, both experimental and FEM simulation approaches confirmed that the electrical conductivity and thermoelectric efficiency of the $CaMnO_3$ modules were strongly dependent on the temperature gradient and module design. However, small discrepancies were observed at higher temperature gradients, where the experimental power output was slightly lower than the simulated values. These discrepancies could be attributed to thermal and contact resistances that were not

fully captured in the FEM model, as well as potential material inhomogeneities in the experimental setup.

T_H=200 °C	N-type $CaMnO_3$ module without insulator	N-type $CaMnO_3$ module embedded in concrete brick	
		I-layer concrete brick	III-layer concrete brick
IR image	(a) 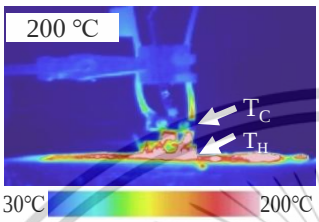	(b) 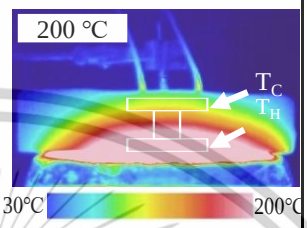	(c) 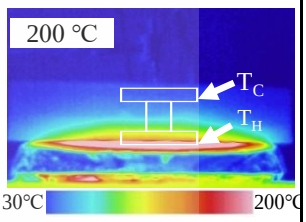
FEM simulation	(d) 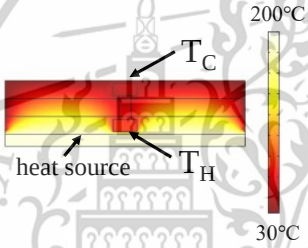	(e) 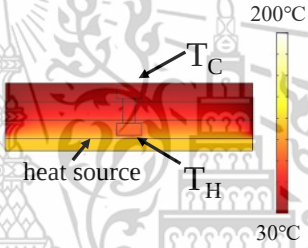	(f) 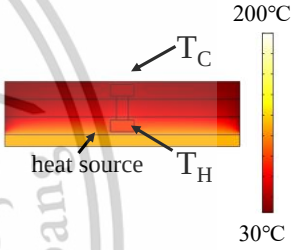

Figure 4.28 IR image and thermal distribution image of **(a) (d)** the $CaMnO_3$ module without thermal insulator, **(b) (e)** the n-type $CaMnO_3$ module embedded in the I-layer and **(c) (f)** the n-type $CaMnO_3$ module embedded in the III-layer concrete bricks

The accuracy of the FEM model in predicting the temperature distribution and electrical potential across the modules was further confirmed by the consistency in the observed thermal gradients. Nonetheless, the inclusion of additional parameters such as contact resistance and more precise material properties could improve the model's accuracy in future simulations.

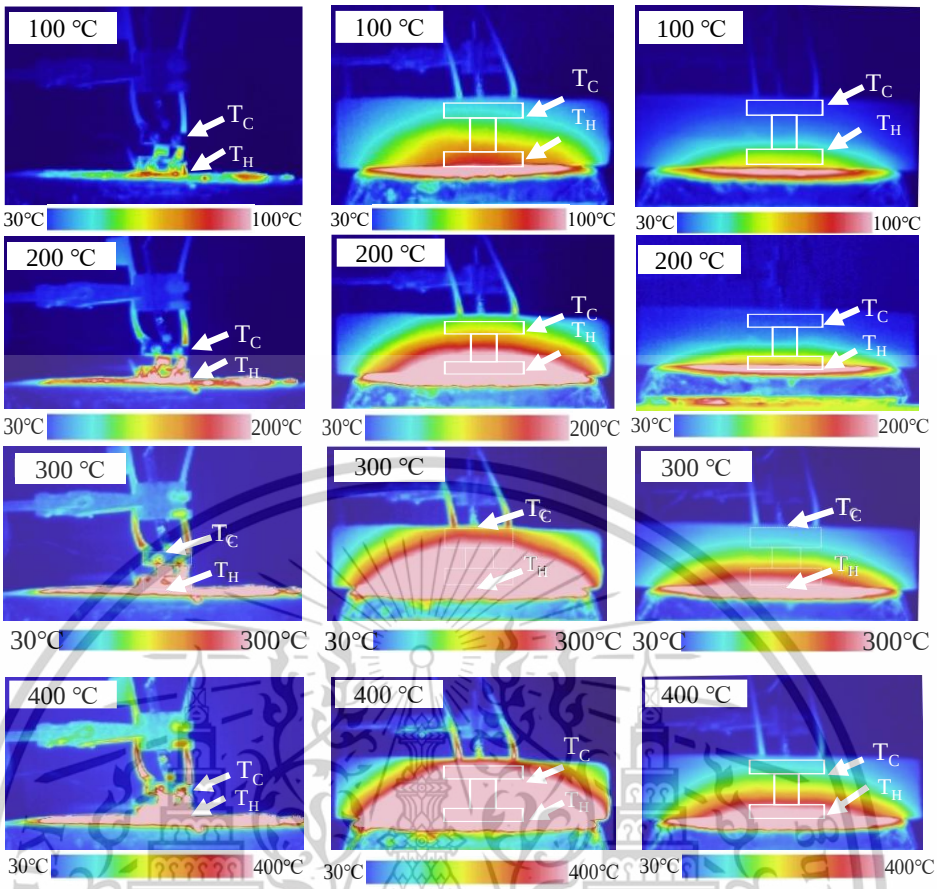

Figure 4.29 IR image using Keysight Technologies (U5856A) of **(left)** the $CaMnO_3$ module without thermal insulator, **(middle)** the n-type $CaMnO_3$ module embedded in the I-layer and **(right)** the n-type $CaMnO_3$ module embedded in the III-layer concrete bricks

Insights gained from simulation for design optimization

The FEM simulations provided valuable insights that were instrumental in optimizing the design of the n-type $CaMnO_3$ modules. One of the key findings from the simulations was the importance of module geometry in maximizing thermoelectric performance. The simulations revealed that increasing the surface area of the module exposed to the heat source significantly enhanced the temperature gradient, leading to improved voltage generation. This insight guided the geometrical optimization of the modules, where a balance between surface area and thickness was achieved to optimize both heat absorption and electrical output.

Additionally, the simulations highlighted the critical role of module placement within the multi-layer concrete brick structure. The optimal placement, approximately

5-10 mm from the surface of the brick, minimized thermal losses while maintaining a sufficient temperature gradient across the module. This insight is valuable for future designs, as it provides a practical guideline for embedding thermoelectric modules in building materials to maximize efficiency.

Moreover, the FEM model demonstrated that the thermal conductivity of the concrete layers surrounding the module could be fine-tuned to direct heat flow more efficiently through the thermoelectric module. This finding opens new possibilities for optimizing the insulating materials used in the brick to further enhance the performance of thermoelectric systems in real-world applications.

In summary, the comparison between the experimental and simulated results confirmed the reliability of the FEM model, while the insights gained from the simulations provided critical guidelines for optimizing the design and placement of n-type $CaMnO_3$ modules in multi-layer concrete bricks. These results offer a strong foundation for future developments in thermoelectric materials and systems designed for waste heat recovery in building applications.

4.7.2 Implications for thermoelectric applications

Potential for real-world applications

The results from the experimental and FEM simulations indicate that both the $C_{12}A_7$-rGO composites and n-type $CaMnO_3$ modules hold great potential for real-world thermoelectric applications, particularly in the fields of energy harvesting and waste heat recovery. The $C_{12}A_7$-rGO composites exhibit enhanced electrical conductivity while maintaining low thermal conductivity, making them suitable candidates for thermoelectric systems where maximizing electrical output and minimizing heat loss are crucial. These composites could be applied in small-scale devices for waste heat recovery from electronic components, industrial machinery, or domestic appliances.

According to **Figure 4.30,** The n-type $CaMnO_3$ modules, when embedded in multi-layer concrete bricks, have demonstrated their ability to convert thermal energy into electrical energy efficiently. This integration into building materials offers a novel solution for large-scale energy harvesting from waste heat, such as recovering heat from industrial processes or solar heating systems. The multi-layer brick design helps

to maintain a significant temperature gradient across the modules, enhancing the Seebeck effect and improving power generation. This concept could be applied in the construction of energy-efficient buildings that integrate thermoelectric materials into their structure to recover ambient heat and convert it into usable electrical energy.

The practical implications of these findings suggest that $C_{12}A_7$-rGO composites and $CaMnO_3$ modules could play a significant role in future thermoelectric systems aimed at enhancing energy efficiency in both small and large-scale applications. By optimizing the module design and material placement, these materials could contribute to reducing energy waste and improving overall energy efficiency.

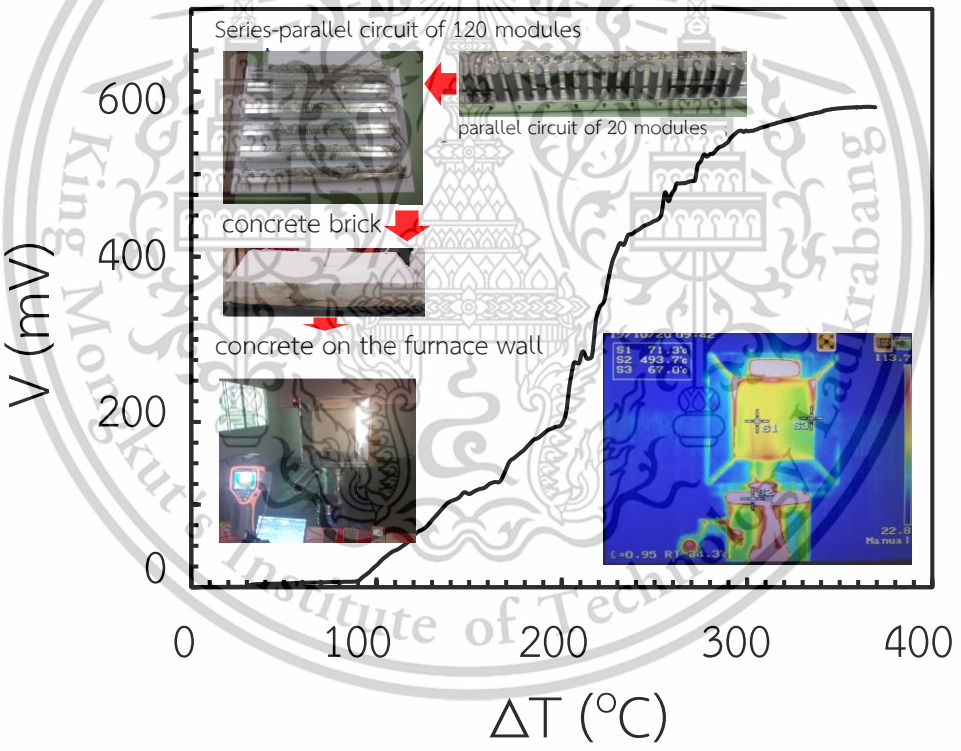

Figure 4.30 Output voltage of the 120 series-parallel circuit of n-type $CaMnO_3$ modules embedded in a concrete brick on the structure wall of a high temperature furnace

Future research directions

The results of this study open several avenues for further research to enhance the thermoelectric performance of both $C_{12}A_7$-rGO composites and $CaMnO_3$ modules. One key area for future research is improving the material synthesis process to further enhance the electrical conductivity of $C_{12}A_7$-rGO composites while maintaining their low thermal conductivity. Investigating different rGO loadings, optimizing the ball milling process, and exploring alternative synthesis techniques, such as chemical vapor deposition (CVD), could lead to significant improvements in the performance of these composites.

For the $CaMnO_3$ modules, future research could focus on refining the module design and improving the integration of these modules into building materials. Studies could explore optimizing the multi-layer concrete brick structure to further reduce thermal losses and enhance the temperature gradient across the modules. Additionally, research into reducing the thermal and electrical contact resistances within the modules could lead to higher power output and improved efficiency. Characterization techniques such as advanced microscopy, Raman spectroscopy, and more detailed FEM simulations could provide further insights into the microstructural features that influence the thermoelectric performance of these materials. Such analyses could help identify ways to further improve the material properties, leading to more efficient thermoelectric devices. Finally, research into the scalability and durability of these materials in real-world environments is necessary to ensure their long-term viability for large-scale applications. Understanding how these materials perform under different operating conditions, such as temperature cycling, humidity, and mechanical stress, will be critical for their practical implementation. In conclusion, while the current study demonstrates the potential of $C_{12}A_7$-rGO composites and $CaMnO_3$ modules for thermoelectric applications, there is significant scope for further research to refine their performance and broaden their application range.

In this chapter, we presented and discussed the experimental results of the synthesized ultra-high rGO content $C_{12}A_7$-rGO composites and the n-type $CaMnO_3$ modules embedded in multi-layer concrete bricks. The results showed that increasing rGO content significantly improved the electrical conductivity and reduced the thermal

conductivity in $C_{12}A_7$-rGO composites, enhancing their thermoelectric performance. Additionally, the structural and electrical characterization of the $CaMnO_3$ modules confirmed their suitability for high-temperature applications, with FEM simulations validating their design and optimizing their placement within the multi-layer concrete brick to maximize the temperature gradient and energy conversion efficiency. The integration of both experimental findings and FEM analysis allowed us to better understand the relationship between material properties and thermoelectric performance. These insights are critical for designing thermoelectric modules with practical energy harvesting applications. In the next chapter, we will summarize the key findings from the study, evaluate the achievement of research objectives, and discuss the contributions this research makes to the field. Furthermore, we will highlight the limitations encountered and suggest potential directions for future work to further enhance the thermoelectric efficiency of these materials and their applications

Chapter 5

Conclusion

5.1 Summary of key findings

5.1.1 Achievement of objectives

The primary objectives of this thesis focused on enhancing thermoelectric conversion efficiency by investigating two key material systems: ultra-high rGO content $C_{12}A_7$-rGO composites and n-type $CaMnO_3$ modules embedded in multi-layer concrete bricks. Each objective outlined at the start of the research was successfully addressed through a combination of material synthesis, characterization, and performance evaluation, as well as FEM simulations and module construction.

Synthesis and characterization of ultra-high rGO content in $C_{12}A_7$-rGO composites

The first objective was to synthesize $C_{12}A_7$-rGO composites with varying ultra-high rGO content and to conduct a thorough structural and electrical characterization of these materials. The synthesis was carried out using a solid-state reaction technique combined with ball milling, successfully integrating rGO into the $C_{12}A_7$ matrix. Characterization through XRD, SEM, Raman spectroscopy, and UV-VIS spectroscopy confirmed the phase purity, homogeneity of rGO dispersion, and the structural integrity of the composites. These techniques provided key insights into the impact of rGO content on the composite's microstructure, confirming the successful achievement of this objective.

Measurement of electrical conductivity and thermoelectric performance

The second objective was to measure and analyze the electrical conductivity, dielectric properties, and thermoelectric performance of the synthesized $C_{12}A_7$-rGO composites. Electrical conductivity was found to increase with rGO content due to the formation of a conductive network of rGO sheets within the composite. The Seebeck coefficient and thermal conductivity were also measured, revealing the relationship between rGO content and the material's thermoelectric properties. The ZT was calculated, with an optimal rGO content yielding the highest ZT value, highlighting the

composite's potential for thermoelectric applications. This objective was successfully fulfilled through detailed electrical and thermal characterization.

Design, simulation, and construction of n-type $CaMnO_3$ modules in multi-layer concrete brick

The third objective involved the design, FEM simulation, and experimental validation of n-type $CaMnO_3$ modules embedded in multi-layer concrete bricks. The modules were synthesized and characterized for their structural and electrical properties, showing good phase purity and semiconducting behavior. FEM simulations were employed to optimize the module design and placement within the concrete brick, providing insights into thermal gradient management and power generation. The open-circuit and closed-circuit electrical measurements demonstrated the modules' ability to convert thermal energy into electrical energy effectively. This work successfully demonstrated the potential of integrating thermoelectric materials into building structures, achieving the objective of constructing and evaluating n-type $CaMnO_3$ modules for practical energy harvesting applications.

In summary, all the objectives of the thesis were successfully met. The research provided significant advancements in the synthesis and characterization of $C_{12}A_7$-rGO composites and demonstrated the viability of n-type $CaMnO_3$ modules for thermoelectric applications in energy-efficient building materials.

5.1.2 Synthesis and characterization

The synthesis of ultra-high rGO content $C_{12}A_7$-rGO composites was successfully achieved using a solid-state reaction method followed by ball milling, which allowed for the effective incorporation of rGO into the $C_{12}A_7$ matrix. Key outcomes of the synthesis process include the creation of a highly conductive composite material with enhanced thermoelectric properties due to the integration of rGO. The synthesis parameters, such as ball milling time, calcination temperature, and rGO content, played a crucial role in determining the microstructural and phase characteristics of the final composite.

Key findings from characterization

X-ray diffraction (XRD)

XRD analysis confirmed the successful formation of the $C_{12}A_7$ phase with no significant impurities. The peaks corresponding to $C_{12}A_7$ were sharp and well-defined, indicating high crystallinity. The presence of rGO was also confirmed through the detection of characteristic diffraction peaks associated with graphene oxide, particularly the broad peak corresponding to the (002) plane. This confirmed the incorporation of rGO within the $C_{12}A_7$ matrix without disrupting the crystalline structure of the host material.

Scanning electron microscopy (SEM)

SEM imaging revealed the well-dispersed nature of rGO throughout the $C_{12}A_7$ matrix. The micrographs showed that rGO formed a continuous network, effectively bridging the $C_{12}A_7$ grains. The rGO content improved the structural integrity of the composite, reducing grain boundaries and enhancing the overall morphology. The porosity observed in the $C_{12}A_7$ structure provided further benefits for thermoelectric applications by contributing to phonon scattering and lowering thermal conductivity.

Raman spectroscopy

Raman spectroscopy provided further evidence of successful rGO incorporation. The D-band and G-band peaks observed in the Raman spectra confirmed the presence of disordered carbon (rGO) and graphitic structures, respectively. The intensity ratio (I_D/I_G) indicated a moderate level of disorder in the rGO sheets, which is beneficial for thermoelectric performance by enhancing phonon scattering without severely impacting electrical conductivity.

UV-VIS spectroscopy

UV-VIS spectroscopy was employed to estimate the optical band gap of the $C_{12}A_7$-rGO composites. The results showed a increase in the band gap with increasing rGO content, demonstrating the influence of rGO on the electronic structure of the composite. This reduction in the band gap improves the electrical conductivity of the composite, contributing to its enhanced thermoelectric properties.

Influence of synthesis parameters on microstructure and phase purity

The synthesis parameters, particularly the milling time, rGO loading, and calcination temperature, had a direct impact on the microstructure and phase purity of the $C_{12}A_7$-rGO composites. Longer milling times improved the uniform dispersion of rGO within the matrix, ensuring homogeneity and enhancing electron mobility. The optimal calcination temperature of 1623 K facilitated the formation of a pure $C_{12}A_7$ phase while preserving the structural integrity of the rGO, preventing it from degrading at high temperatures. These optimized synthesis parameters contributed to the overall enhancement of the composite's thermoelectric performance.

In conclusion, the successful synthesis and characterization of ultra-high rGO content in $C_{12}A_7$-rGO composites demonstrated significant improvements in both structural and thermoelectric properties, highlighting the potential of these materials for energy harvesting applications.

5.1.3 Electrical and thermoelectric properties

The investigation into the electrical and thermoelectric properties of the $C_{12}A_7$-rGO composites revealed key trends that highlight the impact of rGO content on the overall performance of the material. The electrical conductivity, Seebeck coefficient, and thermal conductivity were thoroughly measured to assess the ZT, which is a critical parameter in determining the material's potential for energy harvesting applications.

Main trends in electrical conductivity, Seebeck coefficient, and thermal conductivity

Electrical conductivity

The electrical conductivity of the $C_{12}A_7$-rGO composites increased significantly with rising rGO content. This is due to the formation of a continuous network of conductive rGO sheets within the $C_{12}A_7$ matrix, which enhanced charge carrier mobility. Composites with higher rGO content (e.g., 60-70 wt%) exhibited the highest electrical conductivity, reaching values suitable for thermoelectric applications.

Seebeck coefficient

The Seebeck coefficient, which measures the voltage generated due to a temperature gradient, showed a decreasing trend as the rGO content increased. While

pure $C_{12}A_7$ exhibited a relatively high Seebeck coefficient, the introduction of rGO reduced the coefficient due to the increased charge carrier concentration. However, even at higher rGO content, the Seebeck coefficient remained within a range that contributed positively to the overall thermoelectric performance.

Thermal conductivity

One of the major benefits of incorporating rGO into the $C_{12}A_7$ matrix was the reduction in thermal conductivity. The rGO sheets effectively scattered phonons, thereby minimizing heat transport through the composite. This reduction in thermal conductivity is essential for improving the ZT value, as it helps maintain a high temperature gradient, which is critical for efficient thermoelectric conversion.

Optimal rGO content and its impact on ZT

The optimal rGO content for maximizing the ZT was found to be around 60 wt%. At this concentration, the composite achieved a balance between electrical conductivity and thermal conductivity, leading to an improved ZT value. The increased rGO content enhanced electrical conductivity while the phonon scattering effect of rGO reduced thermal conductivity. These combined effects resulted in an optimal ZT of approximately 0.22, a significant improvement compared to pure $C_{12}A_7$. This balance between electron transport and heat management highlights the importance of optimizing rGO content for maximizing thermoelectric performance.

Temperature dependence and balance between electrical and thermal properties

The temperature dependence of the electrical and thermoelectric properties was also a key factor in evaluating the performance of the $C_{12}A_7$-rGO composites. As the temperature increased, the electrical conductivity improved due to thermal excitation of charge carriers. However, the Seebeck coefficient showed a moderate increase with temperature, reflecting the semiconducting behavior of the composite. The thermal conductivity, on the other hand, exhibited a slight decrease at higher temperatures, further enhancing the ZT value. This balance between electrical and thermal properties as a function of temperature is critical for achieving efficient thermoelectric conversion in practical applications.

In summary, the electrical and thermoelectric characterization of $C_{12}A_7$-rGO composites demonstrated that optimizing rGO content and maintaining a balance between electrical conductivity and thermal management is essential for enhancing the ZT. These findings underscore the potential of these composites for use in energy harvesting and waste heat recovery applications.

5.1.4 FEM simulations and module design

The FEM simulations conducted for the n-type $CaMnO_3$ modules embedded in multi-layer concrete bricks provided critical insights into the thermoelectric performance and guided the design optimization of the modules.

Summary of FEM simulation outcomes

The FEM simulations accurately modeled the heat transfer and electrical potential distribution within the $CaMnO_3$ modules, which were embedded in the concrete brick structure. The simulations demonstrated that maintaining a significant temperature gradient across the module was crucial for maximizing the Seebeck effect and, consequently, the voltage generation. By optimizing the boundary conditions and material properties in the simulations, the thermal and electrical behavior of the modules was closely aligned with experimental results. This provided confidence in the simulation model and its predictions regarding module performance.

Key insights from simulations regarding heat transfer and electrical potential distribution

The FEM simulations revealed several important factors that impacted the thermoelectric performance of the $CaMnO_3$ modules:

Heat transfer

The multi-layer concrete brick structure effectively insulated the module, maintaining a steep temperature gradient between the hot and cold sides. This insulation was critical for enhancing the thermoelectric performance. The simulation showed that placing the module closer to the heat source while maintaining a sufficient insulating layer was the optimal configuration for maximizing the heat flow through the module without significant thermal losses.

Electrical potential distribution

The distribution of electrical potential across the $CaMnO_3$ modules was strongly influenced by the temperature gradient. The simulations revealed that the potential difference generated was highest at the interface between the hot side and the module, gradually decreasing toward the cold side. This distribution is typical of thermoelectric systems and underscored the importance of optimizing the module geometry to enhance electrical output.

The combination of these factors, as revealed by the FEM simulations, helped identify optimal design parameters for both the module geometry and placement within the concrete brick, ensuring improved performance.

Successful design and performance based on experimental and simulated results

The insights gained from the FEM simulations were validated by experimental results, which demonstrated close agreement between simulated predictions and real-world performance. The modules were able to generate measurable voltage and power output under temperature gradients, confirming the effectiveness of the design. The experimentally validated FEM model proved to be a reliable tool for optimizing module design, particularly in terms of maximizing heat absorption and improving electrical potential distribution.

In summary, the FEM simulations played a key role in optimizing the design and placement of n-type $CaMnO_3$ modules within multi-layer concrete bricks, ensuring enhanced thermoelectric performance. The combination of simulation and experimental validation provided a robust framework for further optimization in practical applications.

5.2 Contributions to the field

5.2.1 Advancements in thermoelectric materials

This research demonstrates how rGO significantly improves electrical and thermoelectric performance in $C_{12}A_7$ composites. The study's findings contribute to the understanding of how to balance electrical and thermal conductivity, with an optimal

rGO content yielding the best thermoelectric performance. These advancements open possibilities for designing high-performance thermoelectric materials for energy harvesting and waste heat recovery.

5.2.2 FEM for module design optimization

FEM simulations played a critical role in optimizing the design of n-type $CaMnO_3$ modules. By simulating various geometries and placements within the concrete bricks, the study demonstrated how design adjustments could enhance thermoelectric performance. This work contributes to the development of scalable and efficient energy harvesting systems, especially in the field of building-integrated energy technologies.

5.2.3 Potential applications

The $C_{12}A_7$-rGO composites and n-type $CaMnO_3$ modules hold significant potential for a wide range of applications, from small-scale thermoelectric devices to large-scale waste heat recovery systems. Embedding these materials in building structures could lead to energy-efficient smart buildings, capable of harvesting ambient heat and converting it into electricity.

5.3 Limitations of the study

5.3.1 Experimental limitations

Several experimental challenges were encountered, particularly in controlling rGO content and distribution within the $C_{12}A_7$ matrix. Variations in rGO distribution could have affected the material's performance. Equipment sensitivity limitations in techniques such as SEM and Raman spectroscopy may have introduced inaccuracies in microstructure and property measurements.

5.3.2 FEM simulation limitations

FEM simulations made several simplifications, assuming uniform material properties and ignoring certain heat losses, such as radiation or convection. These assumptions may have led to discrepancies between simulated and experimental results, particularly at higher temperature gradients.

5.4 Future research directions

5.4.1 Further optimization of rGO content

Future research should focus on optimizing rGO content to enhance thermoelectric performance further, exploring different synthesis methods and doping strategies to improve material properties and prevent rGO agglomeration.

5.4.2 Advanced characterization techniques

Nanoscale characterization techniques, such as TEM and atomic-level simulations, should be used to gain deeper insights into the material structure, electronic transport, and phonon scattering mechanisms.

5.4.3 Improved FEM simulations

FEM simulations could be improved by incorporating more realistic boundary conditions and multi-physics models, like electron-phonon interactions, to provide a more accurate understanding of thermoelectric behavior.

5.4.4 New applications

The materials studied could be adapted for flexible thermoelectric devices, wearable energy harvesters, and broader energy conversion technologies, such as waste heat recovery and renewable energy systems. Exploring new applications in smart infrastructure and building materials could lead to innovative energy-efficient solutions.

5.5 Final remarks

5.5.1 Scientific and practical Impact

This research advances the understanding of thermoelectric materials and provides scalable solutions for improving energy efficiency in both industrial and everyday applications. The work paves the way for sustainable energy technologies.

5.5.2 Broader implications for the field

The findings of this research offer significant implications for the future development of thermoelectric materials and devices. The approaches explored in this thesis provide a strong foundation for further innovations in thermoelectric system design and optimization.

References

[1] WANG, H. & ET AL. 2019. Highly efficient thermoelectrics. *Frontiers in Physics*.

[2] RUSS, B. & ET AL. 2018. Organic thermoelectrics: the role of phonons. *Materials Research Express*.

[3] Abedi, H., Migliorini, F., Dondè, R., De Iuliis, S., Passaretti, F., & Fanciulli, C. (2019). Small size thermoelectric power supply for battery backup. *Energy*, *188*, 116061.

[4] TRITT, T. M. & ET AL. 2006. Recent Trends in Thermoelectric Materials Research IV. *Topics in Applied Physics*.

[5] LIU, W. & ET AL. 2017. Novel designs for thermoelectric devices. *Nature Reviews Materials*.

[6] HUANG, J. & ET AL. 2023. Thermoelectric energy conversion and storage. *Energies*.

[7] VULLUM, P. E. & ET AL. 2020. Advances in Thermoelectric Materials Research. *NTNU Open*.

[8] WITTING, I. & ET AL. 2019. The thermoelectric properties of materials with low-dimensional nanostructures. *Journal of Materials Science*.

[9] CHEN, G. & ET AL. 2022. Recent advancements in thermoelectric materials. *PubMed*.

[10] YU, X. & ET AL. 2023. High-performance thermoelectric materials for energy harvesting applications. *Advanced Materials*.

[11] LI, Y. & ET AL. 2023. Progress in thermoelectric energy conversion. *Scientific Reports*.

[12] SHAO, Z. & ET AL. 2015. Thermoelectric materials and devices for industrial applications. *De Gruyter Open*.

[13] TOBERER, E. & ET AL. 2016. Introduction to thermoelectrics. *AIP Advances*.

[14] REDDY, A., PATIL, N. & BOLEGAON, N. N. 2022. Fabrication, Characterization, and Gas Sensing Properties of CaMnO3 Doped Polyaniline Nano Composite Thin Films. *ECS Transactions,* 107**,** 11467.

[15] ZHANG, A. & WANG, B. 2016. Temperature and electric potential fields of an interface crack in a layered thermoelectric or metal/thermoelectric material. *International Journal of Thermal Sciences,* 104**,** 396-403.

[16] LI, C., CHEN, Q. & YAN, Y. 2018. Effects of Pr and Yb dual doping on the thermoelectric properties of CaMnO3. *Materials,* 11**,** 1807.

[17] CHIK, A., ZAKI, R. M., ADEWALE, A. A., PA, F. C. & KEAT, Y. C. 2021. Effect of Vanadium Doping on Thermoelectric Properties of CaMnO3 Using First Principle Calculations. *Solid State Phenomena,* 317**,** 543-548.

[18] SAMIMUTHU, B., MANORANJITHAM, R., MOHAN, K. S., BACKIYALAKSHMI, N. & MUTHUKRISHNAN, M. 2024. A study of the effect of cerium ion doping concentration on the structural, electrical, and thermoelectric properties of CaMnO3 nanoparticles. *Zeitschrift für Physikalische Chemie*.

[19] NUR, M. A. N. & KURNIAWAN, B. 2020. Effect of Ni substitution to structure and morphology of Ca0. 9La0. 05Bi0. 05Mn1-xNixO3 by sol-gel method. *Key Engineering Materials,* 860**,** 117-121.

[20] ALFARUQ, D. S., EILERTSEN, J., THIEL, P., AGUIRRE, M. H., OTAL, E., POPULOH, S., YOON, S. & WEIDENKAFF, A. 2013. High-temperature thermoelectric properties of W-substituted CaMnO3. *MRS Online Proceedings Library (OPL),* 1490**,** 3-8.

[21] POPURI, S. R., SCOTT, A., DOWNIE, R., HALL, M., SUARD, E., DECOURT, R., POLLET, M. & BOS, J.-W. 2014. Glass-like thermal conductivity in SrTiO 3 thermoelectrics induced by A-site vacancies. *Rsc Advances,* 4**,** 33720-33723.

[22] HAN, X., HU, Y., YANG, J., CHENG, F. & CHEN, J. 2014. Porous perovskite CaMnO 3 as an electrocatalyst for rechargeable Li–O 2 batteries. *Chemical Communications,* 50**,** 1497-1499.

[23] MANEESAI, K., KHAMMAHONG, S., SIRIPOOM, P., PHROMPET, C., SRIWONG, C., MAENSIRI, S. & RUTTANAPUN, C. 2023. Fabrication and thermoelectric conversion of thermoelectric concrete brick with buried unileg N-type CaMnO3 thermoelectric module inside. *Scientific Reports,* 13**,** 916.

[24] AZULAY, A. & AMOUYAL, Y. 2019. Tailoring electronic and thermal transport properties of CaO (CaMnO3) m-based (m= 1 and m=∞) composites for thermoelectric power generation. *Acta Materialia,* 164**,** 481-492.

[25] KANAS, N., BJØRK, R., WELLS, K. H., SCHULER, R., EINARSRUD, M.-A., PRYDS, N. & WIIK, K. 2020. Time-enhanced performance of oxide thermoelectric modules based on a hybrid p–n junction. *ACS omega,* 6**,** 197-205.

[26] CHOI, J., TU, N. D., LEE, S.-S., LEE, H., KIM, J. S. & KIM, H. 2014. Controlled oxidation level of reduced graphene oxides and its effect on thermoelectric properties. *Macromolecular Research,* 22**,** 1104-1108.

[27] RAHMAN, J. U., DU, N. V., NAM, W. H., SHIN, W. H., LEE, K. H., SEO, W.-S., KIM, M. H. & LEE, S. 2019. Grain boundary interfaces controlled by reduced graphene oxide in nonstoichiometric SrTiO3-δ thermoelectrics. *Scientific reports,* 9**,** 8624.

[28] AISHWARYA, K., RAJAVARDHINI, R., MARUTHASALAMOORTHY, S., MANI, J., NIRMALA, R., ANBALAGAN, G. & RANGASWAMY, N. 2024. NiMoO4/Reduced Graphene Oxide Nanocomposites for Thermoelectric Power Generation. *ACS Applied Nano Materials*.

[29] KIM, S., BARK, H., NAM, S., CHOI, H. & LEE, H. 2018. Control of electrical and thermal transport properties by hybridization of two-dimensional tungsten disulfide and reduced graphene oxide for thermoelectric applications. *ACS Sustainable Chemistry & Engineering,* 6**,** 15487-15493.

[30] NAM, W. H., LIM, Y. S., KIM, W., SEO, H. K., DAE, K. S., LEE, S., SEO, W.-S. & LEE, J. Y. 2017. A gigantically increased ratio of electrical to thermal conductivity and synergistically enhanced thermoelectric properties in interface-controlled TiO 2–RGO nanocomposites. *Nanoscale,* 9**,** 7830-7838.

[31] MITRA, M., KULSI, C., CHATTERJEE, K., KARGUPTA, K., GANGULY, S., BANERJEE, D. & GOSWAMI, S. 2015. Reduced graphene oxide-polyaniline composites—synthesis, characterization and optimization for thermoelectric applications. *RSC advances,* 5**,** 31039-31048.

[32] ZHENG, J., WEN, Y., WANG, S., LI, Y., WANG, S., ZHAO, Z., LIU, S., LIU, S., GAO, X. & ZHAO, L. 2024. Microstructure Optimization in the Shear‐Exfoliated $Bi_6Cu_2Se_4O_6$ Through Introducing Reduced Graphene Oxide Leads to Wide‐Ranged Thermoelectric Performance. Advanced Functional Materials, 34.

[33] CHEN, D., ZHAO, Y., CHEN, Y., WANG, B., CHEN, H., ZHOU, J. & LIANG, Z. 2015. One-step chemical synthesis of ZnO/graphene oxide molecular hybrids for high-temperature thermoelectric applications. *ACS Applied Materials & Interfaces,* 7**,** 3224-3230.

[34] ALHASHMI ALAMER, F., ALMALKI, G. A. & ALTHAGAFY, K. 2023. Advancements in Conductive Cotton Thread-Based Graphene: A New Generation of Flexible, Lightweight, and Cost-Effective Electronic Applications. *Journal of Composites Science,* 7**,** 476.

[35] DU, C., CAO, M., LI, G., HU, Y., ZHANG, Y., LIANG, L., LIU, Z. & CHEN, G. 2022. Toward precision recognition of complex hand motions: wearable thermoelectrics by synergistic 2D nanostructure confinement and controlled reduction. *Advanced Functional Materials,* 32**,** 2206083.

[36] MARFOUA, B. & HONG, J. 2023. Graphene induced high thermoelectric performance in ZnO/graphene heterostructure. *Advanced Materials Interfaces,* 10**,** 2202387.

[37] MULLA, R., WHITE, A. O., DUNNILL, C. W. & BARRON, A. R. 2023. The role of graphene in new thermoelectric materials. *Energy Advances,* 2**,** 606-614.

[38] CAO, W., WANG, Z., MIAO, L., SHI, J. & XIONG, R. 2020. Role of lone pair electrons in n-type thermoelectric properties of tin oxides. *Journal of Physics: Condensed Matter,* 33**,** 065504.

[39] JIBRI, K. M., ARCHANA, J., NAVANEETHAN, M. & HARISH, S. 2023. Small polaron hopping conduction mechanism and enhanced thermoelectric power factor in the perovskite LaCoO 3 ceramic. *Physical Chemistry Chemical Physics,* 25**,** 12914-12922.

[40] ZHENG, Y., ZOU, M., ZHANG, W., YI, D., LAN, J., NAN, C.-W. & LIN, Y.-H. 2021. Electrical and thermal transport behaviours of high-entropy perovskite thermoelectric oxides. *Journal of Advanced Ceramics,* 10**,** 377-384.

[41] SPOONER, K. B., GANOSE, A. M., LEUNG, W. W., BUCKERIDGE, J., WILLIAMSON, B. A., PALGRAVE, R. G. & SCANLON, D. O. 2021. BaBi2O6: a promising n-type thermoelectric oxide with the PbSb2O6 crystal structure. *Chemistry of Materials,* 33**,** 7441-7456.

[42] EINHORN, M., WILLIAMSON, B. A. & SCANLON, D. O. 2020. Computational prediction of the thermoelectric performance of LaZnOPn (Pn= P, As). *Journal of materials chemistry A,* 8**,** 7914-7924.

[43] KRASUTSKAYA, N. S., KLYNDYUK, A. I., EVSEEVA, L. E., GUNDILOVICH, N. N., CHIZHOVA, E. A. & PASPELAU, A. V. 2024. Enhanced Thermoelectric Performance of Na0. 55CoO2 Ceramics Doped by Transition and Heavy Metal Oxides. *Solids,* 5**,** 267-277.

[44] DING, D., SUN, F., XIA, F. & TANG, Z. 2020. A high-performance and flexible thermoelectric generator based on the solution-processed composites of reduced graphene oxide nanosheets and bismuth telluride nanoplates. *Nanoscale Advances,* 2**,** 3244-3251.

[45] BISWAS, S., SINGH, S., SINGH, S., CHATTOPADHYAY, S., DE SILVA, K. K. H., YOSHIMURA, M., MITRA, J. & KAMBLE, V. B. 2021. Selective enhancement in phonon scattering leads to a high thermoelectric figure-of-merit in graphene oxide-encapsulated ZnO nanocomposites. *ACS Applied Materials & Interfaces,* 13**,** 23771-23786.

[46] HUANG, L., LU, J., MA, D., MA, C., ZHANG, B., WANG, H., WANG, G., GREGORY, D. H., ZHOU, X. & HAN, G. 2020. Facile in situ solution synthesis of SnSe/rGO nanocomposites with enhanced thermoelectric performance. *Journal of materials chemistry A,* 8**,** 1394-1402.

[47] XIANG, M., YANG, Z., CHEN, J., ZHOU, S., WEI, W. & DONG, S. 2020. Polymeric thermoelectric composites by polypyrrole and cheap reduced graphene oxide in towel-gourd sponge fibers. *ACS omega,* 5**,** 29955-29962.

[48] IYER, R. & GHOSH, A. 2023. Investigation of Integrated and Non-Integrated Thermoelectric Systems for Buildings—A Review. *Energies,* 16**,** 6979.

[49] HOTĚK, P., FIALA, L. & ČERNý, R. Thermoelectric properties of metashale geopolymer mortar doped with graphite powder. Journal of Physics: Conference Series, 2023. IOP Publishing, 012006.

[50] TAN, G., OHTA, M. & KANATZIDIS, M. G. 2019. Thermoelectric power generation: from new materials to devices. *Philosophical Transactions of the Royal Society A,* 377**,** 20180450.

[51] WANG, Q., LI, X., CHEN, C., XUE, W., XIE, X., CAO, F., SUI, J., WANG, Y., LIU, X. & ZHANG, Q. 2020. Enhanced Thermoelectric Properties in p-Type Double Half-Heusler Ti2− yHfyFeNiSb2− xSnx Compounds. *physica status solidi (a),* 217**,** 2000096.

[52] MA, T., DONG, B. X., GROCKE, G. L., STRZALKA, J. & PATEL, S. N. 2020. Leveraging sequential doping of semiconducting polymers to enable functionally graded materials for organic thermoelectrics. *Macromolecules,* 53**,** 2882-2892.

[53] XIAO, H., QIU, K., GOU, X., LIU, X. & LI, Z. 2022. Development and heat transfer analysis of thermoelectric self-powered fuel-fired residential boiler. *Energy Science & Engineering,* 10**,** 3344-3357.

[54] FéLIX-HERRáN, L. C., GARCíA-JUáREZ, A., GARCíA-DELGADO, L. A., GONZáLEZ-AGUAYO, P. S., LOZOYA-SANTOS, J. D.-J. & NORIEGA, J. R. 2022. Characterization System for Heat-Energy to Electric-Energy Conversion from Concrete by Means of a Thermoelectric Module. *Sensors,* 22**,** 1881.

[55] MURATA, M., NAGASE, K., AOYAMA, K., YAMAMOTO, A. & SAKURABA, Y. 2021. Prototype fabrication and performance evaluation of a thermoelectric module operating with the Nernst effect. *Iscience,* 24.

[56] LEEPHAKPREEDA, T. 2012. Experimental Determination of Thermoelectric-Module Parameters and Modeling for Cooling/Heating Control Design. *Experimental Techniques,* 36**,** 13-20.

[57] SIPPAWIT, N. & LEEPHAKPREEDA, T. 2015. A study of sensing heat flow through thermal walls by using thermoelectric module. *Thermal Science,* 19**,** 1497-1505.

[58] SAHU, A., RUSS, B., SU, N. C., FORSTER, J. D., ZHOU, P., CHO, E. S., ERCIUS, P., COATES, N. E., SEGALMAN, R. A. & URBAN, J. J. 2017. Bottom-up design of de novo thermoelectric hybrid materials using chalcogenide resurfacing. *Journal of Materials Chemistry A,* 5**,** 3346-3357.

[59] LU, T., LI, Y., ZHANG, J., NING, P. & NIU, P. 2020. Cooling and mechanical performance analysis of a trapezoidal thermoelectric cooler with variable cross-section. *Energies,* 13**,** 6070.

[60] ZHU, Y., NEWBROOK, D. W., DAI, P., DE GROOT, C. K. & HUANG, R. 2022. Artificial neural network enabled accurate geometrical design and optimisation of thermoelectric generator. *Applied Energy,* 305**,** 117800.

[61] ANANT KISHORE, R., KUMAR, P., SANGHADASA, M. & PRIYA, S. 2017. Taguchi optimization of bismuth-telluride based thermoelectric cooler. *Journal of Applied Physics,* 122.

[62] SHITTU, S., LI, G., XUAN, Q., ZHAO, X., MA, X. & CUI, Y. 2020. Electrical and mechanical analysis of a segmented solar thermoelectric generator under non-uniform heat flux. *Energy,* 199**,** 117433.

[63] ZIOLKOWSKI, P., ZABROCKI, K. & MüLLER, E. 2018. TEG design for waste heat recovery at an aviation jet engine nozzle. *Applied Sciences,* 8**,** 2637.

[64] WOLF, M., RYBAKOV, A., HINTERDING, R. & FELDHOFF, A. 2020. Geometry optimization of thermoelectric modules: Deviation of optimum power output and conversion efficiency. *Entropy,* 22**,** 1233.

[65] ZHU, H., YU, J., ZHU, Q. & LI, Y. 2024. Nonlocal numerical simulation of thermoelectric coupling field by using peridynamic differential operator. *Zeitschrift für angewandte Mathematik und Physik,* 75**,** 132.

[66] QIAN, B., ZHAO, Y. & REN, F. 2019. Effect of material anisotropy on the transverse thermoelectricity of layered composites. *International Journal of Energy Research,* 43**,** 181-188.

[67] JIANG, D., ZHOU, Y. T. & LI, F. 2022. The effect of the ratio of the radius of the hole and crack length on the multi‐field behaviors of thermoelectric materials under oblique loads. *ZAMM‐Journal of Applied Mathematics and Mechanics/Zeitschrift für Angewandte Mathematik und Mechanik,* 102**,** e202100370.

[68] DOBOSZ, A., PLEVACHUK, Y., SKLYARCHUK, V., SOKOLIUK, B. & GANCARZ, T. 2019. The influence of Li on the thermophysical properties of liquid Ga–Sn–Zn eutectic alloys. *Journal of Materials Science: Materials in Electronics,* 30**,** 18970-18980.

[69] KHAN, K., TAREEN, A. K., KHAN, U., NAIRAN, A., ELSHAHAT, S., MUHAMMAD, N., SAEED, M., YADAV, A., BIBBò, L. & OUYANG, Z. 2019. Single step synthesis of highly conductive room-temperature stable cation-substituted mayenite electride target and thin film. *Scientific Reports,* 9**,** 4967.

[70] PALLECCHI, I., CAGLIERIS, F., CECCARDI, M., MANCA, N., MARRé, D., REPETTO, L., SCHOTT, M., BILC, D. I., CHAITOGLOU, S. & DIMOULAS, A. 2023. Investigation and field effect tuning of thermoelectric properties of SnSe 2 flakes. *Physical Review Materials,* 7**,** 054004.

[71] SRIWONG, C., PHROMPET, C., TUICHAI, W., KARAPHUN, A., KUROSAKI, K. & RUTTANAPUN, C. 2020. Synthesis, microstructure, multifunctional properties of mayenite Ca12Al14O33 (C12A7) cement and graphene oxide (GO) composites. *Scientific Reports,* 10**,** 1-19.

[72] COMSOL, A. B. 2019. COMSOL Multiphysics® v. 5.5. Stockholm, Sweden: COMSOL AB.

[73] Karnis, I., Krasanakis, F., Sygellou, L., Rissanou, A. N., Karatasos, K., & Chrissopoulou, K. (2024). Varying the degree of oxidation of graphite: effect of oxidation time and oxidant mass. *Physical Chemistry Chemical Physics*, *26*(13), 10054-10068.

[74] Al-Sherbini, A. S., Bakr, M., Ghoneim, I., & Saad, M. (2017). Exfoliation of graphene sheets via high energy wet milling of graphite in 2-ethylhexanol and kerosene. *Journal of advanced research*, *8*(3), 209-215.

[75] Siddarth, R. K., Manopriya, M., Swathi, G., Vijayvenkataraman, G., & Aranganayagam, K. R. (2019). One step synthesis of reduced and moringa oleifera treated graphene oxide: characterization and antibacterial studies. In *Proceedings of the International Conference on Nanomedicine (ICON-2019)* (pp. 54-62). Springer International Publishing.

[76] Ain, Q. T., Haq, S. H., Alshammari, A., Al-Mutlaq, M. A., & Anjum, M. N. (2019). The systemic effect of PEG-nGO-induced oxidative stress in vivo in a rodent model. *Beilstein journal of nanotechnology*, *10*(1), 901-911.

[77] Ji, C., & Gu, F. (2023). XRD analysis determined crystal cage occupying number n of carbon anion substituted mayenite-type cage compound C12A7: n C. *Science and Engineering of Composite Materials*, *30*(1), 20220197.

[78] Park, W., Hu, J., Jauregui, L. A., Ruan, X., & Chen, Y. P. (2014). Electrical and thermal conductivities of reduced graphene oxide/polystyrene composites. *Applied Physics Letters*, *104*(11).

[79] Mitra, A., Sahoo, M. R., Samal, A., Pradhan, S. K., Polai, B., Sahoo, K. R., ... & Nayak, S. K. (2023). Large enhancement of thermal conductivity of aluminum-reduced graphene oxide composites prepared by a single-step method. *Oxford Open Materials Science*, *3*(1), itac015.

[80] Wilk, J., Smusz, R., Filip, R., Chmiel, G., & Bednarczyk, T. (2020). Experimental investigations on graphene oxide/rubber composite thermal conductivity. *Scientific reports*, *10*(1), 15533.

[81] Shahil, K. M. F., & Balandin, A. A. (2012). "Thermal properties of graphene and multilayer graphene: Applications in thermal interface materials." *Solid State Communications*, 152(15), 1331-1340.

[82] Kim, S., Yoo, Y., Lee, J., & Park, J. (2016). "Effects of reduced graphene oxide on the thermal conductivity of epoxy composites." *Composites Science and Technology*, 132, 61-67.

NO THIS PAGE IN APPENDIX

Author biography

Name	Mr. Keerati Maneesai
Date of Birth	25 May 1981
Address	555/130 Moo.1, Tha Song Khon, Mueang Maha Sarakham district, Maha Sarakham, 44000
Education	(2007) Master of Science (Physics) GPA 3.39 (Khon Kaen University) (2003) Bachelor of Science (Physics) GPA 3.35 (Khon Kaen University)
Scholarship	KMITL Doctoral Scholarships, 2018-2021 (KDS2018/007) Development and Promotion of Science and technology Talents project (DPST), 1999-2012
Research Experienced and Interesting	1) Thermoelectric materials and renewable energy 2) Computational physics 3) STEM teaching 4) Innovation coaching
Job history	1) 2014-Present: Lecturer, Department of General Science, Faculty of Science and Engineering, Kasetsart University, Chalermphrakiat Sakon Nakhon Province Campus

Academic Publications

1) Maneesai, K., Thongkam, M., Sriwong, C. and Ruttanapun, C., 2024. Grain boundary, electrical transport and thermoelectric properties of the ultra-high rGO amount of C12A7-rGO composites. *Heliyon*, *10*(8). (IF: 3.4) (ISI, Scimago Q1)
2) Maneesai, K., Khammahong, S., Siripoom, P., Phrompet, C., Sriwong, C., Maensiri, S. and Ruttanapun, C., 2023. Fabrication and thermoelectric conversion of thermoelectric concrete brick with buried unileg N-type CaMnO3 thermoelectric module inside. *Scientific Reports*, *13*(1), p.916. (ISI, IF: 3.8) (Scimago Q1)
3) Maneesai, K., Silakaew, K., Khammahong, S., Phrompet, C., Sriwong, C., Thanachayanont, C. and Ruttanapun, C., 2023. Temperature-dependent electrical transport, Hall effect, and Seebeck properties of bulk chemically reduced graphene oxide with bipolar charge carrier materials. *AIP Advances*, *13*(3). (ISI, IF: 1.4) (Scimago Q3)
4) Maneesai, K., Sriwong, C. and Ruttanapun, C., Effect of Ultra-High Reduced Graphene Oxide Amount of the C12a7/Rgo Composites by a High-Speed 3d Ball Milling Machine on Thermoelectric Properties. *Available at SSRN 4213273*. (ISI, IF:) (Scimago)
5) Phrompet, C., Maneesai, K., Tuichai, W., Karaphun, A., Sriwong, C. and Ruttanapun, C., 2020. Electrochemical properties of tricalcium aluminate hexahydrate– reduced graphene oxide nanocomposites for supercapacitor device. *Journal of Energy Storage*, *30*, p.101474. (ISI, IF: 8.9) (Scimago Q1)
6) Thongsamrit, W., Phrompet, C., Maneesai, K., Karaphun, A., Tuichai, W., Sriwong, C. and Ruttanapun, C., 2020. Effect of grain boundary interfaces on electrochemical and thermoelectric properties of a Bi2Te3/reduced graphene oxide composites. *Materials Chemistry and Physics*, *250*, p.123196. (ISI, IF: 4.3) (Scimago Q1)